

AD-A070 469

UNITED TECHNOLOGIES RESEARCH CENTER EAST HARTFORD CONN F/G 11/2
INVESTIGATION OF SILICON-NITROGEN CERAMICS FOR GAS TURBINES.(U)

JAN 79 G K LAYDEN

N62269-77-C-0248

UNCLASSIFIED

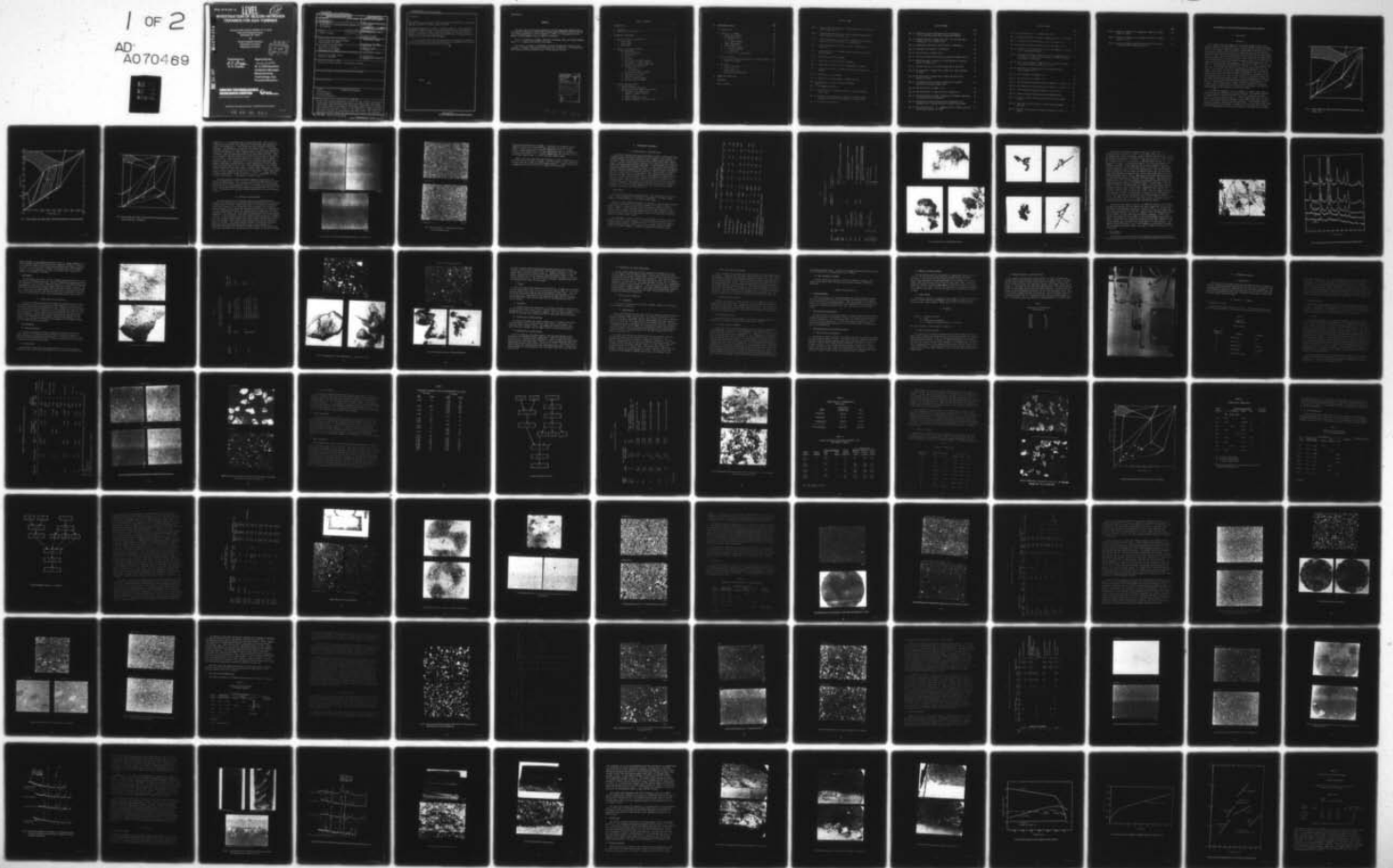
UTRC/R79-914147-4

NADC -77063-30

NL

1 OF 2

AD
A070469



R79-914147-4

LEVEL

12

INVESTIGATION OF SILICON-NITROGEN CERAMICS FOR GAS TURBINES

ADA070469

Prepared Under Contract N62269-77-C-0248

Naval Air Development Center
Warminster, Pa. 18974

for

Naval Air Systems Command
Department of the Navy
Washington, DC 20361

DDC
RECEIVED
JUN 26 1979
C

Prepared by:

G. K. Layden
G. K. Layden

Approved by:

M. A. DeCrescente
M. A. DeCrescente
Assistant Manager
Manufacturing
Technology and
Process Research

DDC FILE COPY

**UNITED TECHNOLOGIES
RESEARCH CENTER**



EAST HARTFORD, CONNECTICUT 06108

"APPROVED FOR PUBLIC RELEASE - DISTRIBUTION UNLIMITED."

79 06 25 044

78-01-254-1

Unclassified

SECURITY CLASSIFICATION OF THIS PAGE (When Data Entered)

19 REPORT DOCUMENTATION PAGE		READ INSTRUCTIONS BEFORE COMPLETING FORM
1. REPORT NUMBER 48 NADC-77063-30	2. GOVT ACCESSION NO.	3. RECIPIENT'S CATALOG NUMBER 9
6. TITLE (and Subtitle) INVESTIGATION OF SILICON-NITROGEN CERAMICS FOR GAS TURBINES		5. TYPE OF REPORT & PERIOD COVERED Final Report September 1977 - October 1978
7. AUTHOR(s) 10 George K. Layden	14 UTRC	6. PERFORMING ORG. REPORT NUMBER R79-914147-4
9. PERFORMING ORGANIZATION NAME AND ADDRESS United Technologies Research Center East Hartford, CT 06108		8. CONTRACT OR GRANT NUMBER(s) 15 N62269-77-C-0248
11. CONTROLLING OFFICE NAME AND ADDRESS Department of the Navy Naval Air Systems Command Washington, D.C. 20361		10. PROGRAM ELEMENT, PROJECT, TASK AREA & WORK UNIT NUMBERS A3200000/001A/7R02200000
14. MONITORING AGENCY NAME & ADDRESS (if different from Controlling Office) Naval Air Development Center Warminster, PA 18974		12. REPORT DATE January 27, 1979
		13. NUMBER OF PAGES 95
		15. SECURITY CLASS. (of this report) Unclassified
		15a. DECLASSIFICATION/DOWNGRADING SCHEDULE
16. DISTRIBUTION STATEMENT (of this Report) Approved for Public Release - distribution unlimited 11 27 Jan 79 12 110p		
17. DISTRIBUTION STATEMENT (of the abstract entered in Block 20, if different from Report)		
18. SUPPLEMENTARY NOTES		
19. KEY WORDS (Continue on reverse side if necessary and identify by block number) SiAlON Liquid Phase Sintering Silicon Nitride Nitrogen Ceramics Gas Turbine Materials		
20. ABSTRACT (Continue on reverse side if necessary and identify by block number) Ceramic bodies having compositions in the β^* , β^* -15R, and β^* -0' phase fields in the Si_3N_4 - SiO_2 - Al_2O_3 - SiO_2 system which are prepared using fine grained constituents cannot be sintered to high density, since little or no liquid forms during normal firing schedules. β^* -X phase bodies, however, sinter to near theoretical density as a result of the presence of a liquid phase under equilibrium conditions at temperatures above about 1750°C. One such body, composition 20e/oAl, 20e/oO, was characterized in terms of room temperature		

DD FORM 1 JAN 73 1473

EDITION OF 1 NOV 65 IS OBSOLETE

Unclassified * Beta' JOB
SECURITY CLASSIFICATION OF THIS PAGE (When Data Entered)

409 252

20 (cont'd)

and 1370°C flexural strength, 1370°C creep, 1000 and 1400°C static oxidation behavior, and Mach 0.8 flame erosion at 1270°C.

* Attempts were made to supply a transient liquid to effect sintering of β' , β' -15R, and β' -0' bodies by controlling particle size distributions of different constituent phases. There was evidence that in fact transient liquids were induced at temperatures above 1750°C, but solid phase particle bridging effects prevented gross shrinkage.

It seems highly likely that the application of pressure at temperature to such formulations could yield the desired result--dense β' based materials that contain neither residual glass nor X phase.

* Beta'

FOREWORD

The work reported herein was performed by United Technologies Research Center, East Hartford, Connecticut, 06108 under Contract Number N62269-77-C-0248 during the period from September 27, 1977 to December 27, 1978. Mr. Irving Machlin of the Naval Air System Command acted as technical consultant.

Dr. M. A. DeCrescente, Manager, Materials Processing, UTRC, was Program Manager, and Dr. G. K. Layden was Principal Investigator.

The author is pleased to acknowledge the help received from D. Moroz, x-ray analysis, L. Jackman, scanning electron microscope, A. Manzione, x-ray fluorescence and scanning electron microprobe, and C. Hulse, machine testing.

Accession For	
NTIS GRA&I	<input checked="" type="checkbox"/>
DDC TAB	<input type="checkbox"/>
Unannounced	<input type="checkbox"/>
Justification	
By _____	
Distribution/_____	
Availability Codes	
Dist	Avail and/or special
A	

79 06 25 044

TABLE OF CONTENTS

	Page
I. INTRODUCTION	1
A. Background	1
B. Objectives and Approaches	5
II. EXPERIMENTAL PROCEDURES	9
A. Characterization of Raw Materials	9
1. Si_3N_4 Powders	9
2. Al_2O_3 Powders	14
3. AlN Powders	17
B. Sample Fabrication Procedures	17
1. Unit Operations	17
a. Batch formulations	17
b. Ball milling	17
c. Drying	22
d. Screening	22
e. Prereaction of master batches.	22
f. Preparation of X phase powders	22
g. Preparation of course Si_3N_4 powder	23
h. Particle size separation	23
1. Screening	23
2. Sedimentation	23
i. Fine-coarse particle blending	24
j. Pressing of test samples	24
k. Calcining test bars	24
1. Firing of pressed samples	24
m. Heat treatment of samples	25
C. Sample Characterization	25
1. Prepared Powders	25
2. Melting Point Determination.	25
3. Characterization of Fired Test Specimens	25
a. Microstructural examination.	25
b. Modulus of rupture testing	26
c. Creep testing	26
d. Static oxidation testing	26
e. Dynamic oxidation - erosion testing.	27

	Page
III. EXPERIMENTAL RESULTS	29
A. Organization	29
B. Process I - β' Bodies	29
1. Compositions Studies	29
2. Prereacted Powders	30
a. X-Phase	30
b. β' and 15R Phases	34
3. Sample Fabrication	34
4. Sample Evaluation	34
a. Process 2, Bodies	40
5. β' - 15R Compositions	44
6. β' Compositions	52
7. β' -O' and β' -O'-X Compositions	61
C. Process 3 Bodies	62
1. Preparation and Microstructure of β' -X Phase Samples	68
2. Powder Pack Studies	68
D. Properties	74
1. Flexural Strengths	74
2. 1370°C Creep	79
3. Oxidation Behavior	79
4. Oxidation-Erosion Behavior	88
IV. SUMMARY AND CONCLUSION	93
REFERENCES	95
LIST OF FIGURES	96

LIST OF FIGURES

		Page
Fig. 1	System $\text{Si}_3\text{N}_4\text{-AlN-Al}_2\text{O}_3\text{-SiO}_2$ 1750°C Isothermal Section (Partial) After Layden (Ref. 3).	2
Fig. 2	System $\text{Si}_3\text{N}_4\text{-AlN-Al}_2\text{O}_3\text{-SiO}_2$, 1750°C Isothermal Section, After Naik, Gauckler, and Tien (Ref. 4).	3
Fig. 3	System $\text{Si}_3\text{N}_4\text{-AlN-Al}_2\text{O}_3\text{-SiO}_2$ 1650°C Isothermal Section Showing Compositions Involved in Process 1 Formulations	4
Fig. 4	Polished and Etched Sections of Process 1 Sample (Ref. 5, Sample 351)	6
Fig. 5	Microstructures of β' -15R Phase Pellets Prepared from Finely Milled Powders	7
Fig. 6	Morphology of KBI Si_3N_4 Powder	12
Fig. 7	Morphology of GTE Sylvania Si_3N_4 Powders	13
Fig. 8	Whisker Mat on Pellet of SN 402 Si_3N_4 Heated to 1460°C	15
Fig. 9	Diffraction Patterns of as-Received and Heat Treated Si_3N_4 Powders	16
Fig. 10	Morphology of Al_2O_3 Powders	18
Fig. 11	Morphology of AFE AlN Powder -325 Mesh Fraction	20
Fig. 12	Morphology of Indussa -325 Mesh AlN Powder	21
Fig. 13	Erosion Test Apparatus	28
Fig. 14	Etched Sections of Crystallized Melts of Proposed X Phase Compositions	32
Fig. 15	Different size fractions of crushed and screened X Phase, $\text{Si}_3\text{Al}_6\text{O}_{12}\text{N}_2$ (Transmission micrographs, 1.720 index oil)	33
Fig. 16	Flow Sheet for Process 1	36

LIST OF FIGURES

	Page
Fig. 17 Morphology of Batch 16A Powder (28.4 w/o $\text{SiAl}_4\text{O}_2\text{N}_4$ + 71.6 w/o Si_2AlON_3) After Spray Drying and Screening	38
Fig. 18 Polished Section of Sample 17A-3 (21.7 w/o -100 +200 Mesh $\text{Si}_3\text{Al}_6\text{O}_{12}\text{N}_2$ + 78.3 w/o Batch 16A)	41
Fig. 19 Compositions Involved in Variou Process 2 Formulation	42
Fig. 20 Flow Sheet for Process 2, β -15R Field	45
Fig. 21 Microstructure of Sample 28.3.1	48
Fig. 22 Particles in Exterior and Interior Regions of Samples 28.3.1	49
Fig. 23 SEM Element Maps in Vicinity of Large Particles in Exterior Region of Sample 28.3.1	50
Fig. 24 Polished Sections of (β' -15R) Samples 28.7.1 and 28.8.1	51
Fig. 25 Microstructure of Sample 28.3.1 After 10 hr. Heat Treatment at 1720°C	53
Fig. 26 Microstructure of Sample 28.6.1 Before and After 10 hr. Heating at 1720°C	54
Fig. 27 Polished Sections of Process 2 Composition 33 Samples Fired With and Without Powder Pack	57
Fig. 28 Polished Section of Sample 33.1.2	58
Fig. 29 SEM Element Maps of Large Particles in Sample 15.2	59
Fig. 30 Polished Sections of Stage 2 Composition 33 Samples Compounded from Different Batch Formulation	60
Fig. 31 Representative Optical Transmissions Micrographs (1.77 Immersion Oil) of Settled Fraction of Ward B Si_3N_4 Powder	63
Fig. 32 Microstructure of β' - 0' - Composition 30.1.2 Before and After 10 hr. Heat Treatment of 1720°C	65

LIST OF FIGURES

	Page
Fig. 33 Microstructure of $\beta - 0$ Composition 30.3.1	66
Fig. 34 Polished Sections of Process 2 Composition 30 ($\beta' - 0$) Sampler	67
Fig. 35 Polished and HF Etched Surfaces of ($\beta'-X$) Sample 27.3.3	70
Fig. 36 Polished and HF Etched Surfaces of ($\beta'-X$) Sample 31.1.1	71
Fig. 37 Comparison of the Microstructure of ($\beta'-X$) Samples 27.3.3 and 31.1.1 at High Magnification	72
Fig. 38 XRD Patterns Obtained from Surfaces of $\beta'-X$ Phase Sample 27.3.2 and Sample 27.3.6 Heat Treated 15 Hours at 1600°C in Powder of Composition $4AlNi SiO_2$	73
Fig. 39 Macro and Micrographs of Sample 27.3.9 after Heat Treatment in $4 AlNSiO_2$ Powder at 1600°C for 50 hrs.	75
Fig. 40 XRD Pattern from Different Areas at Powder Pack Heat Treated Sample 27.3.10	76
Fig. 41 Fracture Surface of Sample 33.1.1	77
Fig. 42 Fracture Surface of Sample 30.4.4	78
Fig. 43 Room Temperature Fracture Origins of Samples 27.1.3 and 27.1.4	80
Fig. 44 Room Temperature Fracture Origins of Samples 27.3.3 and 27.3.4	81
Fig. 45 1370°C Fracture Origins of Samples 27.4.2 and 27.4.3	82
Fig. 46 Flexural Strength of Some Si_3N_4 and $SiAlON$ Materials	83
Fig. 47 Strain vs Time at 1370°C and 10,000 psi Stress for Sample 27.3.15	84
Fig. 48 Creep Rate vs Applied Stress for Some Si_3N_4 and $SiAlON$ Materials	85
Fig. 49 Polished Cross Sections of Samples Oxidized for 72 hrs, at 1400°C	87

	Page
Fig. 50 Surface of Sample 27.3.2 Subjected to Mach 0.8, 1270°C Flame for 3 hrs.	89
Fig. 51 Surface of Samples 27.3.1 Subjected to Mach 0.8, 1400°C Flame for 2 hrs.	91
Fig. 52 Surface of Sample of Hot Pressed Si ₃ N ₄ (NC 132) Subject to Mach 0.8 1270°C Flame for 2 hrs.	92

Investigation of Silicon-Nitrogen Ceramics for Gas Turbines

I. INTRODUCTION

A. Background

Hot pressed Si_3N_4 would appear to have potential applications in gas turbines operating at high temperature. The great expense of machining parts from this material is prohibitive however, and alternative materials are sought that could be formed to near net shape by conventional sintering techniques. Early reports indicated that mixtures of Si_3N_4 and Al_2O_3 could be sintered to fully dense bodies having the same crystal structure as, and properties comparable to, Si_3N_4 . These reports stimulated further research in the fabrication and characterization of β' solid solutions. More recent work has shown that β' solid solutions have an extended narrow homogeneity range in the Si-Al-O-N diagram given by the formula $\text{Si}_{3-x}\text{Al}_x\text{O}_x\text{N}_{4-x}$. Solid phase compatibility relations for the system have been proposed by Guackler et al (Ref. 1) and by Jack (Ref. 2). Previous work at UTRC done under contract to the Department of the Navy (Ref. 3) has shown that the β' $\text{Si}_{3-x}\text{Al}_x\text{O}_x\text{N}_{4-x}$ compositions, like pure Si_3N_4 , do not sinter, and that the reason Si_3N_4 - Al_2O_3 mixtures do sinter is because some liquid is present at sintering temperature. The extent of the liquid and liquid-solid regions at 1650°C and 1750°C were determined in Ref. 3. Recent work by Naik et al. (Ref. 4) has confirmed the essential features of the isothermal sections proposed in Ref. 3 and has established tie-lines between β' solid solutions and equilibrium liquid phase compositions at 1750°C. The 1750°C isothermal sections of Layden and Naik et al are presented in Figs. 1 and 2, respectively. Figure 1 has been replotted in equivalent percent from the original work and reoriented to correspond to the style of representation used by Gauckler, by Jack, and by Naik.

Prior work by the author (Ref. 5) attempted to produce single phase β' solid solutions by a transient liquid phase process. The technique employed can be understood in terms of the 1650°C and 1750°C isothermal sections. The 1650°C section is shown as Fig. 3. Several compositions have been indicated on the figure which are relevant to the following discussion. As with Fig. 1, this section has been replotted from Ref. 1. Two preacted compositions were prepared: composition a (X phase) which is liquid above about 1750°C and composition c which consists of a mixture of β' and 15R solid solutions. These two complementary compositions were mixed in the proper ratio to yield

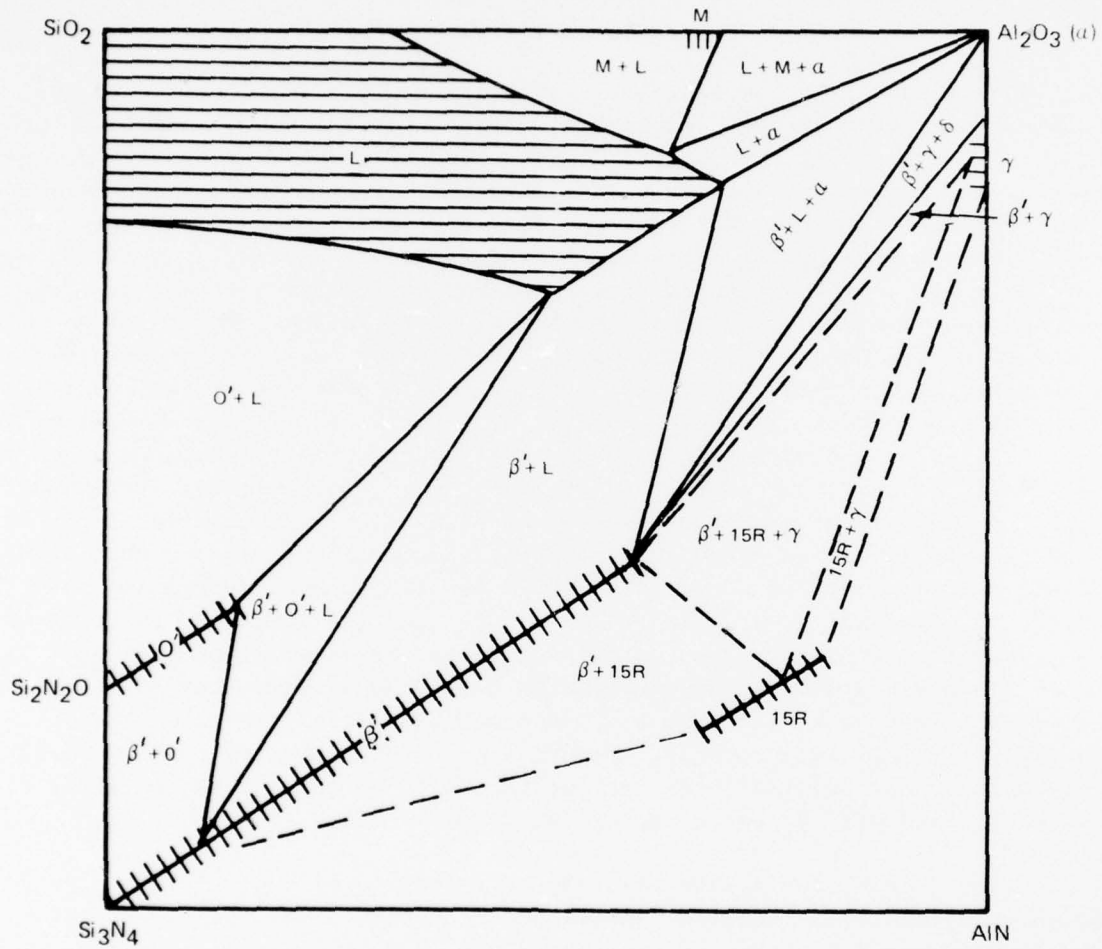


Fig. 1 System $\text{Si}_3\text{N}_4\text{-AlN-Al}_2\text{O}_3\text{-SiO}_2$ 1750°C Isothermal Section (Partial) After Layden (ref. 3)

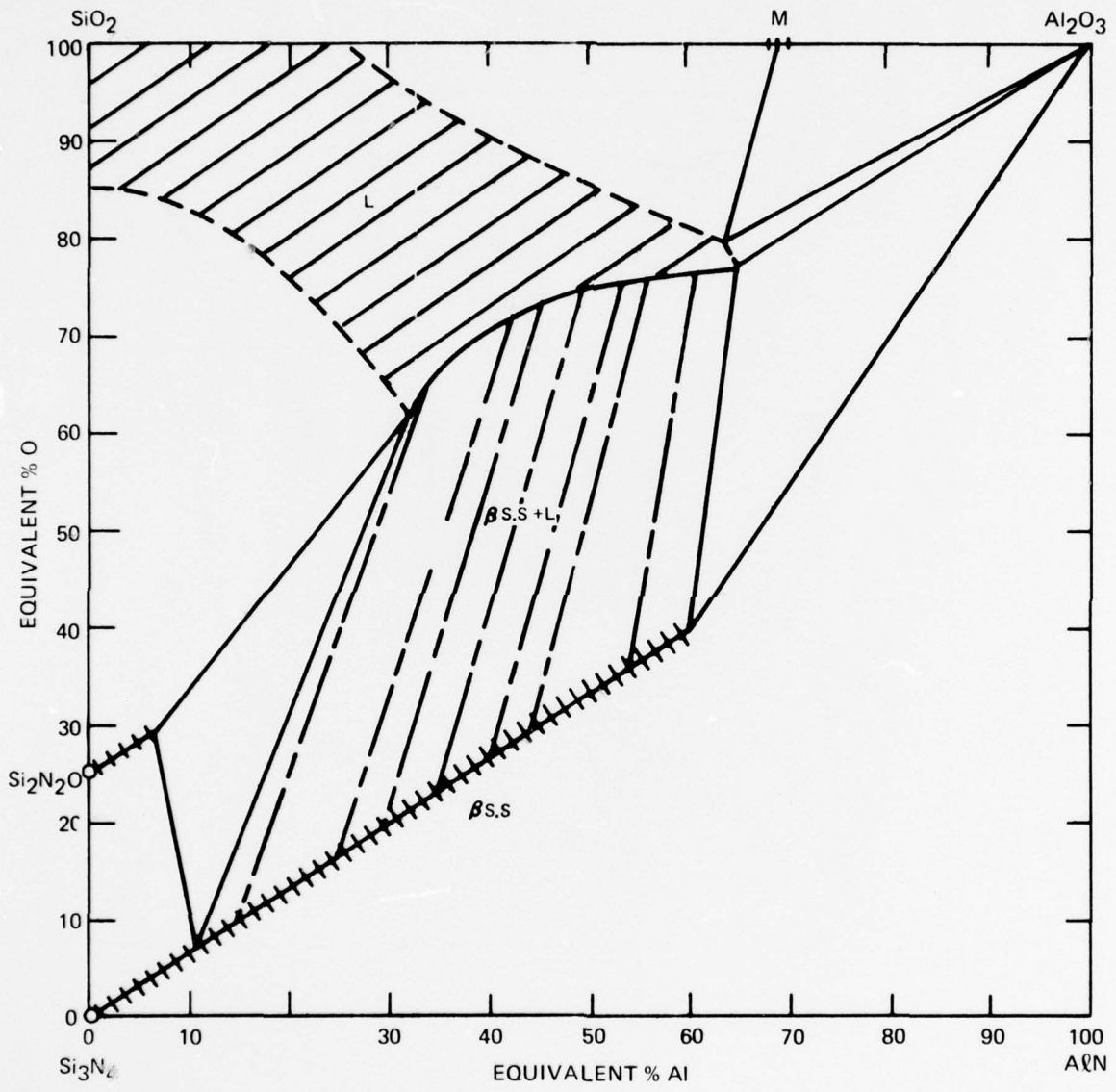


Fig. 2 System Si_3N_4 -AlN- Al_2O_3 - SiO_2 , 1750°C Isothermal Section, after Naik, Gauckler,

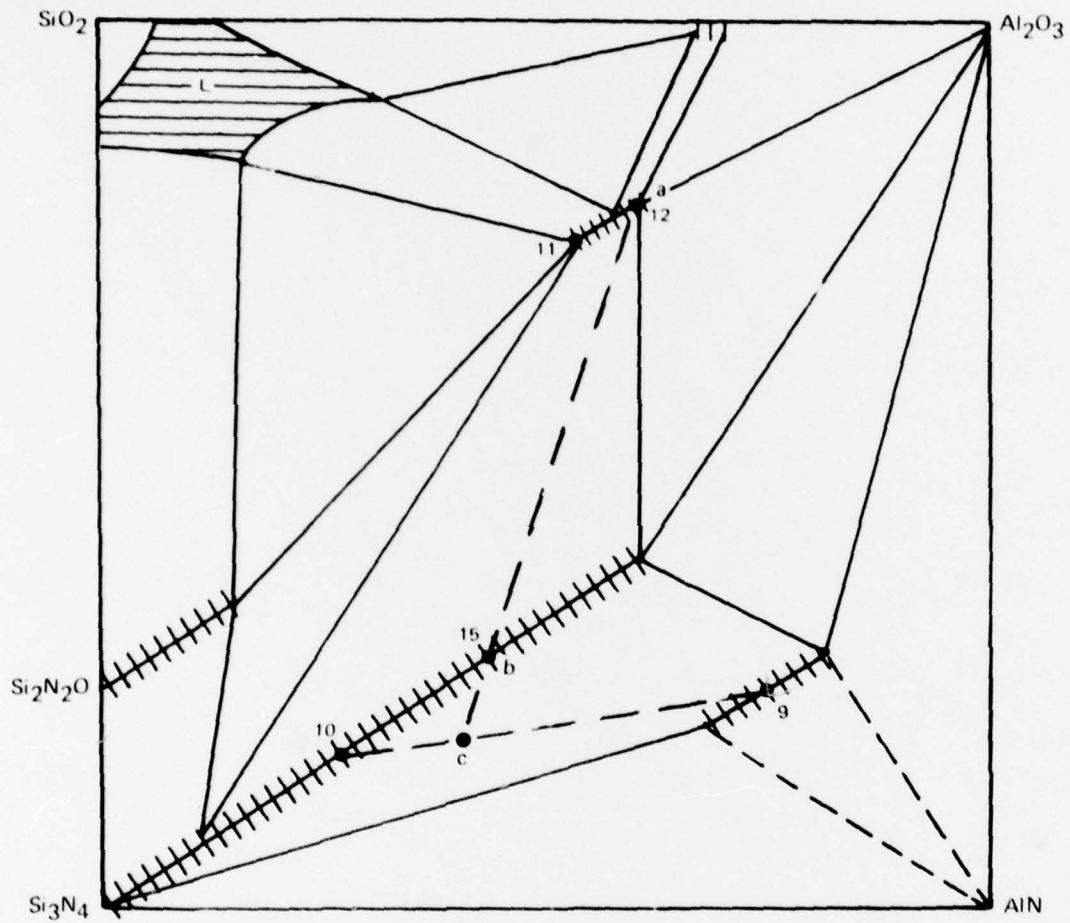


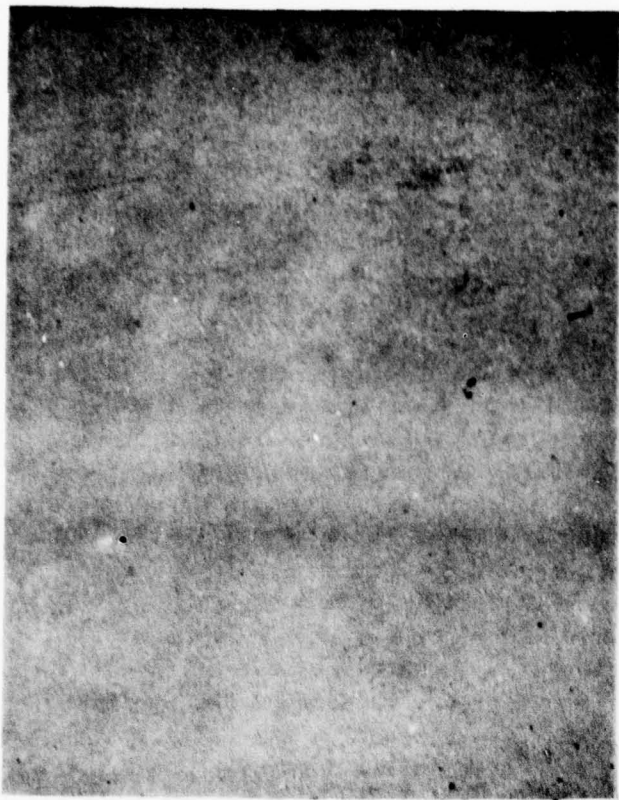
FIG. 3 System $\text{Si}_3\text{N}_4\text{-AlN-Al}_2\text{O}_3\text{-SiO}_2$ 1650° Isothermal Section Showing Compositions Involved in Process 1 Formulations

composition b. It was assumed that at temperatures above 1750°C liquid of composition a would react with composition c constituents and homogenize to single phase composition b. Fully dense bodies were produced using these techniques. Micrographs of one such body are shown in Fig. 4. Such bodies frequently appeared to be single phase to x-rays, but microscopic examination disclosed the presence of a grain boundary phase or phases (presumably glass or X-phase), and the mechanical properties of these bodies were poor. Mean room temperature flexural strength of 210 MPa (30 ksi) falling to 180 MPa (26 ksi) at 1370°C. Long term heat treatments of such bodies did not improve properties, and it was concluded that either 1) residual glassy phase in the bodies is difficult to crystallize, or 2) unaccounted-for deviations from assumed stoichiometry placed the true overall compositions in the two-phase field β' -X rather than on the β' line. Altering compositions so as to move assumed compositions away from X phase resulted in some improvement in properties to a point, but also resulted in more porous bodies. Bodies whose overall composition fell unambiguously inside the β' - 15R or β' - $\text{Si}_2\text{N}_2\text{O}$ fields did not sinter appreciably. By way of contrast to Fig. 4, micrographs of some sintered fine grained β' - 15R samples are shown in Fig. 5.

The above studied processing techniques employed co-milling of the prereacted compositions a and c in order to achieve intimate mixing of finely ground constituent phases. Such fine mixtures can react in the solid state during heat-up to firing temperature, and it is possible under such conditions that no liquid forms unless overall compositions actually fall in the β' - X field. This appears to be the most probably explanation of results presented in Ref. 5.

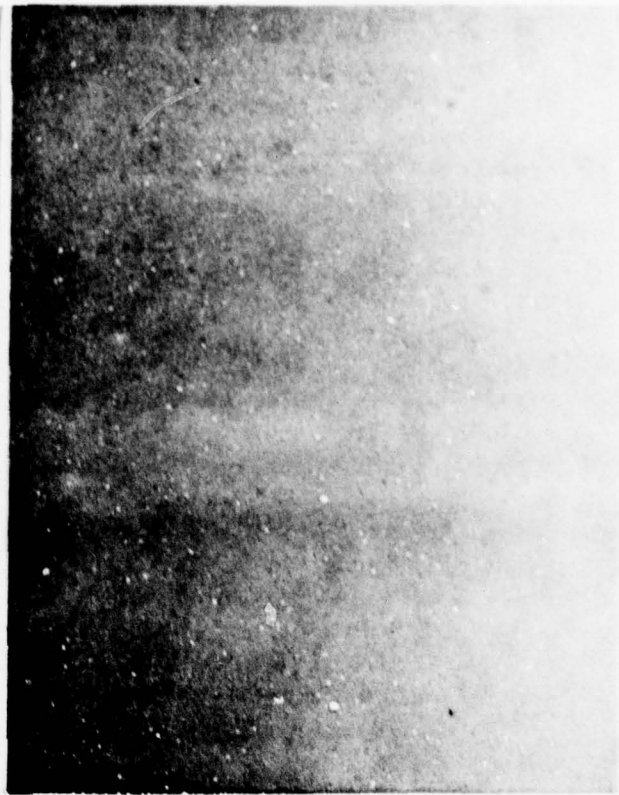
B. Objectives and Approaches

The initial objective of the present work was to develop processing techniques to produce densely sintered SiAlON bodies which were free of either residual glass or X phase. Several approaches to this goal were considered, but the basic premise in all of them was that the presence of a liquid of composition near that of X phase was required during part of the firing schedule. The approaches differed in the conceptual way of supplying, and later "drying-up," the liquid. The first approach employed mixtures of fine grained compatible β' and 15R phases, with coarse grained X phase constituent (composition 12). It was assumed that lack of intimate contact between the incompatible X and 15R phases would prevent their reaction until the melting point of X phase was reached, at which point X phase liquid would "wet-out" the solid phase constituents. The second approach employed a fine grained mixture of Si_3N_4 and Al_2O_3 constituents which would react to form a mixture of β' and liquid, and coarse size fraction of AlN which would not all react in the solid state during heat up, and could serve as a reserve to dry-up the X phase

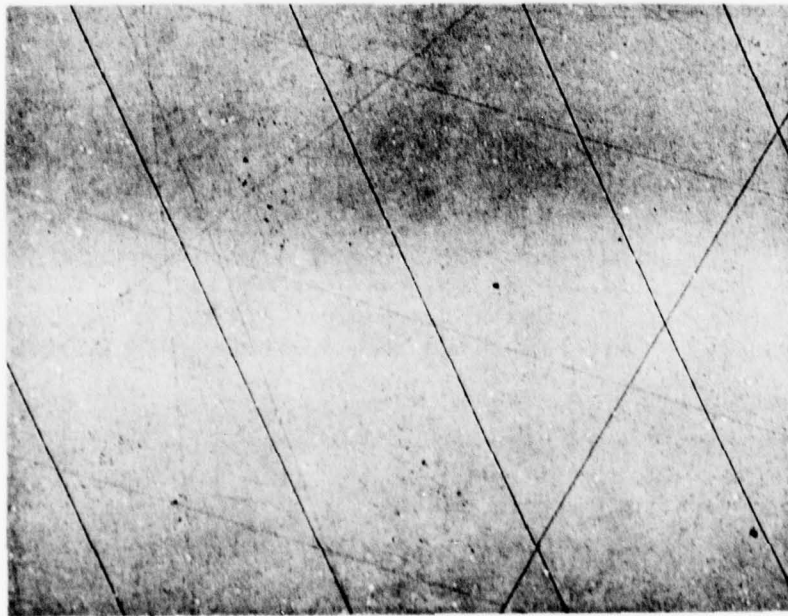


A. POLISHED

200 μ



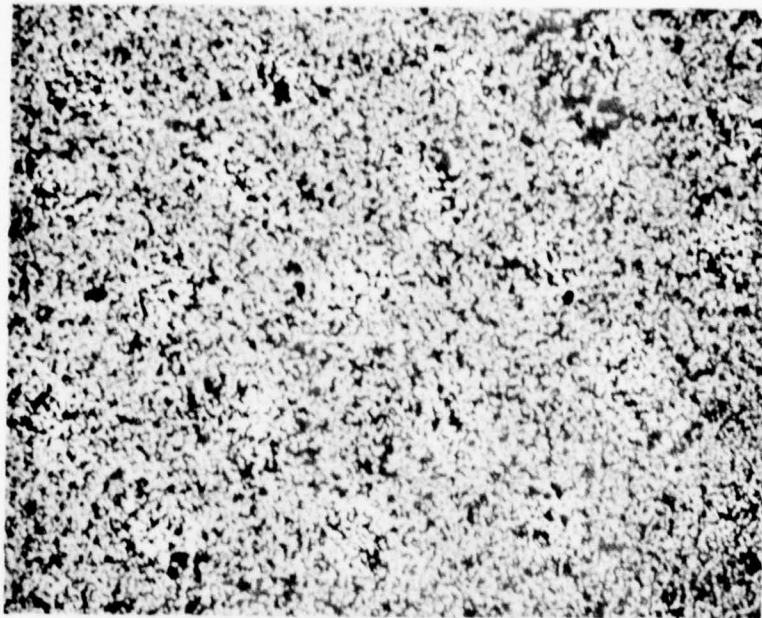
50 μ



B. HF ETCHED

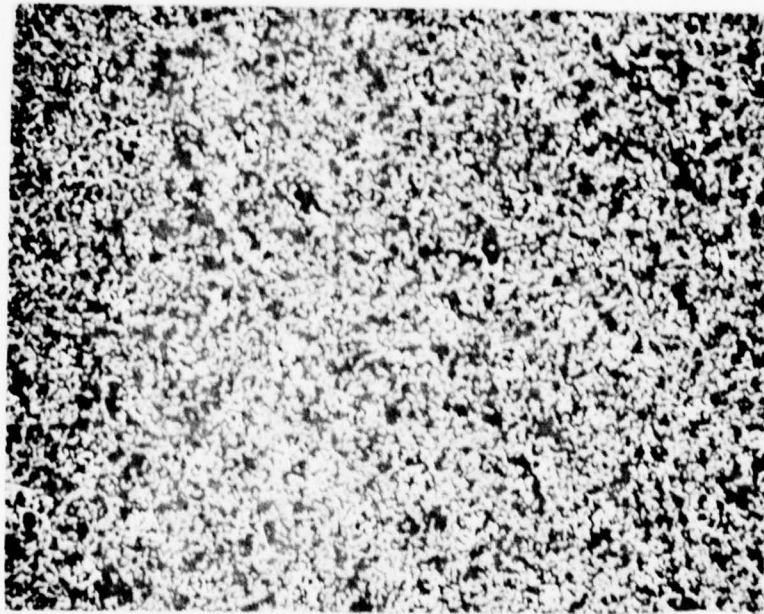
50 μ

Fig. 4 Polished and Etched Sections of Process 1 Sample (ref. 5, Sample 351)



a.) SAMPLE 28-1-1

100 μ



b.) SAMPLE 29-1-1

100 μ

Fig. 5 Microstructures of β' -15R Phase Pellets Prepared from Finely Milled Powders

liquid during extended heat treatment. A variation of the second approach employed a mixture of fine grained Al_2O_3 and Si_3N_4 with coarse grained Si_3N_4 to produce bodies with an overall composition in the β' - $\text{Si}_2\text{N}_2\text{O}_{ss}$ field. A third approach was to use fine-grained mixtures of Si_3N_4 and Al_2O_3 to produce dense bodies of β' - X phase compositions, and later heat treat these in 15R phase powder packs to convert the grain boundary phase.

None of the above approaches was successful in terms of producing a fully dense body devoid of glass or X phase. The fourth quarter of the program was therefore devoted to producing and characterizing a β' - X phase body having a composition as close to the β' - O' phase field as possible.

II. EXPERIMENTAL PROCEDURES

A. Characterization of Raw Materials

A variety of raw materials was investigated in order to choose the types of powders that would be most suitable for the purposes of this program. In general, powders were characterized in terms of phase by x-ray diffraction techniques, (XRD), morphology by scanning electron microscopy (SEM), metallic impurity content by spectrochemical analysis, and volatile impurity content by weight loss measurements and mass spectrometry. Spectrochemical analyses for the various powders are presented in Table I. In the case of nitride powders, oxygen content was determined by fast neutron activation analyses performed by the Union Carbide Corporate Research Laboratory. These data are included in Table I. In the case of two Si_3N_4 powders - GTE Sylvania SN402 and SN502 - mass spectrographic analysis of products of room temperature outgassing and of pyrolysis to 700°C were performed. Attempts were made to determine total nitrogen content using the Kjeldahl method of various size fractions screened from AlN powder, but results were not reproducible to the accuracy required and are not reported. The handling and processing characteristics imparted to batches as a result of powder morphologies were also observed and were important criteria in selecting materials.

1. Si_3N_4 Powders

Silicon nitride powders investigated were: KBI high purity 85 percent β phase - 325 mesh powder, GTE Sylvania SN402 "amorphous", and SN502 α phase powders, and Ward Chemical Co. -325 mesh β phase Si_3N_4 .

Results of spectrochemical analyses for impurities, and activation analyses for oxygen in the various nitride starting materials are given in Table 1. Weight changes of pressed pellets during various heat treating regimes are given in Table 2. X-ray diffraction data for SN402 powder subjected to the various heat treatments, and other observations, are also included in Table 2. Scanning electron microscope photographs of particles of KBI and GTE Sylvania powders are shown in Figs. 6 and 7.

The KBI powder is seen to consist of a broad range of particle sizes and shapes typical of a milled product. A similar appearance was exhibited by the Ward Chemical powders. The SN402 consists of a very narrow size range of roughly spherical particles about 0.2 to 0.8 μ in diameter, while the SN502 consists of whisker fragments of submicron diameters and variable length.

TABLE 1

CHEMICAL ANALYSES OF RAW MATERIALS

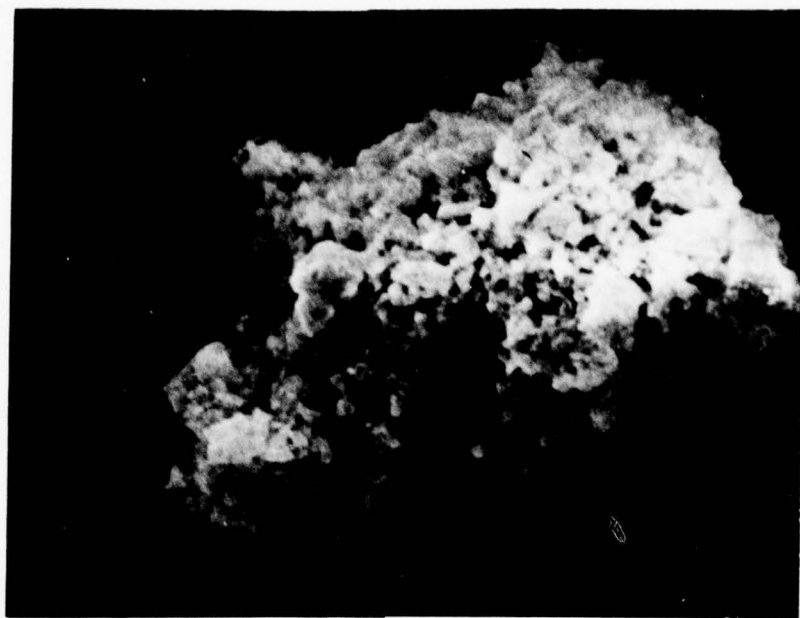
Powder	Impurity, Weight Percent									
	Co	Fe	Si	Al	Mg	Cr	Ni	Cu	Ca	O*
XBI Lot 606-138 Si_3N_4	<.01	.10	Major	<.01	<.01	.01	<.01	.01	<.01	.84
GTE SN-402 Si_3N_4	<.01	.01	Major	<.01	<.01	<.01	<.01	<.01	.02	2.20
GTE SN-402 A**	-	-	-	-	-	-	-	-	-	2.88
GTE SN-502 Si_3N_4	<.01	.01	Major	<.01	<.01	<.01	<.01	<.01	<.01	2.97
Ward Chemical	.03	1.0	Major	0.10	.02	0.10	<.01	<.01	.02	
Indussa AlN	<.01	0.5	1.0	Major	.01	<.01	<.01	.03	.02	1.06
AEE AL 106 AlN	0.5	.05	.15	Major	.01	.03	.01	.01	<.01	6.55
Linde A Al_2O_3	<0.1	<.01	<.01	Major	<.01	<.01	<.01	<.01	<.01	
Apache Amorphous Al_2O_3	<0.1	<.01	.02	Major	.01	<.01	<.01	<.02	.02	

*Determined by fast neutron activation analysis.

**Vacuum heat treated

TABLE 2
WEIGHT CHANGES ACCOMPANYING VARIOUS HEAT
TREATMENTS OF Si_3N_4 POWDERS

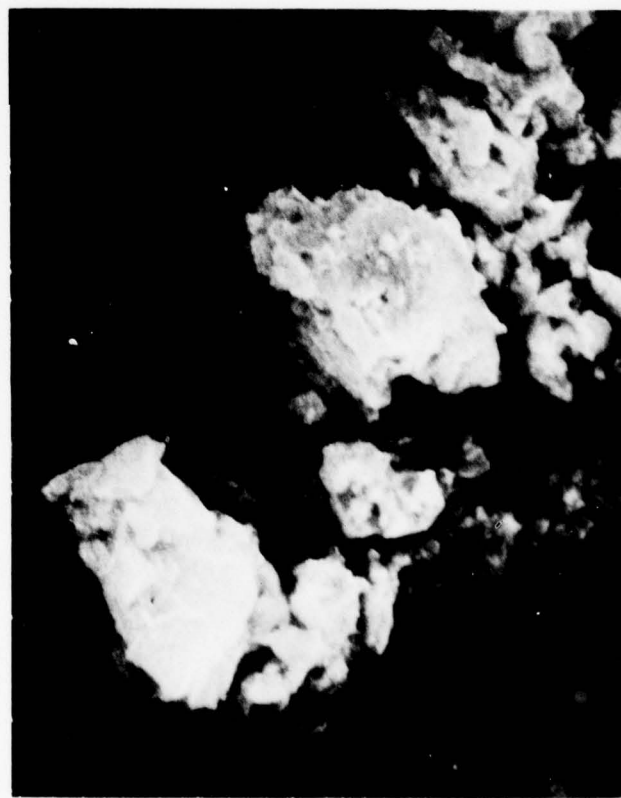
Material	Sample	Heat Treatment	Subsequent Material Designation	Weight Change (percent)	Observation
KBI	a			-0.6	
KBI	b			-0.5	
SN402	a	heated to 1460°C		-6.7	Grew a Si_3N_4 whisker mat on exterior of pellets, and changed color from white to tan.
SN402	b	in nitrogen for 2 hours		-6.3	
SN502	a			-1.5	
SN502	b			-1.5	
SN402	c	heated to 1270°C in vacuum	SN402-2		Changed color from white to tan. Exhibited strong x-ray diffraction pattern.
SN402-2		subsequently heated to 600°C in air, 1 hr.			Retained buff color, a x-ray pattern.
SN402	d	heated to 600°C in air for 1 hour	SN402-1	+0.02	Remained white, exhibited weak a pattern comparable to that of raw material.
SN402-1		subsequently heated to 1190°C in vacuum for 1 hour	SN402-3	-0.47	Retained white color, exhibited weak a diffraction pattern only slightly stronger than that of original material.
SN402	e			-4.0	Dense whisker mat.
SN402	f			-5.4	
SN402-1	a	heated to 1490°C		-5.2	Light whisker growth.
SN402-1	b	in nitrogen for 2 hours		-5.0	
SN402-3	a			-4.4	Essentially whisker free.
SN402-3	b			-4.4	
SN402-3	c			-4.9	
SN402-3	d			-4.5	



5 μ



2 μ



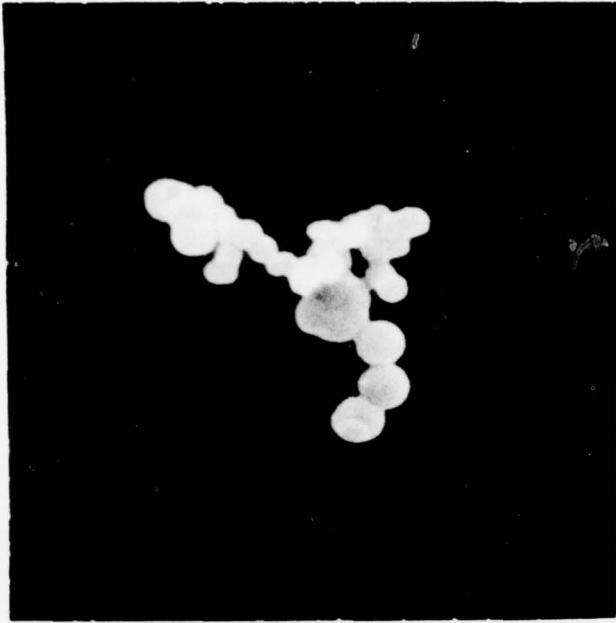
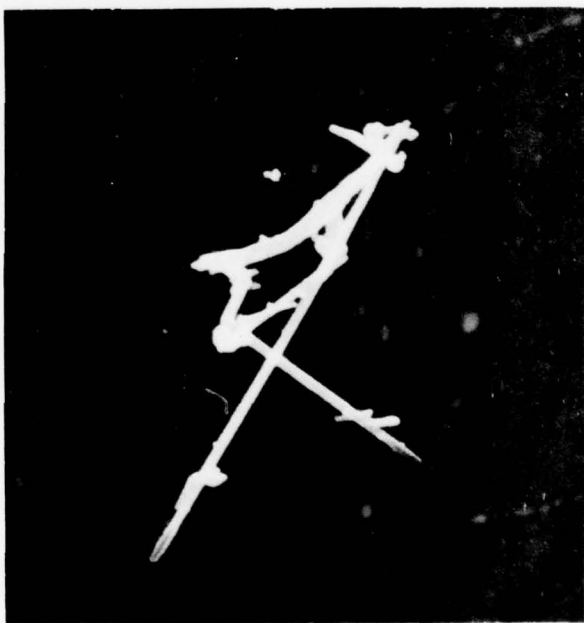
2 μ

Fig. 6 Morphology of KBI Si₃N₄ Powder

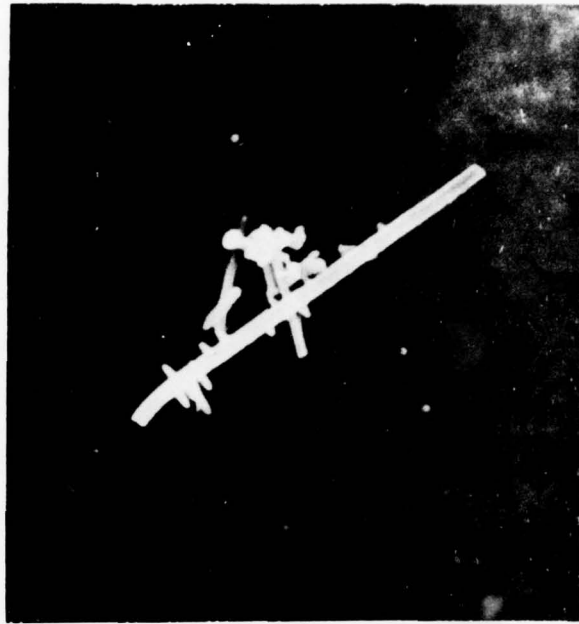
a) SN 402



b) SN-502



1 μm



2 μm

Fig. 7 Morphology of GTE Sylvania Si₃N₄ Powders

During the initial heating of small pellets (< 1 gram) of these powders in nitrogen (entries 1 through 5 of Table 2), the SN402 powder exhibited a substantial weight loss of about 6 percent. A mat of whiskers and particulate material was found on the outside of the SN402 pellets, and the interior of the originally white pellets had taken on a tan color. A SEM micrograph of a portion of this mat is shown in Fig. 8. X-ray diffraction analysis showed the mat to consist primarily of a Si_3N_4 . An unidentified peak at 2.95 Å was also present in the diffraction pattern. It was suspected that a volatile impurity, possibly chloride, was present in the SN402 powder which contributed to a vapor phase transport mechanism responsible for the whisker growth. Mass spectrographic analysis showed that both the SN402 and SN502 materials gave off water vapor during room temperature outgassing, and low molecular weight hydrocarbons and hydrogen when pyrolyzed to 700°C. SN502 also evolved some NH_3 during pyrolysis, otherwise the spectra of SN402 and SN502 were similar. No chlorides were detected in the 700°C pyrolysis products of either powder. Experiments were conducted to see if various outgassing procedures were effective in reducing the whisker-growing tendency of the SN402 powder. A large compact (about 30 grams, 1.5" dia.) of the SN402 powder was placed in a boron nitride crucible and heated slowly to 1250°C under vacuum. Some material was spilled from the crucible during unloading so that accurate weight loss data could not be retrieved. The material had turned tan in color, similar to SN502, and gave an x-ray pattern of a Si_3N_4 . Reproductions of portions of the diffraction patterns of this and other as-received and heat treated powders are shown in Fig. 9. This material was subsequently heated in air to 600°C in order to see if the discoloration was due to a carbonaceous residue that would burn off. The material retained the tan color after the 600°C treatment.

A second 30 gram compact of as-received SN402 was heated in air to 600°C. This material remained white and exhibited a small weight gain of 0.02 percent. This material was subsequently heated in vacuum to 1180°C. It retained the white color, and exhibited a diffraction pattern only slightly stronger than the as-received material (see Fig. 9). Samples of both the SN402 powder heated in air to 600°C, and that which was subsequently outgassed to 1180°C, were then fired (along with control samples of as-received SN402) in nitrogen to 1490°C. The weight losses from these variously treated SN402 powders were all nearly the same, but the tendency to whisker growth was quite different. The control samples again exhibited dense overgrowths of a Si_3N_4 whiskers. The samples of material heated in air to 600°C showed a lesser growth of whiskers, and the samples subsequently heated in vacuum to 1180°C were essentially free of whiskers.

2. Al_2O_3 Powders

Two powders were investigated; Linde A alumina micropolish (0.3 μ particle size) and a nominally 0.03 μ particle size amorphous alumina from Apache Chemicals.

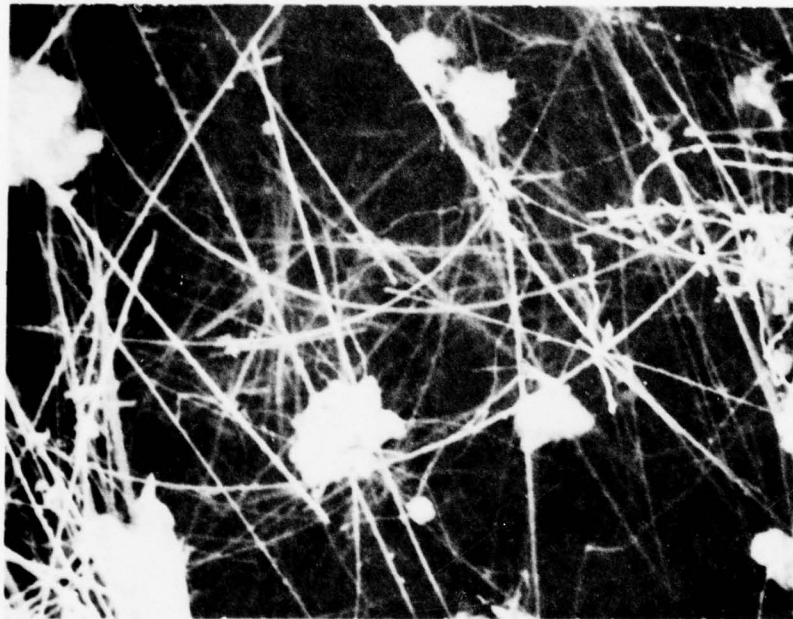


Fig. 8 Whisker Mat on Pellet of SN 402 Si_3N_4 Heated to 1460°C

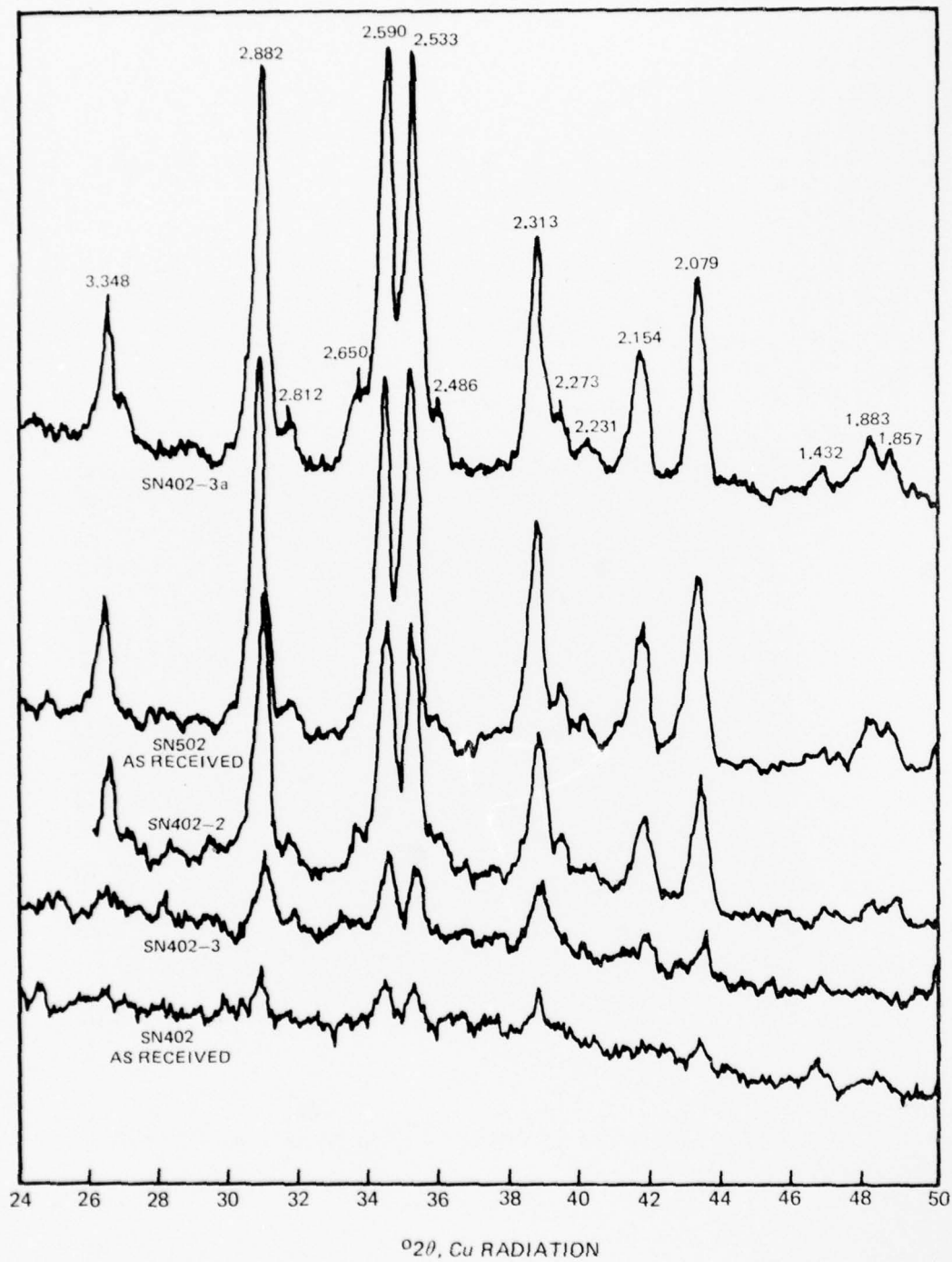


Fig. 9 Diffraction Patterns of as-Received and Heat Treated Si_3N_4 Powders

78-01-177-3

SEM micrographs of these powders are shown in Fig. 10. Weight changes of the alumina powders resulting from various heat treatments are given in Table 3. It is clear from Table 3 that unless special handling and storage procedures are used, it is not possible to assign a fixed Al_2O_3 content to the Apache alumina. This is undoubtedly the result of variable water content which changes with atmospheric conditions.

3. AlN Powders

Two AlN powders were used: Atlantic Equipment Engineers AL106, and a-325 mesh powder from Indussa Industries. Optical transmission photographs of particles dispersed in oil having a refractive index of 1.77, and SEM micrographs of representative particles of the two powders are shown in Figs. 11 and 12. The AEE material is seen to have higher average particle size than the Indussa powder. In general, the former material was selected for screening and settling into fairly narrow particle size fractions when these were required, and the latter was used when ball milled, fine grained master batches were required.

B. Sample Fabrication Procedures

A variety of sample preparation techniques were employed over the course of the program, the specifics of which are best presented in Section III of this report along with the experimental results. However, all of the fabrication techniques can be considered as built up of several unit operations which will be described shortly. Generally, batch preparations fall into one of two broad categories: 1) Those in which all the constituents are added in the initial formulation and 2) those in which subformulations having different particle size distributions are blended to yield the end composition. For clarity, these two types of batches will be referred to as 1) master batches, and 2) blended batches, respectively.

1. Unit Operations

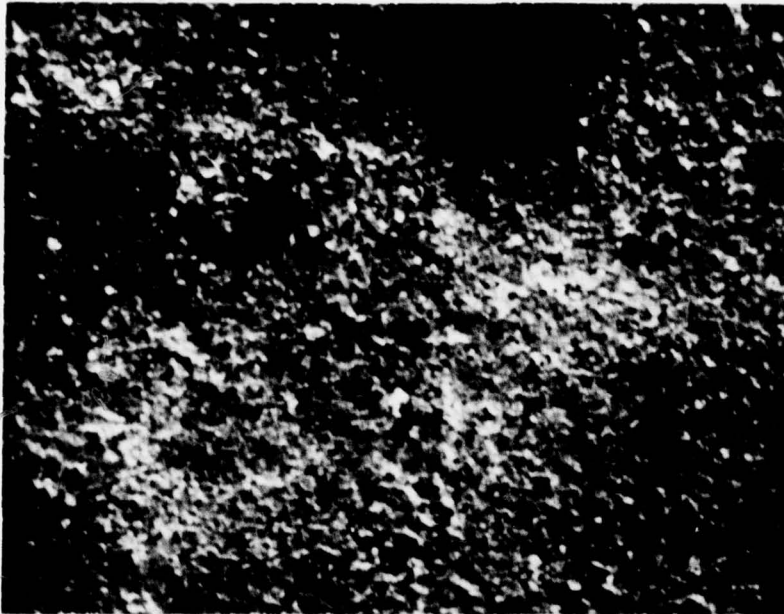
a) Batch formulations

In general, 100 gram master batch formulations took into account the oxygen content of the Si_3N_4 and AlN constituents, and also the amount of major contamination from ball milling operations. In order to do this, logs were kept of the grinding media weight so that material from this source could be predicted with reasonable accuracy.

b) Ball milling

Master batch constituents were added directly to 16 oz. wide mouthed polyethylene bottles which were approximately half filled with a known weight

a) APACHE



b) LINDE A (AGGLOMERATE)

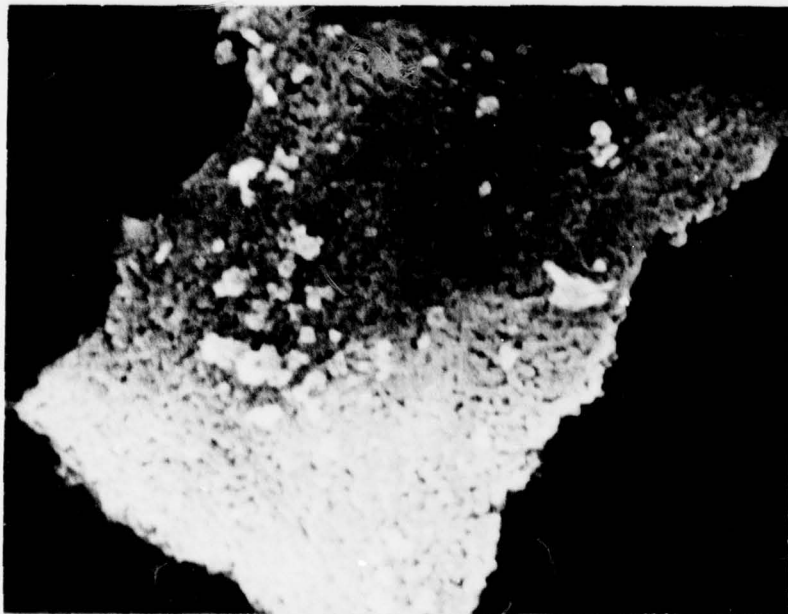


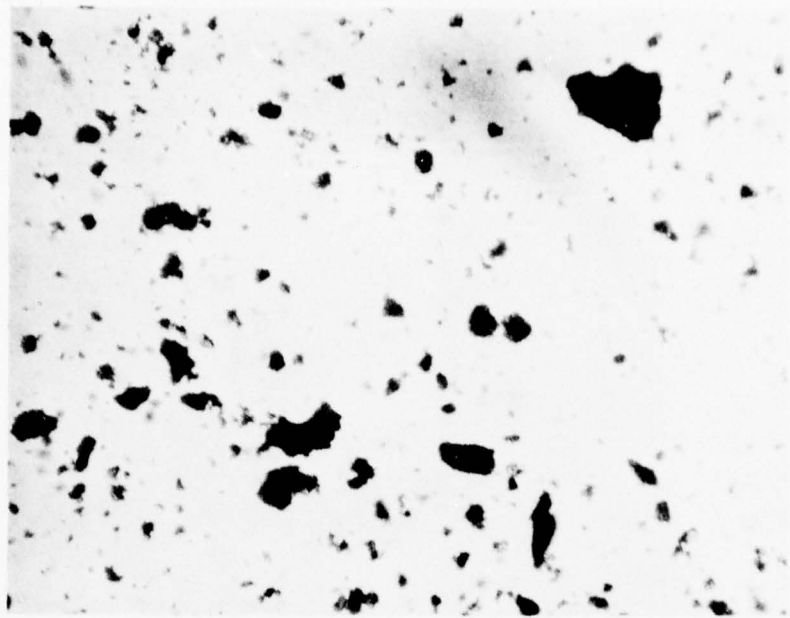
Fig. 10 Morphology of Al₂O₃ Powders

78-01-103-6

TABLE 3

WEIGHT CHANGES ACCOMPANYING VARIOUS
HEAT TREATMENTS OF Al_2O_3 POWDERS

<u>Material</u>	<u>Run Number</u>	<u>Heat Treatment</u>	<u>Weight Change (%)</u>
Linde A	1	Heated to 600°C in air. Material from run 1 sub- sequently heated to 900°C in air.	-0.64
	2		0.0
Apache	1	Heated to 600°C in air Material from run 1 sub- sequently held at ambient laboratory conditions for 48 hours. Material from run 2 sub- sequently heated to 900°C in air.	-6.6
	2		+3.7
	3		-5.3



200 μ

b) SEM MICROGRAPHS



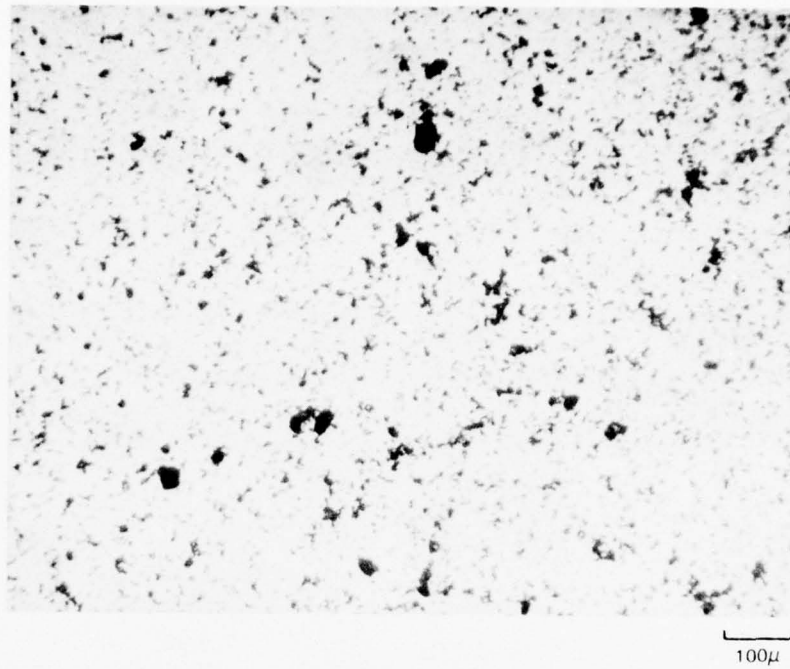
5 μ



2 μ

Fig. 11 Morphology of AEE AlN Powder – 325 Mesh Fraction

a.) OPTICAL TRANSMISSION MICROGRAPH



b.) SEM MICROGRAPHS



Fig. 12 Morphology of Indussa -325 mesh AlN powder

of either reaction-sintered Si_3N_4 grinding media manufactured by Miracle Ceramics, or Norton high-alumina media. The chemical composition of the high-alumina media is given in Table 4, page 27. Methanol was added to cover the charge, and was milling carried out for the predetermined length of time. Rolling speed was set for the different media by adjusting by ear for maximum uniform grinding action. The motor control setting so established was used in all subsequent runs using the given media.

c) Drying

Mill jar contents were emptied into wash bottles. A large tray of aluminum foil was constructed, placed on a hot plate, and a smaller plate of 1/4" aluminum was placed in the center of the tray and heated to about 100°C. The wash bottle was continuously agitated while the contents were sprayed onto the hot alumina plate. Evaporation of the methanol was rapid, and the dry powder was periodically scraped from the plate into the surrounding tray using a teflon scraper.

d) Screening

In instances where test samples were to be made from master batch materials, this was passed through either a 20 or 100 mesh screen in order to break up larger agglomerates prior to cold pressing of samples. This step was eliminated if the master batch was to be prereacted before blending with other constituents.

e) Prereaction of master batches

The spray dried powder was lightly tamped into a 2" diameter BN crucible. A lid was fixed to the crucible which was then placed in the chamber of a carbon resistance element furnace. The chamber was slowly evacuated, then back-filled with nitrogen, and the sample fired to the desired temperature.

f) Preparation of X phase powders

Prior to preparing the X-phase powders, some melting experiments were performed on two proposed X-phase compositions. These will be described in Section II, C2. Following these experiments, a batch of composition $\text{Si}_3\text{Al}_6\text{O}_{12}\text{N}_2$ was prereacted as described above. Pellets of the prereacted powder were cold pressed and placed in a BN crucible, and melted at 1760°C. The cooled (crystallized) material was crushed using a tool steel mortar and pestal. A magnet was passed through the crushed material until no further pick up of steel particles was observed.

g) Preparation of coarse Si₃N₄ powder

Coarse grained Si₃N₄ was initially obtained by crushing some of the Miracle Ceramics Si₃N₄ grinding cylinders with the steel mortar and pestle to obtain material in the -100 mesh range. Finer material was produced by dry ball milling the -100 mesh powder using Si₃N₄ media. After each one hour increment of milling, the -325 mesh fraction was collected, and the remainder returned for further milling. An attempt was made to remove iron contamination introduced from the steel mortar, but it was discovered that the crushed powder itself contained a magnetic impurity. (Even the original grinding cylinders were attracted to a strong magnet). After some initial experiments using the crushed grinding cylinders, a source of fairly coarse grained Si₃N₄ was located (Ward Chemical Corporation).

h) Particle size separation

1) Screening

Particle size fractions in the ranges -100+200, -200+325, and -325 mesh were obtained by screening.

2) Sedimentation

The screened nominal particle size fractions contained substantial amounts of finer material ranging in size down to the limits of resolution of the optical microscope. The coarse fractions were "cleaned up", and the -325 mesh fractions of X-phase, AL106 AlN, and the crushed and milled Si₃N₄ cylinders were cut to about -44 +10 μ fractions by the following technique. The screened fractions were placed in graduated cylinders which were filled with methanol to a height of about 10 cm. These were stoppered and shaken, then allowed to stand for 10 minutes after which the liquid holding the fine suspended particles was decanted. This was repeated five times and removed most of the material below about 10 μ.

The above technique was not suitable for use with the Ward -325 mesh Si₃N₄ powder because of the relatively higher concentration of -10 μ material, and the tendency for this to agglomerate in methanol. The fine material was removed from this material using the following technique. About 35 grams of Ward Si₃N₄ and 2 drops of Tergitol 15S-9 were added to 900 ml of distilled water in a 1000 ml beaker. This was stirred vigorously, allowed to settle for 20 minutes, then the liquid decanted. Fresh water was added, and the procedure repeated four times. The sediment was then stirred in a fresh change of acetone several times, then allowed to dry.

i) Fine-coarse particle blending

Three techniques for blending fine and coarse grained powders were employed. These were: 1) tumbling the processed constituents dry in a twin shell blender, 2) preparing a slurry of the constituent powders and acetone in a large mortar and stirring this with a nylon rod until sufficient acetone had evaporated so that the slurry became "stiff". The stiff slurry was then allowed to dry without further agitation. The dried cake was broken up by light hand grinding, then passed through a 20 mesh screen. 3) The constituent powders were milled for 2 hours under methanol in polyethylene jars using 1/2" diameter polystyrene balls. In some instances, 2 w/o (solids basis) of carbowax was added to the mill to serve as a binder when the powders were pressed into bars. The ball mill charge was then spray dried as described in Section II B1c above.

j) Pressing of test samples

Samples were pressed in either cylindrical or rectangular steel molds at a pressure of about 10,000 psi. These were then placed into rubber bags and isostatically repressed. Early samples were pressed to 60 psi. Failure of the large isostatic press limited later samples to 30 psi. Pressure will be indicated in subsequent tables. Rectangular bars had dimensions approximately 4 cm x 0.95 cm x 0.40 cm.

k) Calcining test bars

Bars which were pressed from powders containing carbowax binder were heated in air to 600°C to burn out the binder prior to firing.

l) Firing of pressed samples

Pressed bars were fired in BN crucibles in one of several configurations. In configuration 1, samples were free standing in the crucibles with bar samples standing vertically. In configuration 2, samples were packed in powder of one of the master batch compositions. In configuration 3, previously fired SiAlON bars were used to construct a chamber inside the BN crucible in which the unfired bars were nested. The spaces between the chamber and the BN crucible were filled with a mixture of unfired powder and grog obtained by crushing some previously fired SiAlON bars. The configuration and powder pack composition, if used, will be identified in the appropriate tables. BN lids were placed on the crucibles which were then placed in graphite holders which had screw tops to hold the lids in place during evacuation. The crucible and holder assemblies were placed in a graphite resistance element furnace. The furnace chamber was evacuated and back-filled with nitrogen to atmospheric pressure a total of three times, then a slow flow of nitrogen maintained through

the furnace during firing. A variety of heating schedules were employed which will be identified in the appropriate text or tables.

m) Heat treatment of samples

Selected samples were packed in powder of composition $\text{SiAl}_4\text{O}_2\text{N}_4$ (15R phase) inside BN crucibles and heated on different schedules in nitrogen atmosphere.

C. Sample Characterization

1) Prepared Powders

Phase identification of prereacted powders was made using XRD techniques. Particle size and morphology of milled batches were assessed by SEM examination of ultrasonically dispersed powders. The various particle size fractions obtained by screening and sedimentation were examined by optical transmission microscopy of powders dispersed in oil under cover glasses on microscope slides.

2) Melting Point Determination

Pellets pressed from prereacted powders of X phase composition were placed in small BN crucibles in the graphite furnace. The furnace was then heated to different temperatures, and a W-Re thermocouple in close proximity to the pellets recorded their temperature. The melting temperature was bracketed by visual and metallographic examination of the crucible contents following cool down to room temperature.

3) Characterization of Fired Test Specimens

a) Microstructural examination

Bulk density, specific gravity, and apparent porosity of sintered specimens were determined by ASTM test C373-5. Microstructures were examined on polished and etched sections of test samples using optical microscopy and, in selected instances, SEM and EDAX^R (Energy Dispersive Analyses of x-rays). Also in selected instances, x-ray diffraction patterns were obtained either from the surfaces test bars or from crushed and ground samples. Surfaces of selected samples that had been heat treated in packed powder were examined by XRD after successive depths of material had been removed by surface grinding.

b) Modulus of rupture testing

Test bars were ground flat and parallel to approximate dimensions 0.10" x 2.5" x 1.25", and one surface was polished through 600 grit SiC paper. The edges of the polished tensile surface were beveled about 0.01" at a 45° angle. Room temperature strength measurements were conducted in four-point flexure with the outer span of 0.75" and the inner span 0.375". Cross-head speed was 0.02"/min. strength measurements at 1370°C were conducted in three-point flexure with a span of 0.75". Selected fracture surfaces were examined in the SEM in an attempt to identify the nature of the flaws that controlled strength.

c. Creep testing

Specimens in the above configuration were loaded to 10 ksi in three-point flexure at 1370°C under argon atmosphere using tungsten loading pins, and deflection-time curves obtained. Strain was calculated from the formula

$$\epsilon = \frac{2h (n+2)}{L^2} y_L$$

where h = specimen thickness

L = span

y_L = cross-head displacement

n = the empirical stress exponent of creep rate.

The stress exponent n was assigned the number 1.75.

d. Static oxidation testing

All surfaces of rectangular specimens were polished through 600 grit SiC paper, and the geometrical surface area of the specimen was measured. Samples were weighed to the nearest tenth of a milligram and placed on a platinum tray that was constructed so as to support the specimens along two lines of contact and leave all surfaces exposed to the atmosphere. The samples were introduced into a preheated furnace in air atmosphere and removed from the furnace periodically, and weighted. X-ray diffraction patterns were obtained from the oxidized surface, then the sample mounted in resin, polished, and examined metallographically.

e. Dynamic oxidation - erosion testing

The erosion test apparatus is shown in Fig. 13. The test sample was clamped between refractory brick jaws mounted on a traverse table. The sample and table were aligned in front of the orifice of a propane - oxygen torch prior to ignition so that the flame would impinge on the sample surface at 20° incidence. The sample was then withdrawn from position, and torch ignited and brought to approximate steady state operating conditions. The sample was then driven into the predetermined position, and the torch fine-tuned to give the desired surface temperature and flame velocity. Surface temperature was sensed by a radiation pyrometer focused on the hottest spot of the sample and was recorded throughout the run. Flame velocity was calculated from chamber pressure. Erosion was judged qualitatively by SEM examination of eroded surfaces.

TABLE 4

Composition of High Alumina
Grinding Media

Al ₂ O ₃	88
SiO ₂	10
CaO	0.5
Na ₂ O	0.7
K ₂ O	0.3
Fe ₂ O ₃	0.3
TiO ₂	0.1

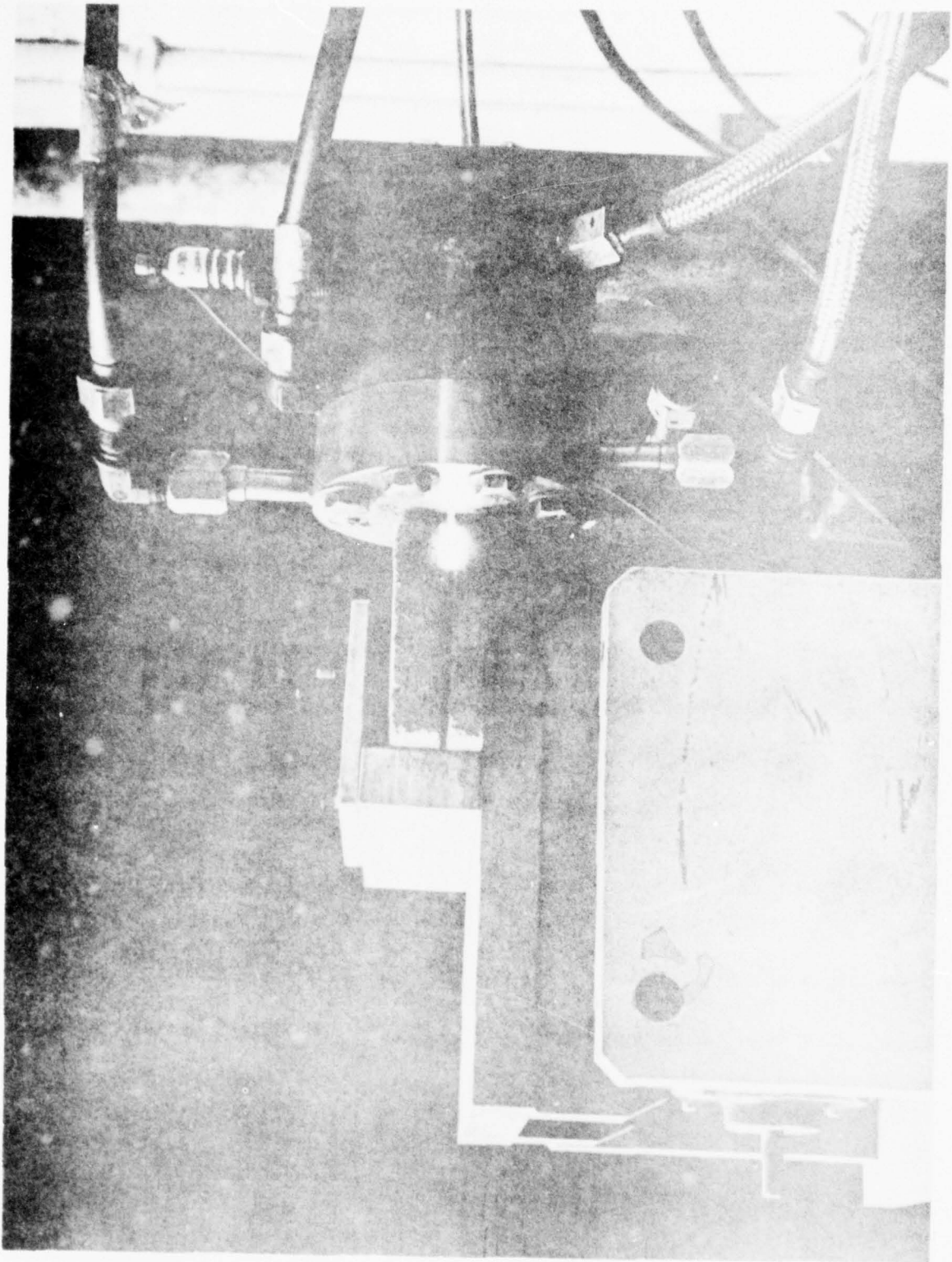


Fig. 13 Erosion Test Apparatus

III. EXPERIMENTAL RESULTS

A. Organization

The results of the various processing investigations will be organized in terms of the different approaches that were set forth in the introduction and the phase field in which the composition of the body under consideration lies. The sintering and microstructural characteristics of the variously formulated bodies will be considered first, then the physical properties of those bodies that were tested will be discussed.

B. Process I - β' Bodies

1) Compositions Studied

Compositions studied are plotted on Fig. 3. The chemical formulae and assumed phase identities for the indicated compositions are listed in Table 5.

TABLE 5

PROCESS I COMPOSITIONS

(See Figure 3)

<u>Composition Number</u>	<u>Formula</u>	<u>A Phase</u>
9	$\text{SiAl}_4\text{O}_2\text{N}_4$	15R
10	$\text{Si}_2\text{Al}_6\text{O}_3\text{N}_3$	β'_1
11	$\text{Si}_{10}\text{Al}_{15}\text{O}_{32}\text{N}_7$	X (Niak ³)
12	$\text{Si}_3\text{Al}_6\text{O}_{12}\text{N}_2$	X (Layden ¹)
15	$\text{Si}_{1.5}\text{Al}_{1.5}\text{O}_{1.5}\text{N}_{2.5}$	$\beta'_{1.5}$

Recent work by Naik et al. (Ref. 4) has assigned the composition $\text{Si}_{10}\text{Al}_{15}\text{O}_{32}\text{N}_7$ to X-phase. Our previous work (Ref. 3) found $\text{Si}_3\text{Al}_6\text{O}_{12}\text{N}_2$ to be essentially single phase X, and our interpretation of the phases observed in adjacent compositions cooled from different temperatures suggested that the homogeneity range of X phase probably extended to about $\text{Si}_{3.5}\text{Al}_{5.5}\text{O}_{11.5}\text{N}_{2.5}$ as shown in Fig. 3. This may be written as $\text{Si}_{9.8}\text{Al}_{15.4}\text{O}_{32.2}\text{N}_7$ which is essentially identical with the composition assigned by Naik. The end members of the 15R solid solution series have not been established precisely, nor have the tie lines between 15R and β' compositions, but we assume them to be approximately as indicated on Fig. 3.

2) Prereacted Powders

Batch data, firing schedules, and XRD data for prereacted phases are given in Table 6. Except for X-phase powders, the initial firing was insufficient to convert the powders to the desired phase. These powders were lightly hand ground in a procelain mortar and refired as indicated in Table 6. The prereacted phases were characterized and further processed as described below.

a. X-Phase

The assumed end members of the X-phase homogeneity range were prepared. Both gave very similar diffraction patterns corresponding to X-phase (Ref. 3, p. 16), however, the pattern from the $\text{Si}_{10}\text{Al}_{15}\text{O}_{32}\text{N}_7$ composition exhibited sharper peaks of greater intensity, as was also observed by Naik (Ref. 4). The melting behavior of both compositions was observed as described in Section II. Pellets of both compositions showed no evidence of melting when heated to 1700°C , and both appeared to have been molten when cooled from 1750°C . The crystallized melts were mounted, polished, etched with HF, and examined metallographically. Micrographs are shown in Fig. 14. Both samples are seen to consist of large crystals of X-phase which contain inclusions of small lath like crystals, probably β' . The $\text{Si}_{10}\text{Al}_{15}\text{O}_{32}\text{N}_7$ composition also exhibited some glassy phase in grain boundaries. It is not clear whether the small inclusions represent undissolved material in the melts or (perhaps more likely on the basis of morphology) precipitates that formed in the melts as a result of changes in melt composition because of disproportionation. The crystallized melts were full of bubbles, and appear to disproportionate at temperatures only slightly above the melting point at one atmosphere of nitrogen pressure.

Several large pellets of the prereacted X-phase (Batch 12.1) were melted, crushed, and screened to different particle size distributions as described in Section II. Optical transmission photographs of different size fractions dispersed in 1.72 index oil are shown in Fig. 15.

TABLE 6

PROCESS 1 PRERACTED COMPOSITIONS FIRING AND XRAY DATA

Composition	Batch Number	Constituents (1)			Firing Conditions Temp (°C)	Time (hrs)	X-Ray Data
		Si ₃ N ₄	SiO ₂	Al ₂ O ₃			
9	9.1	20.97(2)		21.67	57.25(3)	1680	2 s U ₁ , (5) + m β'
	9.2	20.97		21.67	57.25	1680	2 s U ₁
						1725	2 ms 15 R + m β'
	9.3		26.82		73.18(4)	1650	2 s 15 R + w β'
10	9.4		26.82		73.18	1650	2
						1700	2
	10.1	66.59		20.50	12.90(3)	1690	2 s β' + w α
	10.2	66.59		20.50	12.90	1690	2
11						1725	3 s β' + tra
	11.1	19.40		58.91	21.57	1700	3 s X
	12.1	19.55		82.03	23.42	1600	3 m X

(1) Compensated for ball mill pick-up (Si₃N₄) and oxygen content in nitride starting materials

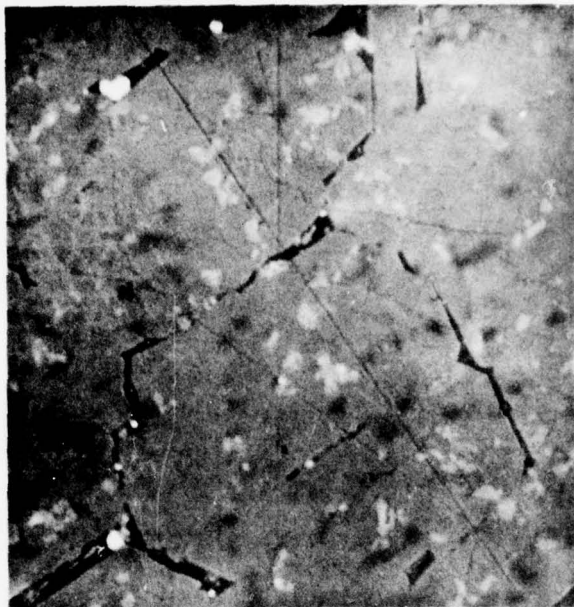
(2) KBI

(3) AEE AL106 AlN

(4) Degussa AlN

(5) Unidentified diffraction pattern. See Table 7.

a.) $\text{Si}_{10}\text{Al}_{15}\text{O}_{32}\text{N}_4$



b.) $\text{Si}_3\text{Al}_6\text{O}_{12}\text{N}_2$

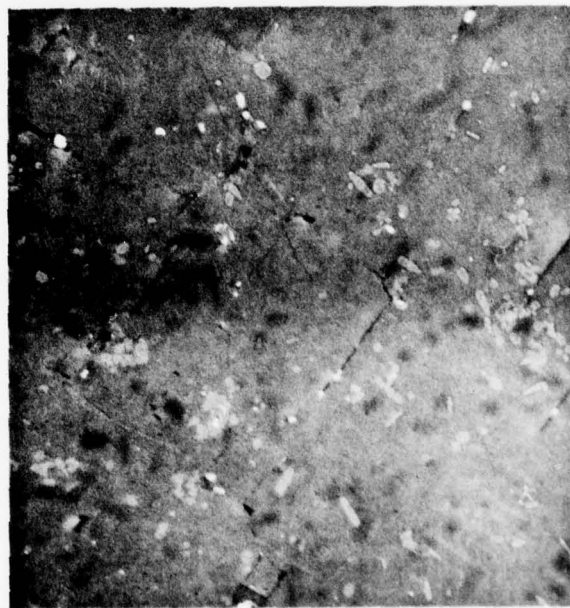
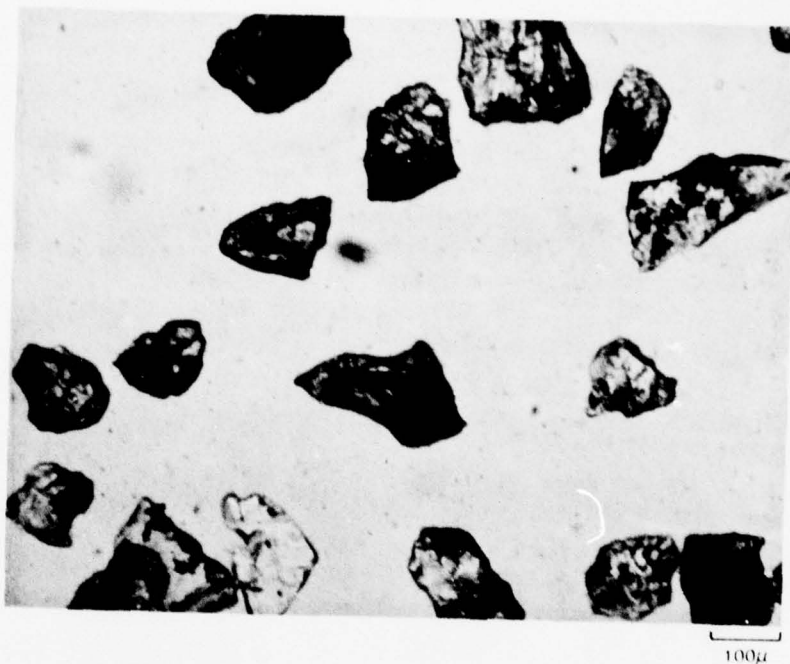


Fig. 14 Etched Sections of Crystallized Melts of Proposed X Phase Compositions

78-05-73-2

a.) -100 + 200 MESH



b.) -325 MESH

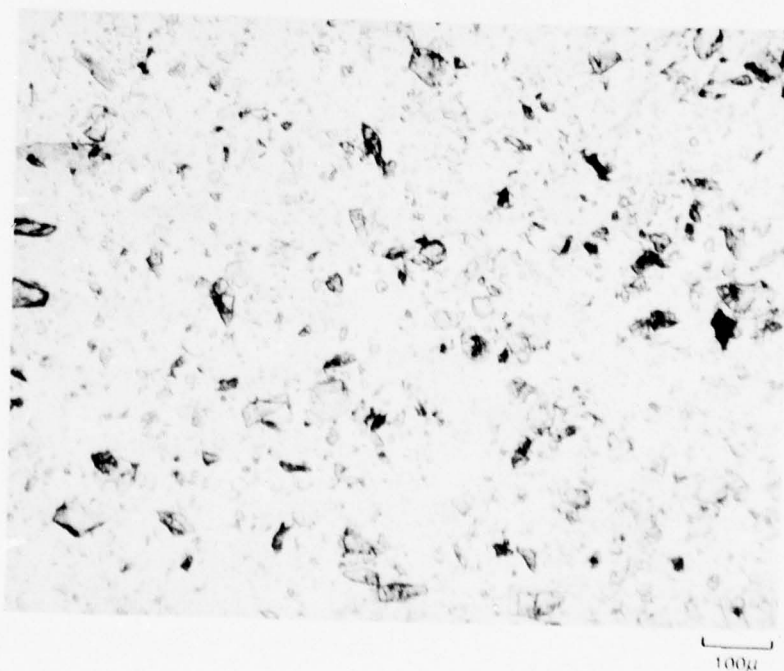


Fig. 15 Different size fractions of crushed and screened X phase, $\text{Si}_3\text{Al}_6\text{O}_{12}\text{N}_2$
(Transmission micrographs, 1.720 index oil)

78-05-73-6

b. β' and 15R Phases

The 15R phase composition batched from Si_3N_4 , Al_2O_3 and AlN (batches 9.1 and 9.2 of Table 6), even after the second heat treatment, did not exhibit the standard diffraction pattern we had previously reported for the composition $\text{SiAl}_4\text{O}_2\text{N}_4$ (Ref. 3, p. 17) although the patterns were similar. These patterns are given in Table 7. It is possible that a mistake was made in the batching of this composition. A second batch was prepared from SiO_2 and AlN which yielded material which exhibited the standard diffraction pattern (plus a trace of β') after the second firing. The β' composition (composition 10, Table 6) was found to be β' plus a trace of Si_3N_4 after the second firing.

3. Sample Fabrication

Steps in the fabrication of process 1 samples are shown in the flow sheet, Fig. 16, and process details and batch numbers are presented in Table 8. SEM micrographs of the finely milled constituent powders (mixture of β' and 15R phase) are shown in Fig. 17. The formulation for the ternary mixture of β' , 15R, and X phase is given in Table 9. Cylindrical pellets were uniaxially pressed from the different composition 17 batches, then isostatically repressed at 40 ksi, and fired in BN crucibles without powder fill (configuration 1, see section IIb11) on a schedule consisting of an approximately linear ramp requiring 1 hour to reach maximum temperature, followed by a 1 hr soak at temperature.

4. Sample Evaluation

Firing temperature, weight loss, and density data are recorded in Table 10. Two pellets were placed in the crucibles for each firing, and the first listed of each pair was uppermost in the crucible. Note that the weight losses increased with firing temperature, and that the uppermost of the two samples in each firing exhibited the larger weight loss and apparent porosity. In the firings, care was taken to position the crucibles in the flat portion of the thermal gradient of the furnace, so that the variations in weight loss and density are not likely to be the result of a thermal gradient. Although the crucibles were covered, they were not gas tight, and vapors generated by the samples escaped at the top. Thus a gradient in the partial pressures of vapor species over the samples existed, and this in all probability accounts for the variable weight loss and density of samples occupying different positions of the crucibles.

TABLE 7

DIFFRACTION PATTERNS OF 15R AND UNIDENTIFIED (U_1) PHASES

15R Phase		U_1 Phase	
$d(\text{\AA})$	I/I0	$d(\text{\AA})$	I/I0
2.786	70	2.79	16
		2.73	70
2.597	100	2.69	32
		2.61	100
2.493	30	2.55	25
		2.49	20
2.390	50	2.45	35
		2.36	70
2.331	15		
2.215	12	2.21	20
2.149	12		
		2.05	8
1.992	4		
1.967	12	1.97	8
		1.89	16
1.847	25	1.84	6
		1.82	40
1.792	20		
1.679	7	1.68	4
1.536	10	1.55	14
1.507	60	1.52	70
1.491	12	1.50	16
1.409	4	1.41	10
1.369	17	1.39	11
1.325	25	1.33	35

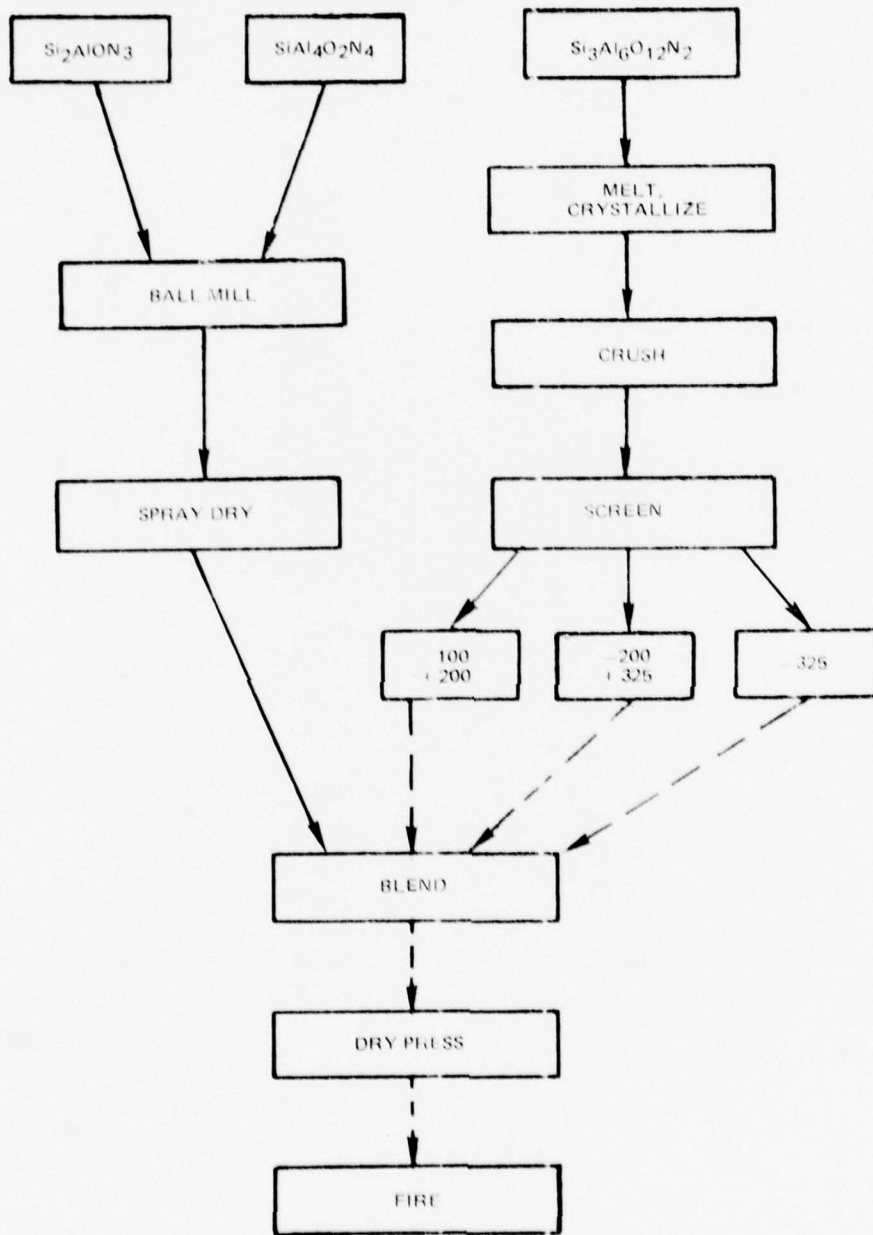


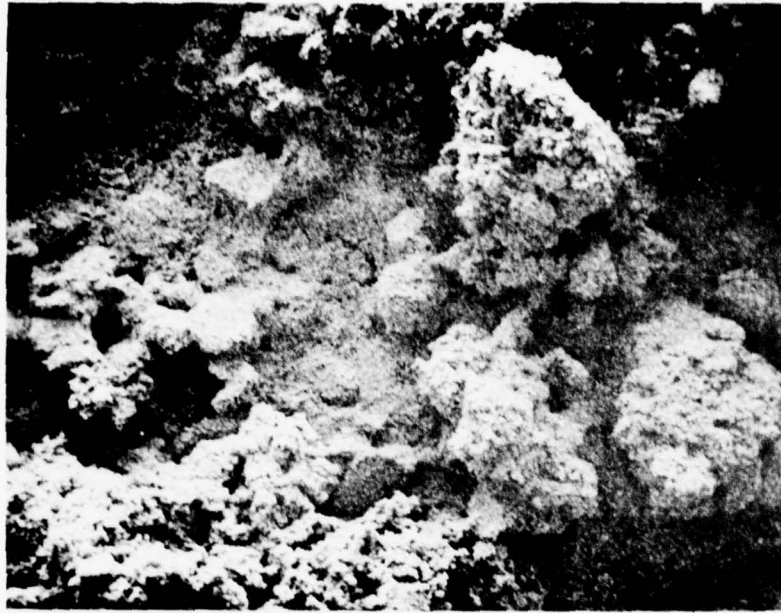
Fig. 16 Flow Sheet for Process 1

TABLE 8

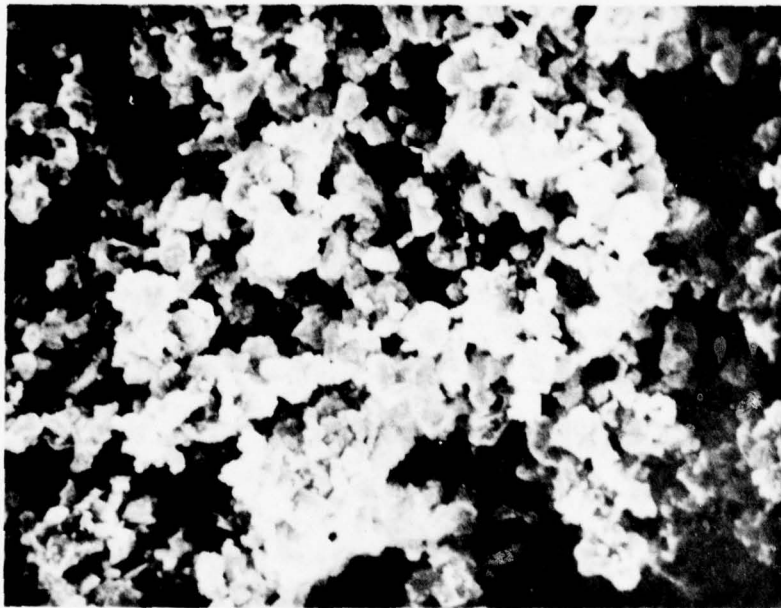
BATCH DATA OF PROCESS 1 SAMPLES

Sample Number	Phase	Batch Constituents Batch Number	w/o	Processing
12.2	X	12.1	100	Melted, crystallized
12.3	X	12.2	100	- 100 + 200 mesh fraction (Fig. 15A)
12.4	X	12.2	100	- 325 mesh fraction (Fig. 15B)
16	{ β' 15R	10.2 9.4	71.60 28.40	blended, ball milled *4 hrs, then spray dried
16A	{ β' 15R	16	71.60 28.40	ball milled 30 hrs, then spray dried. (Fig. 17)
17	{ X 15R β'	12.3 16	21.76 78.24	tumbled dry in twin shell blender
17A	{ X 15R β	12.3 16A	21.76 78.24	tumbled dry in twin shell blender
17B	X 15R β	12.4 16A	21.76 78.24	blended in acetone slurry till stiff

*Al₂O₃ Media



200μ



50μ

Fig. 17 Morphology of Batch 16A Powder (28.4 w/o $\text{SiAl}_4\text{O}_2\text{N}_4$ + 71.6 w/o Si_2AlON_3)
After Spray Drying and Screening

78-05-73-1

TABLE 9
FORMULATION OF β' COMPOSITION 17
($\text{Si}_3\text{Al}_3\text{O}_3\text{N}_5$)

<u>Phase</u>	<u>Stoichiometric Weight (g)</u>	<u>w/o</u>
$12\text{Si}_2\text{AlON}_3$	1694.28	56.02
$3\text{SiAl}_4\text{O}_2\text{N}_4$	672.15	22.22
$1\text{Si}_3\text{Al}_6\text{O}_{12}\text{N}_2$	658.17	21.76
<hr/>	<hr/>	<hr/>
= (10 $\text{Si}_3\text{Al}_3\text{O}_3\text{N}_5$)	(3024.60)	(100.00)

TABLE 10
FIRING CONDITIONS, WEIGHTLOSS AND DENSITY DATA
FOR PROCESS 1 SAMPLES

<u>Sample Number</u>	<u>Config- uration</u>	<u>Firing Conditions</u>		<u>Firing Weight Loss (%)</u>	<u>Density Data</u>		
		<u>Temp (°C)</u>	<u>Time (hrs.)</u>		<u>Apparent Porosity (%)</u>	<u>Specific Gravity (g/cc)</u>	<u>Bolk Density (g/cc)</u>
17.1	1	1750	1	5	35	3.07	2.00
17.2				4			
17A.1	1	1750	1	5	26.6	2.92	2.14
17A.2				4	23.3	2.89	2.22
17A.3	1	1775	1	11	34.7	2.91	1.90
17A.4				9	33.5	2.98	1.98
17B.1	1	1790	1	29	52.9	3.23	1.52
17B.1				13	37.1	3.10	1.95

(1) See section II.B.1.1

Micrographs of the top (more porous) and bottom sections of sample 17A.3 are shown in fig. 18. These are typical of the appearance of all the Table 10 samples. If one compares the appearance of the large voids in the body with the appearance of the -100+200 mesh X-phase constituent shown in Fig. 15, it is clear that when the X-phase particles melted, liquid penetrated the surrounding matrix of fine grained 15R and β' particles, leaving behind voids having the shapes of the original particles. Since the 15R and β' particles were already bridged into a reasonably rigid structure prior to the melting of X-phase, no gross shrinkage of the body occurred.

The non-shrinking characteristic of these bodies which therefore retain a high interconnected porosity, aggravates the vaporization of molten X-phase. However, even where loss of X-phase liquid was low, as in Fig. 18B, no substantial shrinkage occurred, and the voids appear to be near perfect replicas of the original X-phase particles. It thus does not appear feasible to develop this concept into a successful pressureless sintering process for dense single phase β' bodies. It is quite possible that dense single phase bodies could be produced from such a system using pressure sintering technique (uniaxial or isostatic hot pressing).

c. Process 2, Bodies

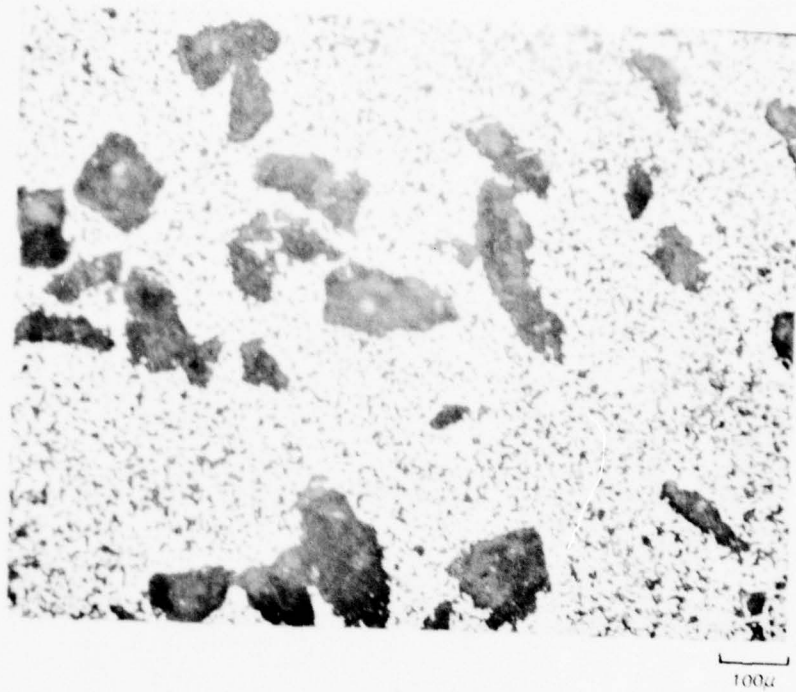
Compositions involved in process 2 formulations are plotted on the 1650C isothermal section of the $\text{Si}_3\text{N}_4 - \text{AlN} - \text{Al}_2\text{O}_3 - \text{SiO}_2$ system in Fig. 19, and are expressed in terms of equivalent percent aluminum and oxygen and in mole % of the constituents in Table 11. In terms of Process 2, compositions which fall

TABLE 11

PROCESS 2 COMPOSITIONS

Composition Numbers	Equivalent Percent		Mole Percent		
	Al	O	Si_3N_4	Al_2O_3	AlN
27	20	20	66.67	33.33	0
28	29.4	17.7	46.15	23.08	30.77
30	10	10	81.22	18.18	0
31	39.50	30.25	38.30	38.30	23.40
32	44.62	27.69	31.03	31.03	37.94
33	42.86	28.57	33.33	33.33	33.33
34	15	15	89.47	10.53	0
35	33.33	33.33	50	50	0

a.) AREA 1 (NEAR TOP OF CRUCIBLE 1)



b.) AREA 2 (NEAR BOTTOM OF CRUCIBLE)

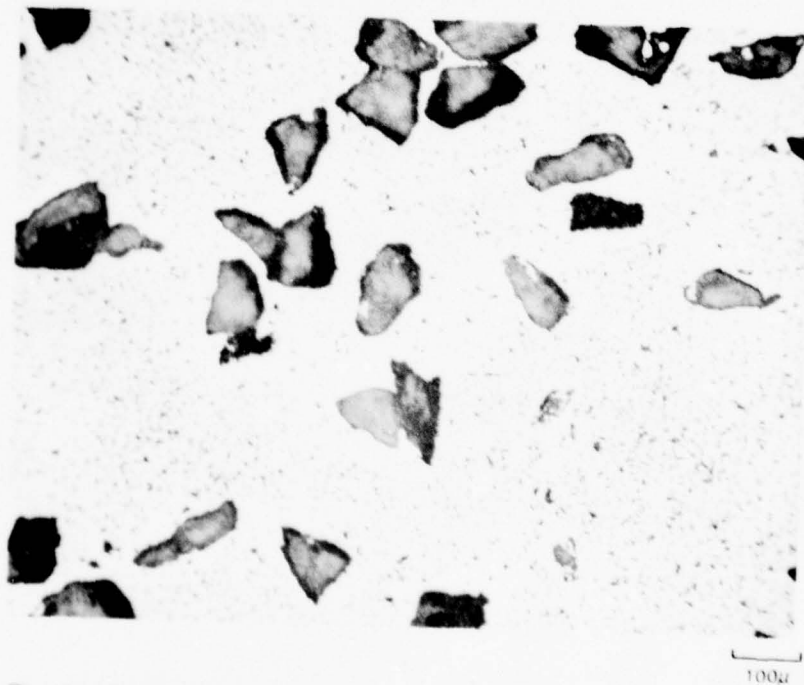


Fig. 18 Polished Section of Sample 17A-3 (21.7 w/o -100 +200 Mesh $S_3Al_6O_{12}N_2$ + 78.3 w/o Batch 16A)

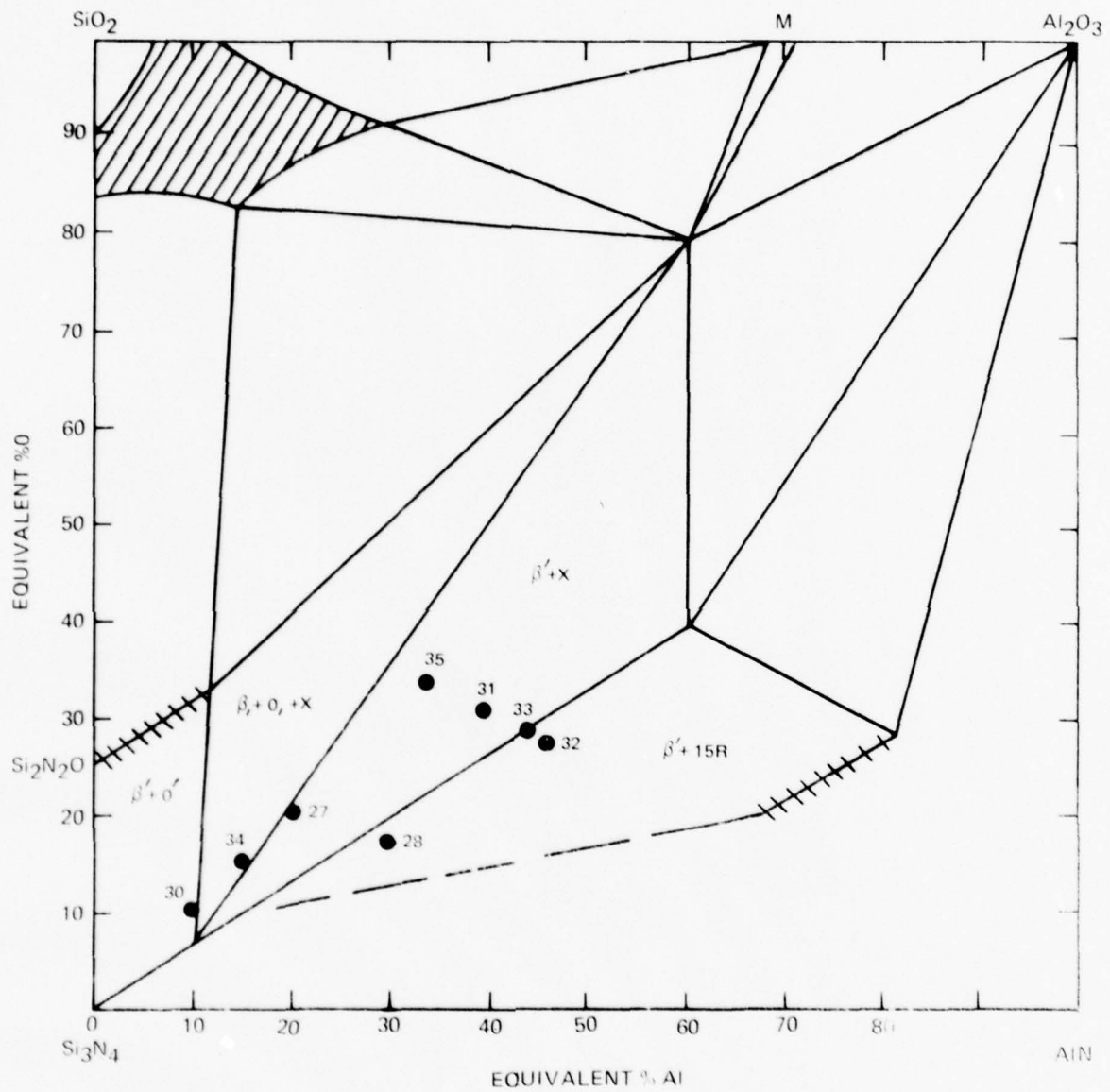


Fig. 19 Compositions Involved in Various Process 2 Formulation

TABLE 12
MASTER BATCH FORMULATIONS

Batch Number	Constituents (grams)			Milling* Technique	
	Si ₃ N ₄				
	Al ₂ O ₃	AIN			
	KBI	Sn-402	Ward		
27.1	36.67		13.33	0	1
27.3	64.18		20.68**	0	2
27.4		36.67	13.33	0	1
28.1	32.09		11.66	6.25	1
30.5			86.1	13.9	3
31.1	48.00		34.87	8.57	1
34.1	92.12		5.23	0	2
35.1		17.37	12.63	0	1
35.2	49.53		36.00	0	1

- *1) 16 hours, Si₃N₄ media
- 2) 90 hours, alumina media
- 3) 3 hours, alumini media

**It was anticipated that 2.64 grams of Al₂O₃ would be contributed by media wear.

in the β' -X field (i.e., 27, 31 and 35) served as master batches supplying the fine grained Si_3N_4 and Al_2O_3 constituents. Formulation and processing date of these and other master batches are given in Table 12. Processing and properties of blended-batch bodies with compositions falling in different phase fields will be discussed separately.

1) β' - 15R Compositions

With the exception of Sample 28.1.1 which was prepared from fine grained powder (master batch 28.1), bodies with compositions in the β' - 15R field were prepared following the flow sheet, Fig. 20. The formulations and batch blending methods (see section IIB1i) are presented in Table 13. Both as-screened and

TABLE 13
FORMULATION AND PROCESSING
OF β' -15R BLENDED BATCHES

Batch Number	Master Batch		Constituents			Carbowax	Blending Technique
	Number	Weight	-100+200	AlN -200+325	-325		
28.3	27.1	2.188	0.312				2
28.4	27.1	2.188		0.312			2
28.5	27.1	2.188			0.312		2
28.6	27.3	2.188			0.312		2
28.7	27.1	43.76			6.24*	1	3
28.8	27.1	28.88		4.13*			3
32.2	31.1	32.0		3.0*			3
32.3	31.1	32.0			3.0*		

*Settled

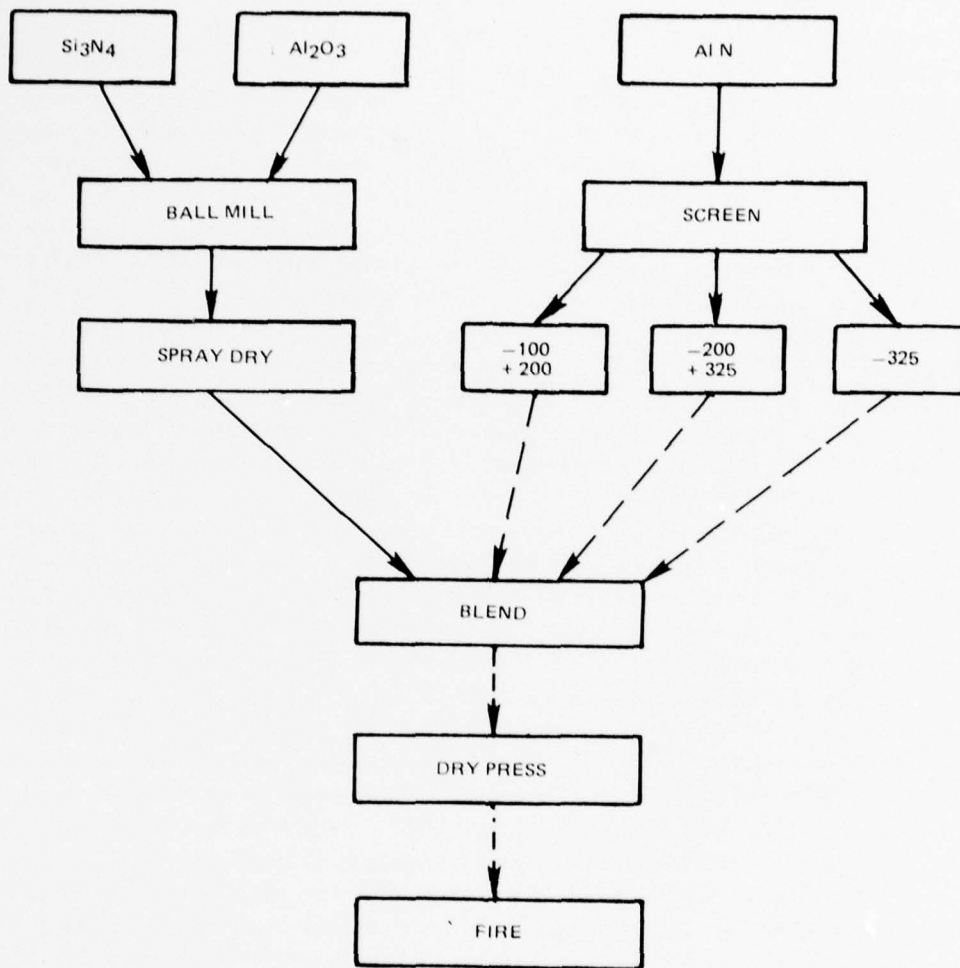


Fig. 20 Flow Sheet for Process 2, β -15 R Field

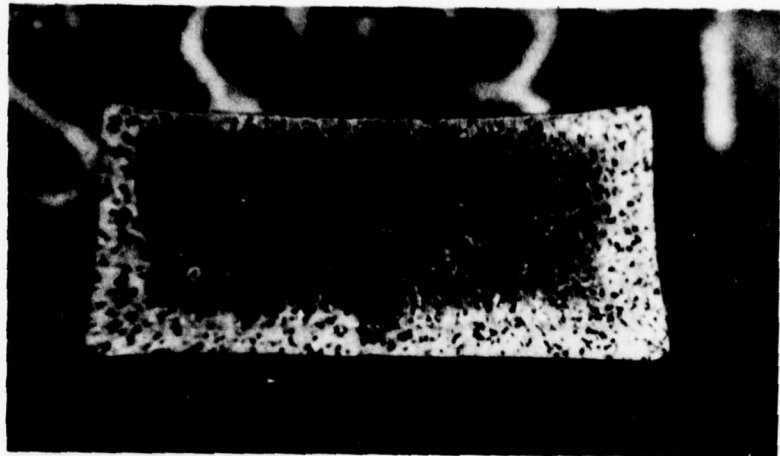
settled AlN fractions were employed. Sample fabrication and test data are presented in Table 14. The density data appear to be quite variable, but some general trends are apparent. All of the fired samples of composition 28 prepared from particle size blends sintered to substantially higher density than did the control sample (28.1.1) prepared from the fine grained master batch. (The microstructure of 28.1.1 was shown as Fig. 5). The initial grouping of comparatively thick cylindrical samples (28.3.1, 28.4.1 and 28.5.1) prepared using non-settled fractions of AlN, slurry blending, and high isostatic pressure were substantially more dense than the subsequent bar samples. The most probable reason for this variability in density has to do with the sample geometry as will be seen shortly. The density data for the bar shaped samples suggests that packing the samples in powder of the same composition for firing tends to increase porosity of fired sample rather than decrease it as was at first supposed would be the case. (Compare data for samples 28.7.1 and 28.7.2, and .3 and .4. On the other hand, packing samples in powder having the composition of the fine grained constituents results in a substantial increase in density compared to samples fired without powder packs. (Compare data for samples 32.1.1 and .2 with that for samples 32.2.3 and .4). These effects are probably the result of diffusion of liquid formed by the reaction of the fine grained Si_3N_4 and Al_2O_3 constituents, 1) out of the sample and into the powder pack (and thence to the atmosphere) in the former case and, 2) into the samples from the powder pack in the latter case. The microstructure of sample 28.3.1 is shown in Fig. 21. Note that the (diametrically sectioned) pellet shrank more on one face than the other, and that a less dense (depletion) zone of varying thickness is found near surfaces of the pellet. It may be assumed that details of placement of samples in the crucible created a differential loss of X phase so that shrinkage was favored at the upper surface as pictured. The height of the fired cylinders is about 0.25". Note that the less dense region near the lower surface extends into the cylinder about .06". The thickness of the fired bar samples was about 0.125" so that given symmetrical depletion, virtually the entire sample becomes depleted, accounting for the low density of these samples. Micrographs of samples 28.7.1 and 28.8.1 are shown in Fig. 24. Note the resemblance of these microstructures to that of the depletion zone in Fig. 21B.

The remnants of the original AlN particles are easily discerned in Fig. 21B, but one must use imagination to distinguish the remnants in the interior region in Fig. 21C. Higher magnification micrographs of these remnants are shown in Fig. 23 where it can be seen that no clear interface exists which defines the original particles, there being only a gradient of porosity and reflectivity. EDAX silicon and aluminum maps taken in the neighborhood of a large particle remnant in the exterior region of sample 28.3.1 are shown in Fig. 23 and indicate that the composition is essentially uniform over the area (save for the voids). Similar observations were made in the interior of sample 28.3.1 and from samples 28.4.1 and 28.5.1. One can conclude that samples of the subject formulations approach a uniform composition (if not microstructure) under the given firing

TABLE 14

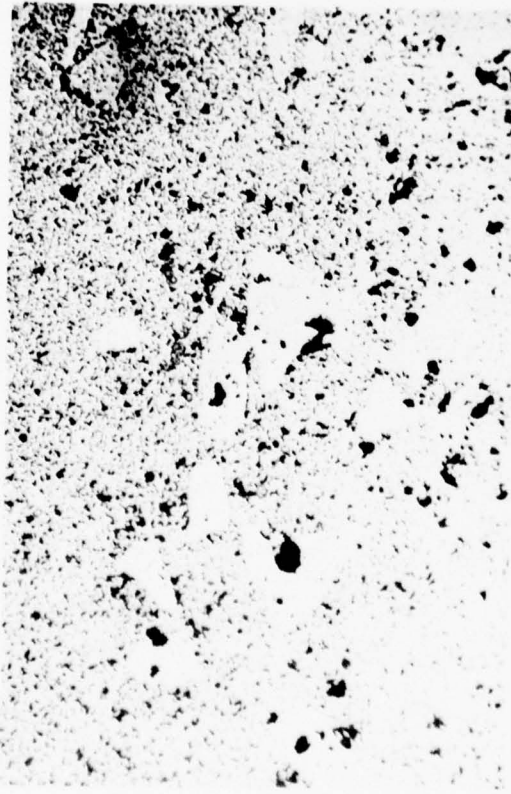
FABRICATION AND TEST DATA
FOR β' -15R PHASE, PROCESS 2 SAMPLES

Sample Number	Pressing Conditions			Firing Conditions			Test Results			
	Sample Shape	Isostatic Pressure (ksi)	Configuration	Pack Powder (Batch#)	Temp. ($^{\circ}$ C)	Time (hrs.)	Apparent Porosity (%)	Bulk Density (g/cc)	Specific Gravity (g/cc)	XRD
28.1.1	Cylinder	60	2	28.1	1760	2	44.8	1.74	3.17	
28.3.1							8.0	2.85	3.10	
28.4.1							4.0	2.94	3.06	
28.5.1							5.4	2.92	3.08	
28.6.1	Cylinder	40	2	28.1	1760	2	8.0	2.74	3.00	s β' -w15R+w4.5A
28.6.2							6.8	2.75	2.95	
28.7.1	Bar	30	2	28.1	(1760 1700)	2 7	34.2	2.08	3.18	
28.7.2							33.6	2.05	3.00	
28.8.1	Bar	30	2	28.1	1760	2	41.1	1.85	3.14	
28.8.2	Bar	30	1		1780	1	29.4	2.24	3.17	
28.8.3							29.7	2.27	3.23	
28.8.4							29.3	2.22	3.14	
32.2.1	Bar	30	1		1780	2	23.3	2.42	3.16	
32.2.2							20.4	2.66	3.03	
32.2.3	Bar	30	2	31.1	1780	2	10.4	2.66	2.96	
32.2.4							8.1	2.68	2.92	
32.3.1	Bar	30	1		1780	2	19.3	2.36	2.92	
32.3.2							24.4	2.29	3.04	
32.3.3							29.8	2.59	3.04	
32.3.4							21.9	2.07	2.65	



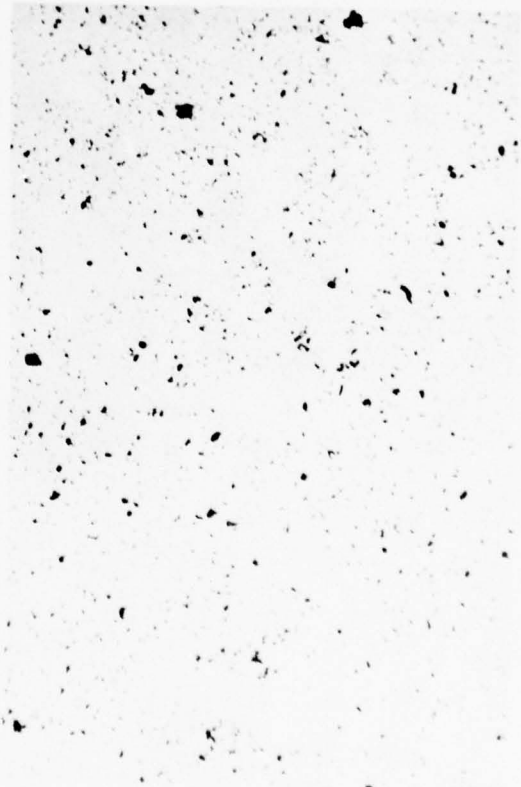
a.) OVERALL

1430 μ



b.) EXTERIOR REGION

100 μ

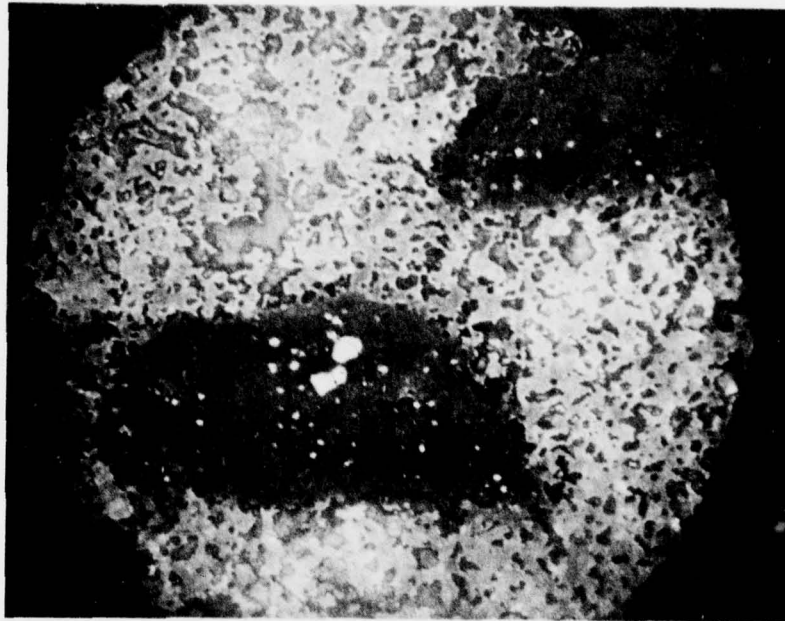


c.) INTERIOR REGION

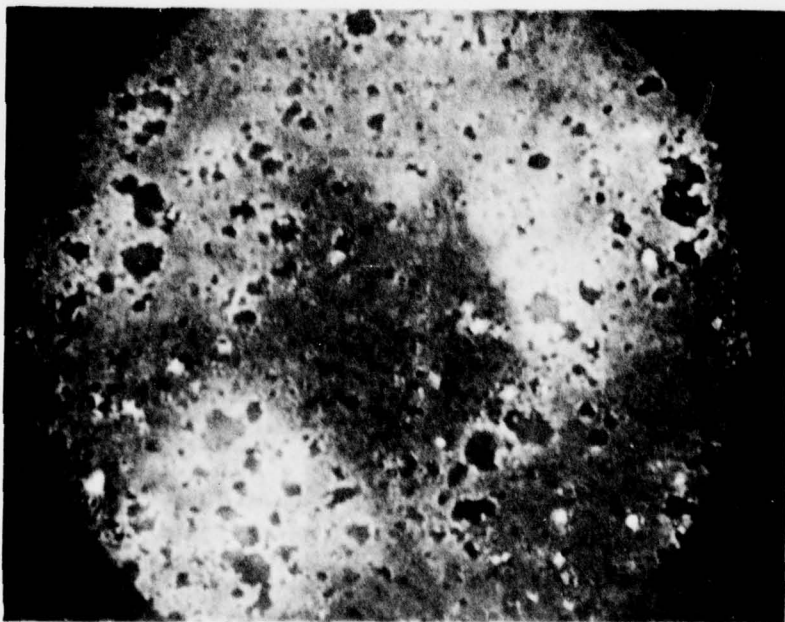
100 μ

Fig 21 Microstructure of Sample 28-3-1

78-08-77-5



a.) EXTERIOR

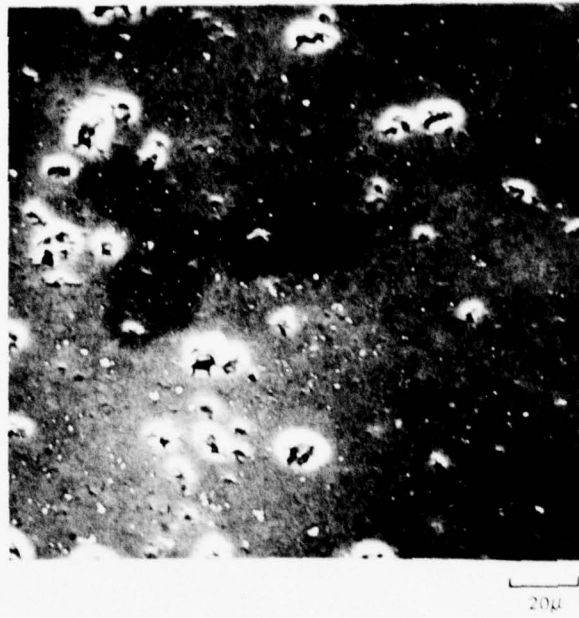


b.) INTERIOR

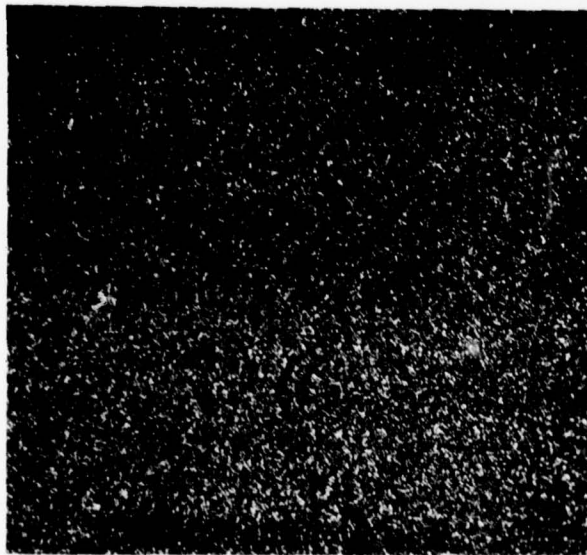
20 μ

Fig. 22 Particles in Exterior and Interior Regions of Samples 28.3.1

a) SEM



b) ALUMINUM MAP



c) SILICON MAP

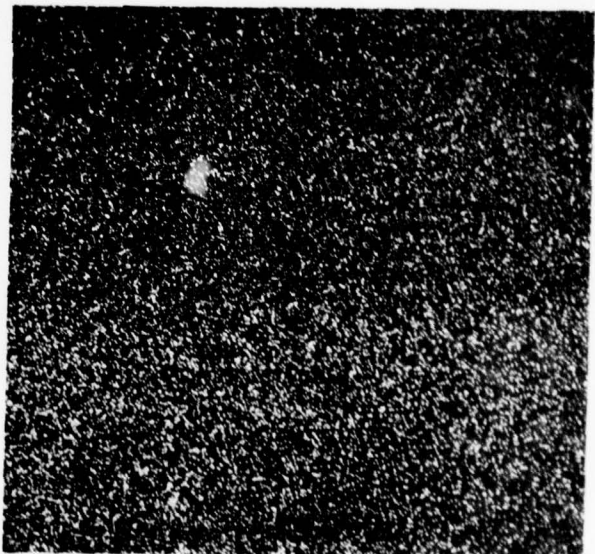
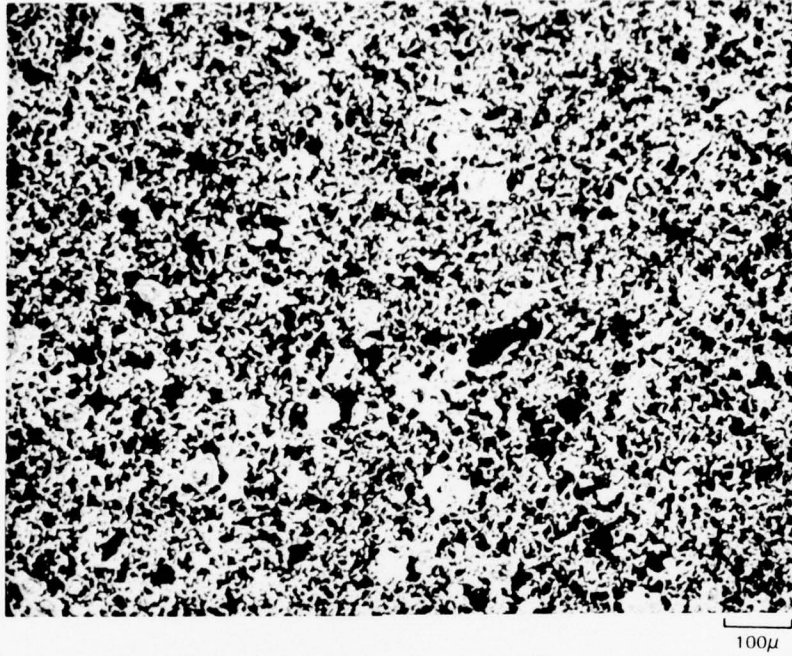


Fig. 23 SEM Element Maps in Vicinity of Large Particles in Exterior Region of Sample 28.3.1

A. SAMPLE 28.7.1



B. SAMPLE 28.8.1

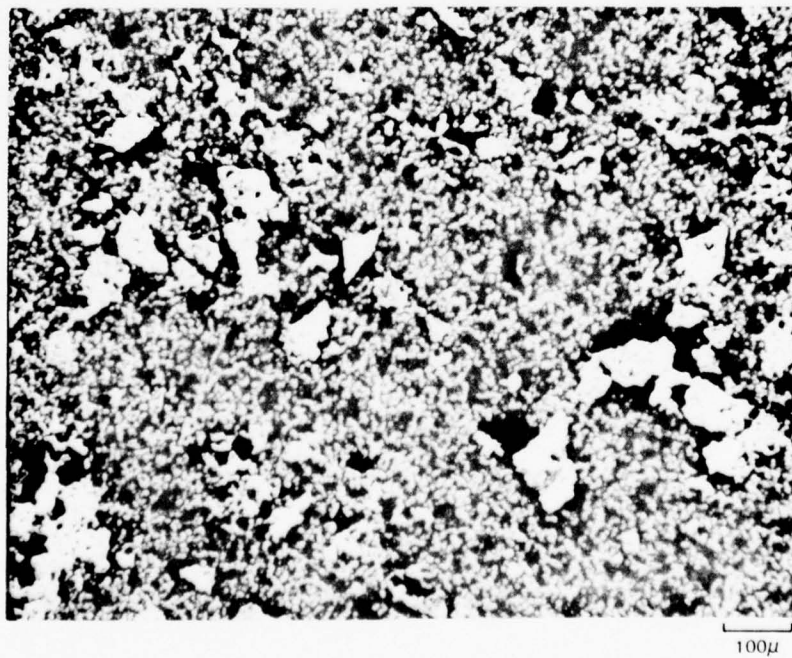


Fig. 24 Polished Sections of (β' - 15R) Samples 28.7.1 and 28.8.1

conditions. As will be seen shortly, this is not always the case with process 2 samples. One of the fired samples (28.6.1) was crushed, ground to -200 mesh and subjected to XRD. The diffraction pattern showed a strong pattern for β' , a weak pattern for the 15R phase, plus an unidentified weak peak at 4.5 Å.

The unmounted halves of samples 28.3.1, 4.1 and 5.1 were packed in powder of composition 27.1 and heat treated for 10 hrs at 1720°C. It was found that the result of the additional heat treatment was to increase further the density of the samples, as can be seen by comparing the microstructures of heat treated sample 28.3.1, Fig. 25, with the original untreated half shown in Fig. 21. EDAX of the sample again showed a homogeneous distribution of aluminum and silicon. XRD from the polished surface following heat treatment showed a pattern for β' only. The mechanism for densification of the pellet packed in composition 27.1 powder has not been established, but in all probability involved the surface diffusion of X phase constituents from the powder pack into the sample, thereby altering the overall sample composition.

The powder pack experiment was repeated with sample 28.6.2 (same nominal composition as 28.3.1, except for the impurities introduced by ball milling) using composition 28.1 powder pack. The microstructures of samples 28.6.2 before and after heat treatment are compared in Fig. 26. It can be seen that again a densification has occurred, though not to the same degree as with sample 28.3.1.

2) β' Compositions

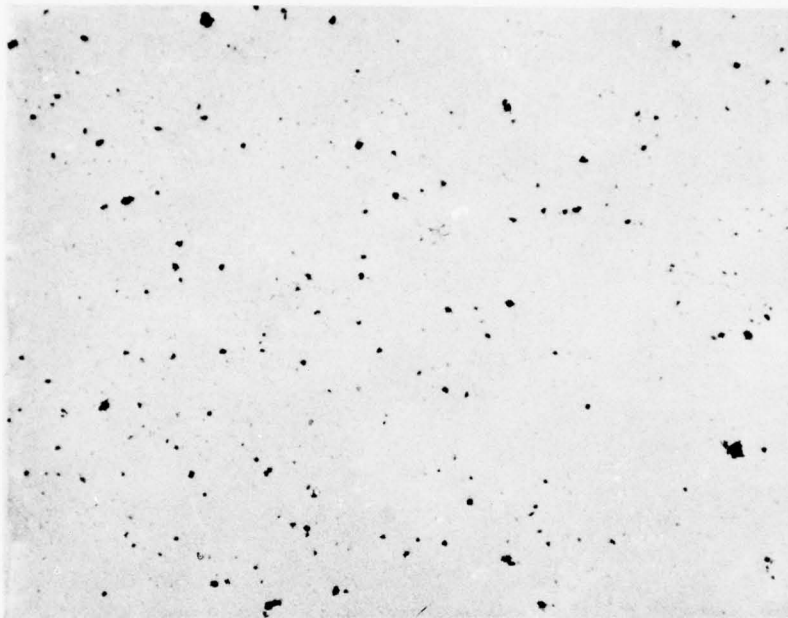
Since the fired process 2 bodies of β' -15R compositions were excessively porous unless fired or heat treated in a β' -X phase powder pack which altered the sample stoichiometry, attention was redirected to single phase β' compositions. These were formulated using the master batches described in Table 12 and different AlN fractions, as described in Table 15. Sample preparation and test data are presented in Table 16.

TABLE 15

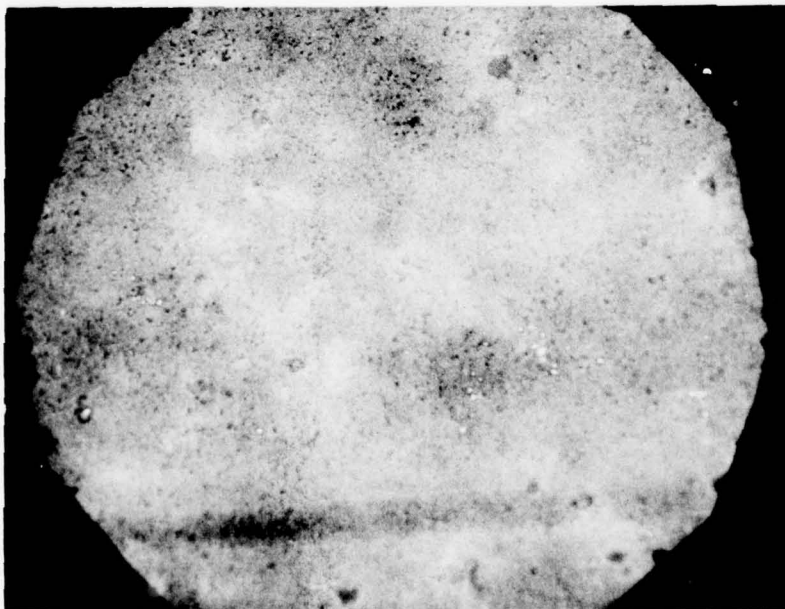
FORMULATION AND PROCESSING OF β' BLENDED BATCHES

Batch Number	Masterbatch		Constituents (grams)			Blending Technique
	Number	Weight	Unscreen	AlN -200+325	-325	
33.1	35.1	5.0		0.85		1
33.2	31.1	33.03	2.03			3
33.3	31.1	33.03			2.03*	3
33.4	35.2	85.53			14.47	Mill 1 hour Si ₃ N ₄ media

*Settled



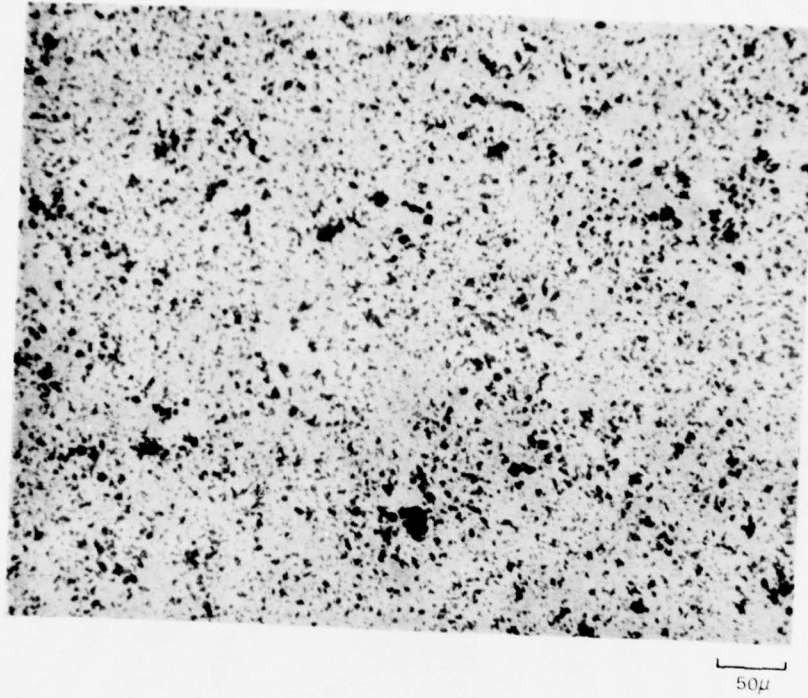
100 μ



20 μ

Fig. 25 Microstructure of Sample 28.3.1 After 10 Hr. Heat Treatment at 1720°C

a) FIRED TO 1760°C FOR 2 HRS



b) FURTHER HEATED FOR 10 HRS AT 1720°C

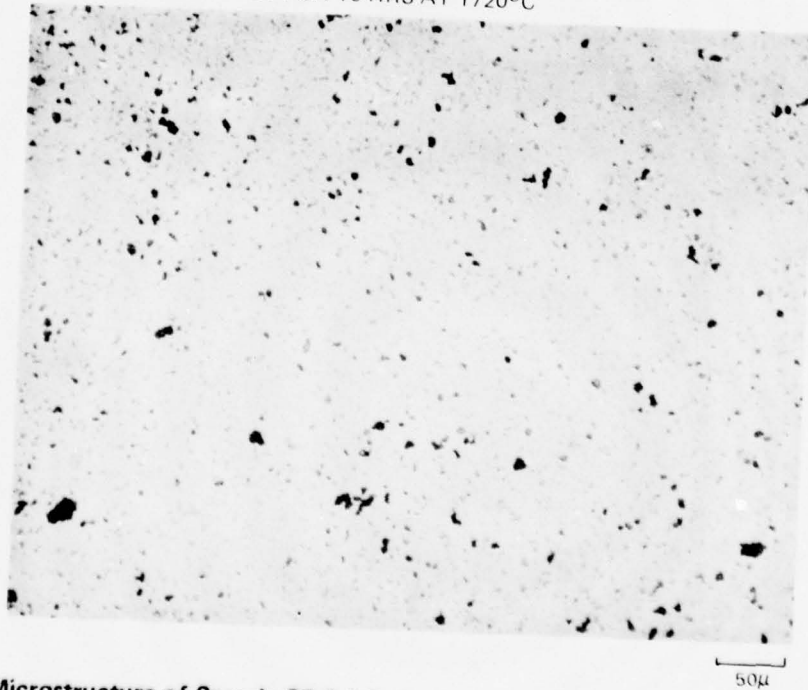


Fig. 26 Microstructure of Sample 28.6.1 Before and After 10 Hr Heating at 1720°C

TABLE 16

FABRICATION AND TEST DATA FOR PROCESS 2 B' COMPOSITIONS

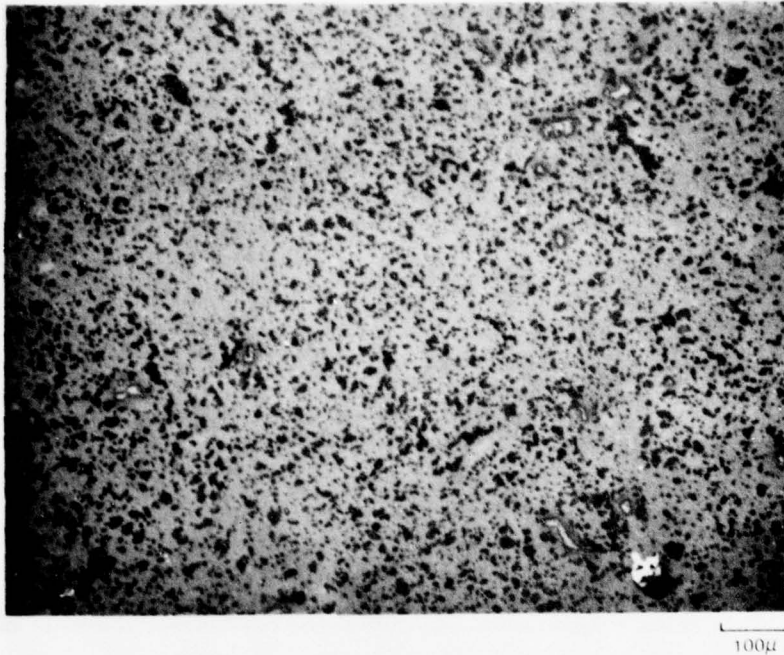
Sample Number	Pressing Conditions			Firing Conditions				Tests Results							
	Sample Shape	Isostatic Pressure(ksi)	Config-uration	Pack Powder	Temp (°C)	Time (Hrs)	Weight Loss (%)	Shrinkage (%)	Apparent Porosity (%)	Bulk Density (g/cc)	Specific Gravity (g/cc)	Test Temp (°C)	MPa	Ksi	Other Tests
33.1.1 } 33.1.2 }	cylinder "	40	1		1750	1	6 7		6.3 10.7	2.73 2.64	2.91 2.96				
33.1.3 } 33.1.4 }	" "	40	1		1780	1	12 15		20.5 26.6	2.41 2.26	3.03 3.03				
33.2.1 } 33.2.2 }	bar	30	1		1780	2	3.2	12	10.0 9.5	2.66 2.68	2.98 2.97				
33.2.3 } 33.2.4 }	"	30	2	31.1	1780	2			1.6 0.2	2.88 2.92	2.98 2.93	25 25	120 125	17 18	
33.3.1 } 33.3.2 } 33.3.3 } 33.3.4 }	bar	30	1		1780	1	2.3	13.3	8.3 8.4 5.1 3.7	2.67 2.66 2.78 2.79	2.92 2.90 2.90 2.90	25 25 25 25	105 85	15 12	
33.3.5 } 33.3.6 } 33.3.7 }	bar	30	3		1780	4	5.5		17.8	2.44	2.96	25	125	18	1370°C oxidation XRD, E'
33.4.1 } 33.4.2 }	bar	30	2	33.3	1710	1	0.5	5.4	17.3 12.2	2.44 2.55	2.96 2.91	25 25	90 120	13 17	

Many of the same observations that were made regarding the process $2\beta'$ -15R samples also apply to the β' samples. However, as anticipated, in general the latter samples were more dense. For example, test bars of 33.3 composition fired to 1780°C for 1 hr had an average bulk density of 2.73 g/cc compared to that of the closely adjacent β' -15R composition 32.2 bars fired under the same condition which had an average density of 2.44 g/cc. Again, firing of test bars in a powder pack of the master batch 31.1 resulted in enhanced densification, as seen from Table 16 and Fig. 27, which compares the microstructure of samples 33.2.1 and 33.2.3.

Note also in Fig. 27, that both samples contained a few remnants of some of the larger original AlN particles. Similar remnants were observed in 33.1 samples, as shown in Fig. 28. This shows many particles in the size range around 25 to 100 μ that are separated from the surrounding material by reaction zones. Two such particles are flagged with arrows in the upper micrograph of Fig. 28, and pictured at higher magnification below. The polished section was examined with SEM and EDAX, and silicon and aluminum distribution maps obtained. These are shown in Fig. 29. It can be seen that, as nearly as can be judged from the element maps, the reaction zones have an Al/Si ratio characteristic of the reacted body, whereas the material inside the reaction zone is devoid of Si, high in Al, and in all probability is unreacted AlN. Note that the chief differences between samples 33.1.1 and 33.2.1 were the particle size fractions of AlN, and the firing schedules. Both factors would favor a faster reaction of AlN in the case of 33.2.1. These trends are verified in examining the microstructure of samples 33.3.7 and 33.4.1 shown in Fig. 30. Sample 33.3.7, which used settled -326 mesh AlN and was fired to 1780°C, is virtually free of unreacted AlN, whereas in the case sample 33.4.1 which was fired to only 1710°C (below the solidus temperature), virtually all of the larger AlN particles shown thin reaction zones, with most of the AlN remaining unreacted.

Figure 30 is most instructive in terms of understanding the failure of the process $2\beta'$ and β' -15R samples to densify fully in spite of the fact that considerable liquid forms initially when samples are fired at temperatures of 1750 and above. Examination of Fig. 30B shows that considerable bridging of the coarse particles has occurred which prevents a uniform fine-grained-matrix shrinkage. Instead, a distribution of large pores associated with bridging of coarse particles is generated. If one compares the distribution of pores in samples 33.3.7 and 33.4.1, one can infer that when the solidus temperature is reached, large voids tend to spheroidize and shrink as a result of general shrinkage of the body in response to liquid surface tension forces. Simultaneously, however, the system begins to solidify as liquid is used up in reaction. The end result is the spheroidize characteristic microstructure consisting of a distribution of pores delineating an interconnected structure of higher than average density.

A. SAMPLE 33.2.1



B. SAMPLE 33.2.3

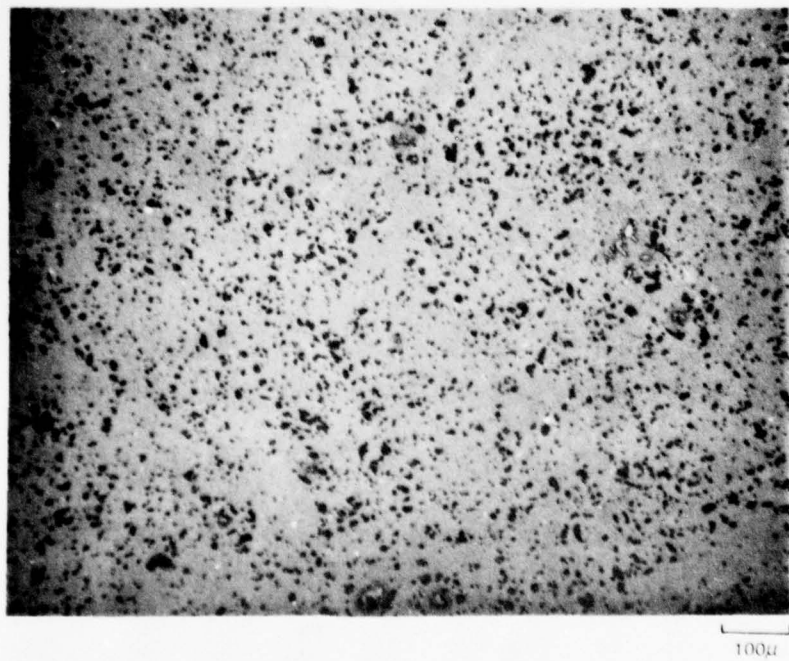
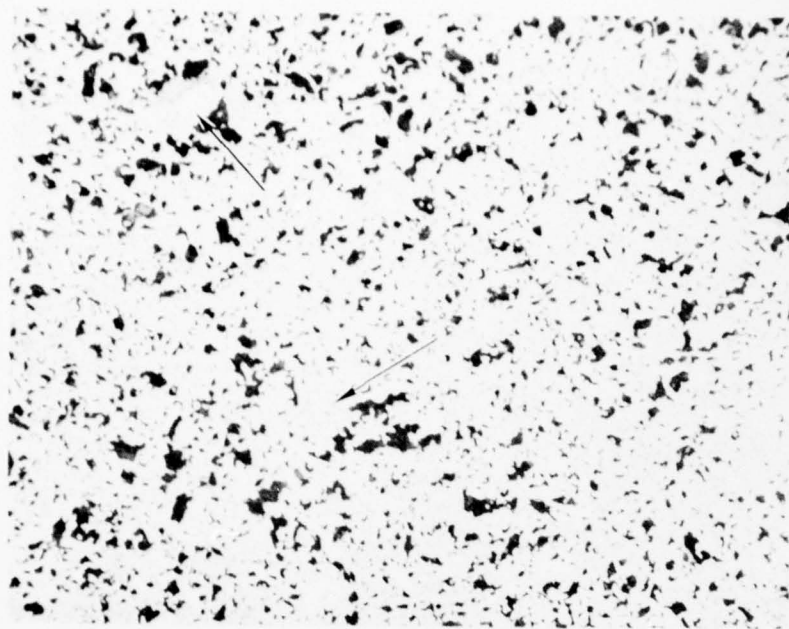


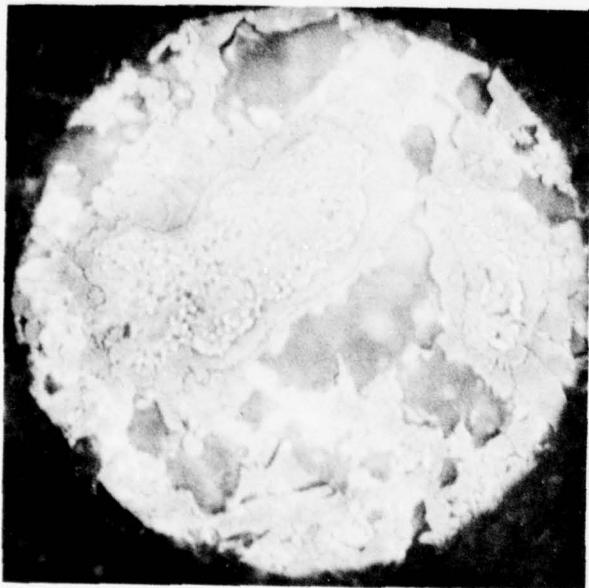
Fig. 27 Polished Sections of Process 2 Composition 33 Samples
Fired With and Without Powder Pack



100 μ

AREA A

AREA B



20 μ



20 μ

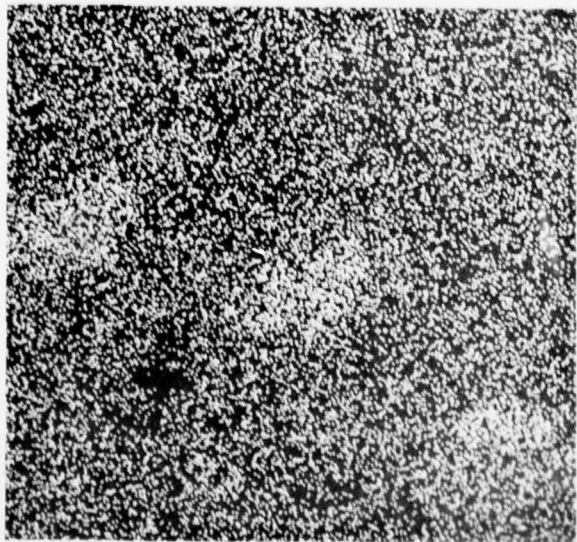
Fig. 28 Polished Section of Sample 33.1.2

78-05-73-3

a.)



b.) ALUMINUM



20μ

c.) SILICON

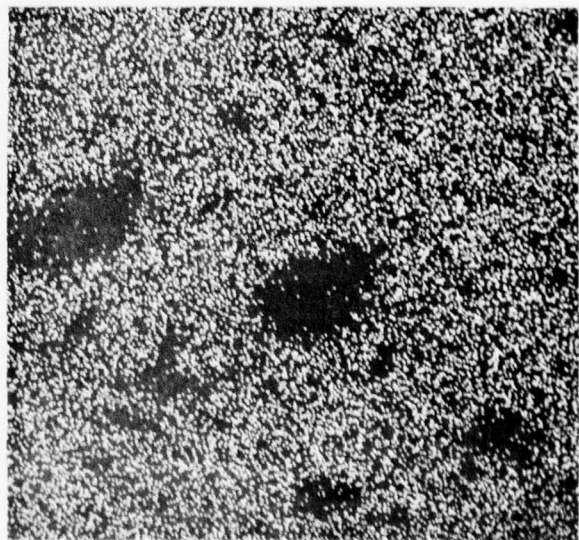
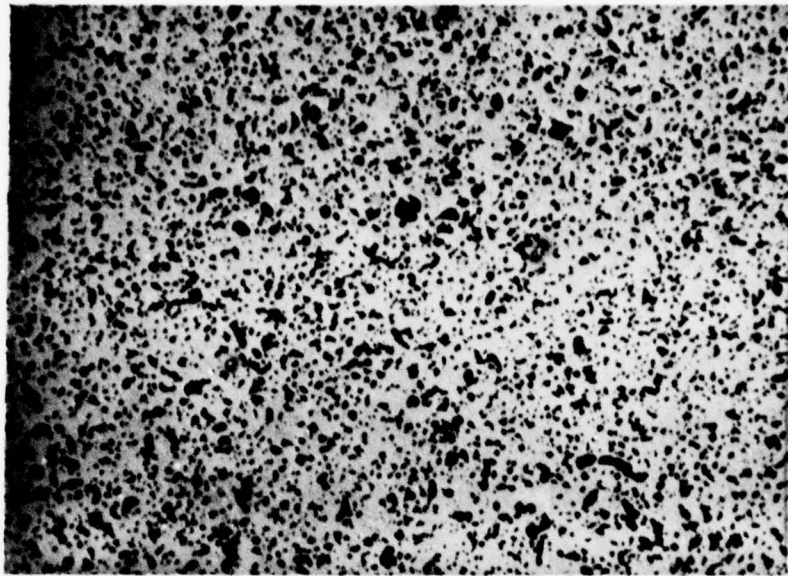


Figure 29 SEM Element Maps of Large Particles in Sample 15.2

A. SAMPLE 33.3.7



B. SAMPLE 33.4.1

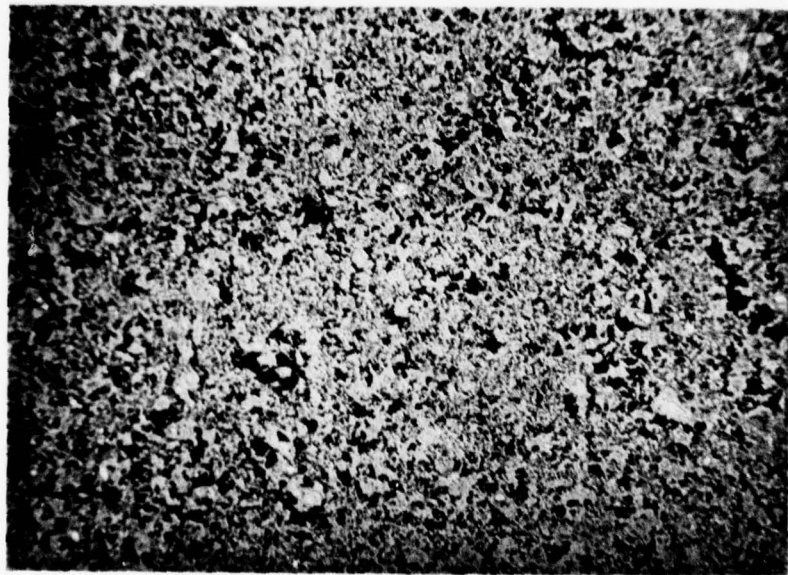


Fig. 30 Polished Sections of Stage 2 Composition 33 Samples Compounded from Different Batch Formulation

The degree to which pores have become isolated can be assessed by examining the apparent (open) porosity, bulk density, and specific gravity data. Of all the samples for which specific gravity data listed in Table 16, the only samples that exhibited an average specific gravity value equal to the X-ray density of $\text{Si}_3\text{Al}_3\text{O}_3\text{N}_5$ ($\rho_x = 3.08$) were the 33.4 compositions fired at 1710°C. Under these firing conditions all the porosity was interconnected, and the apparent porosity equaled the total porosity calculated from the ratio of bulk density to specific gravity. The remaining samples have lower specific gravities indicating that closed porosity exists. The total porosity can be calculated from ratio of the bulk density to X-ray density, and the difference between this and the apparent porosity is the closed porosity. Thus for sample 33.2.3 (Fig. 27B) the total porosity is 6.5 percent, apparent (open) porosity 1.6 percent, and closed porosity 4.9 percent. The total porosity thus calculated is in agreement with porosity measured by statistical methods from Fig. 27B.

Because a mechanism exists which tends to entrap closed porosity during process 2 fabrication, the goal of fabricating fully dense bodies by this technique appears difficult to achieve.

3) β' -O' and β' -O'-X Compositions

The various composition 30 blended batches are given in Table 17. Batches

TABLE 17
FORMULATION AND PROCESSING
 β' BLENDED BATCHES

Batch Number	Masterbatch Number Weight		Constituents (grams)			Blending Technique	
			Si_3N_4				
			-100+200	-200+325	-325		
30.1	27.1	1.305		1.195		} crushed cylinders	2
30.2	27.1	1.305	0.800		0.325		2
30.3	27.3	1.305			1.195*		2
30.4	27.1	35.0				320* Ward	3**

*Settled

** 2 w/o carbowax added

30.5 and 34.1 were master batches included in Table 12. Representative optical transmission micrographs of the settled-out fraction of Ward $\beta\text{Si}_3\text{N}_4$ powder used as a constituent in batches 30.4 and 30.5 are shown in Fig. 31. Fabrication and test data for the various composition 30 and 34 samples are presented in Table 18.

The cylindrical test specimens were cut in half diametrically. One of each of the halves were prepared for metallographic examination. The other halves were packed in batch 27.1 powder and heat treated for 10 hrs at 1720°C , then prepared for metallographic examination. Figures 32 and 33 show the microstructures of fired and heat treated samples 30.1.2 and 30.3.1 respectively. Microstructures of samples 30.4.1 and 30.5.1 are shown in Fig. 34.

Again, the main conclusion to be drawn from these test data and microstructures is that bridging of the coarse particles (which is aggravated in the case of the composition 30 samples because of the higher percentage of the coarse fraction) prevents a uniform bulk shrinkage, and leads to the entrapment of very large voids. (The coarse β' grains are visible under the microscope and in the original micrographs, but the very low contrast may render these undiscernable in the report figures). It is also apparent in the micrographs that the samples prepared using the crushed and sized grinding cylinders for the coarse Si_3N_4 fraction sintered to a much higher density than the samples prepared using the Ward Si_3N_4 . This was particularly the case with the samples prepared using master batch 27.3 as the fine fraction. This enhanced densification is undoubtedly the result of the fluxing action of the very high iron concentration in the Si_3N_4 grinding cylinders. This has led to the generation of a very high concentration of iron silicide inclusions in the sintered bodies particularly evident in Fig. 33B.

C. Process 3 Bodies

Processes 1 and 2 both led to bodies that exhibited high porosity, although the porosity appeared to be generated by different mechanisms in the two cases. Process 2 studies, however, did indicate that bodies containing very disparate particle sizes of constituents could be made chemically homogeneous (within the resolution of EDAX) by diffusional processes. This suggested the possibility that reasonably small, dense β' -X phase bodies could be converted to β^V bodies by diffusional processes.

Dense β' -X phase bodies were fabricated, and some base line test data generated. Concurrently, pack diffusion studies were begun. Property data will be discussed later. The fabrication and pack diffusion studies are described below.

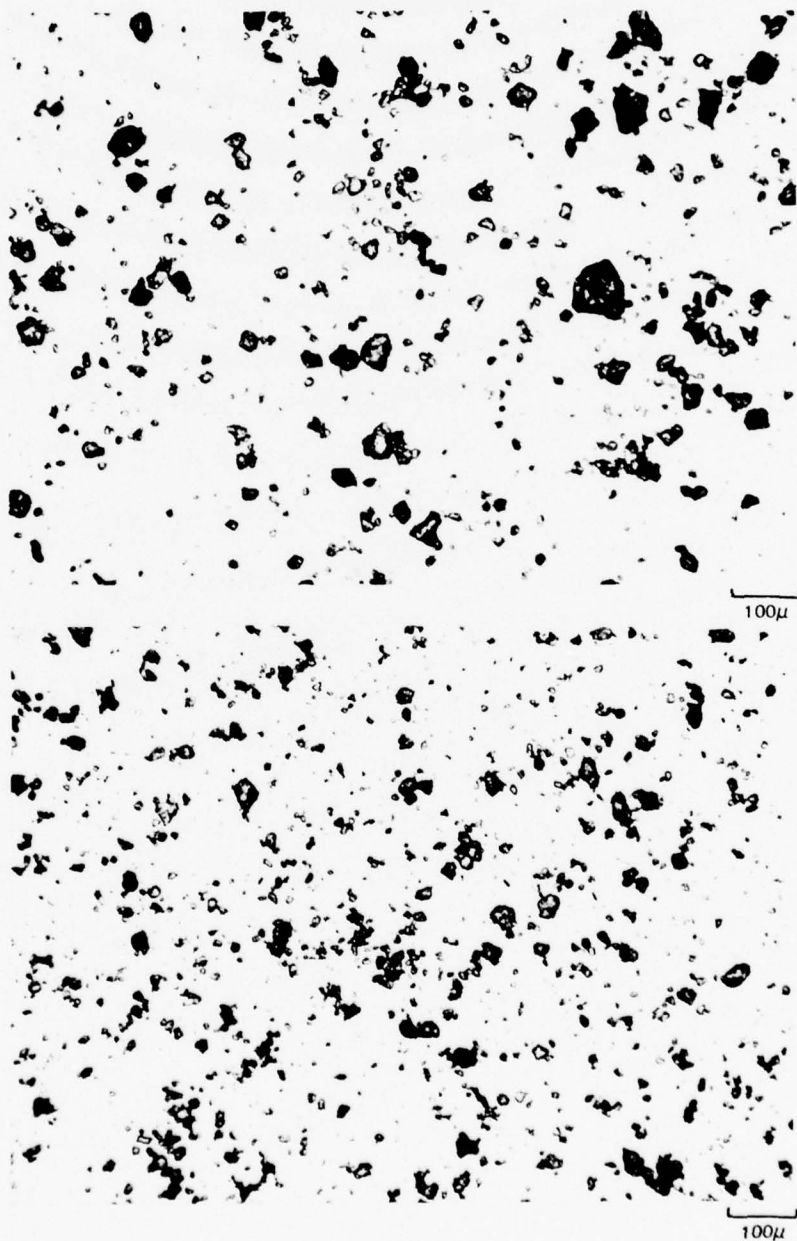


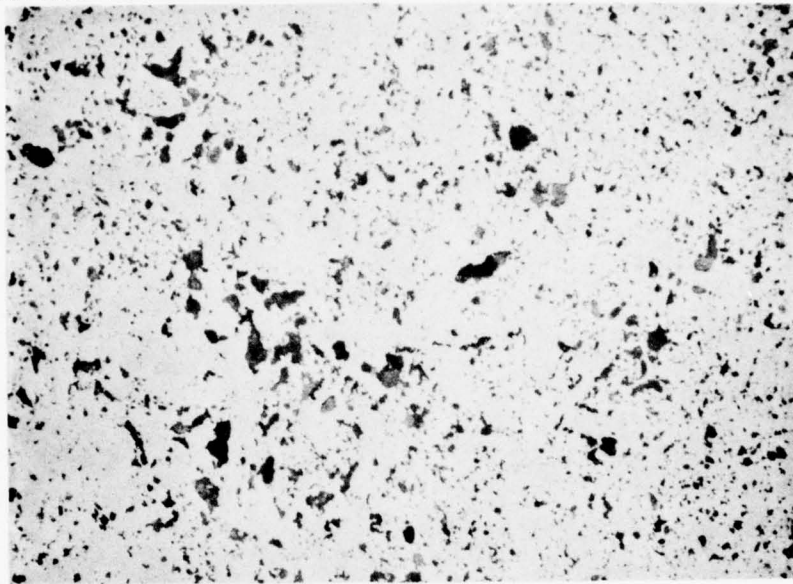
Fig 31. Representative Optical Transmissions Micrographs (1.77 Immersion Oil) of Settled Fraction of Ward β Si_3N_4 Powder

TABLE 18

FABRICATION AND TEST DATA FOR PROCESS 2 SAMPLES HAVING COMPOSITIONS IN THE z^{1-0} AND z^{1-0-x} FIELDS

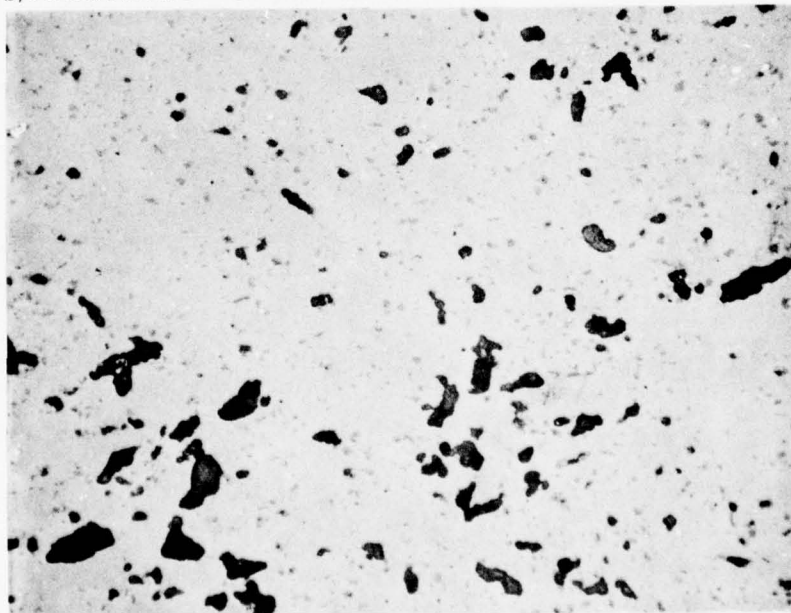
Sample Number	Pressing Condition			Firing Conditions					Test Results					Other Tests	
	Sample Shape	Isostatic Pressure (ksi)	Configuration	Pack Powder	Temp (°C)	Time (hrs)	Temp (°C)	Time (Hrs)	Weight Loss (%)	Shrinkage (%)	Apparent Porosity (%)	Bulk Density (g/cc)	Specific Gravity (g/cc)		Flexural Strength Test Temp (°C)
30.1.1	Cylinder	0	2	28.1	1760	3			10	12	16.5	2.60	3.11		
30.2.1								10	12	19.5	2.59	3.17			
30.1.2	Cylinders*	60	2	28.1	1760	3		11	9	20.5	2.49	3.14			
30.3.1	Cylinder	40	2	28.1	1760	3		10	13	3.8	2.99	3.12			
30.3.2	Cylinders*	40	2	28.1	1760	3		8	12	6.9	2.84	3.05			
30.4.1	Bars	30	2	27.1	1760	1	1720	9	4.6	9.2	13.2	2.71	3.12		
.2											16.5	2.59	3.10		
.3											15.0	2.67	3.14	1370°C oxidator	
.4	Bars	30	2	27.1	1760	1	1720	9			16.3	2.61	3.12		
.5											16.9	2.61	3.14		
.6											17.0	2.66	3.21		
.7											26.3	2.34	3.17		
.8	Bars	30	2	28.1	1760	4	-	-	7.8	-	25.8	2.35	3.16		
.9											27.0	2.30	3.16		
.10	Bar	30	2	28.1	1760	0.5	-	-	7.2		31.0	2.19	3.17		
.11															
.12	Bars	30	2	27.1	1760	2	1700	10		9.8	19.6	2.66	3.19		
.13											19.2	2.56	3.16		
30.5.1											19.4	2.54	3.15		
.2	Bars	30	2	27.1	1780	2	-	-	4.8		13.6	2.45	2.83		
.1											15.0	2.40	2.82		
30.1.1	Bars	30	2	28.1	1780	1	-	-	6.6	11.0	21.5	2.44	3.11		
.2											21.9	2.41	3.08		

a) FIRED TO 1760°C FOR 2 HRS



50μ

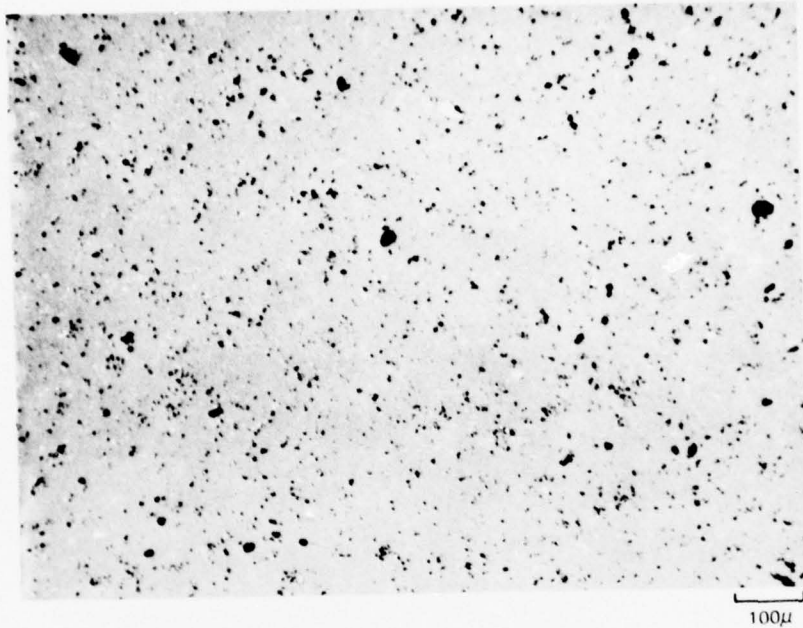
b) FIRED AN ADDITIONAL 10 HRS AT 1720°C



50μ

Figure 32 Microstructure of β' - O' - Composition 30.1.2 Before and After 10 Hr Heat Treatment of 1720°C

A



B

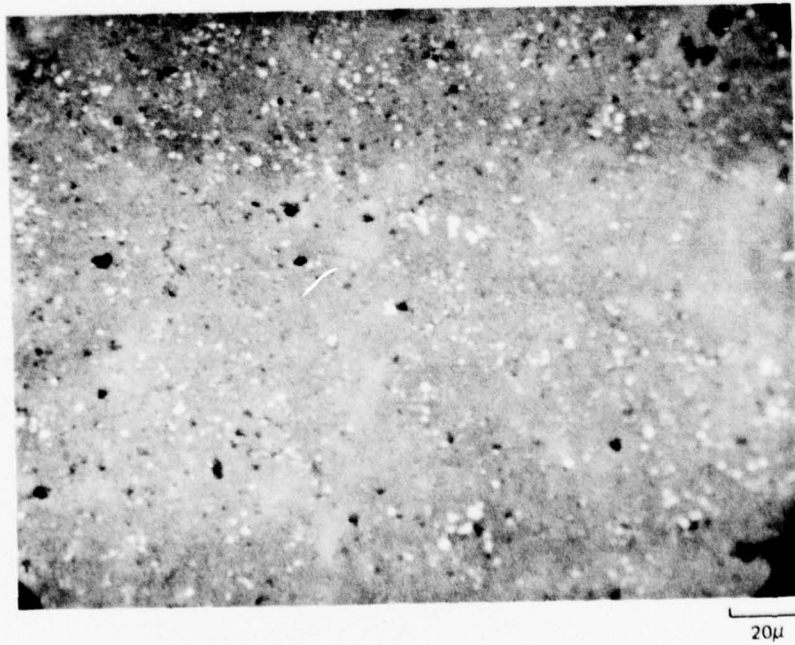
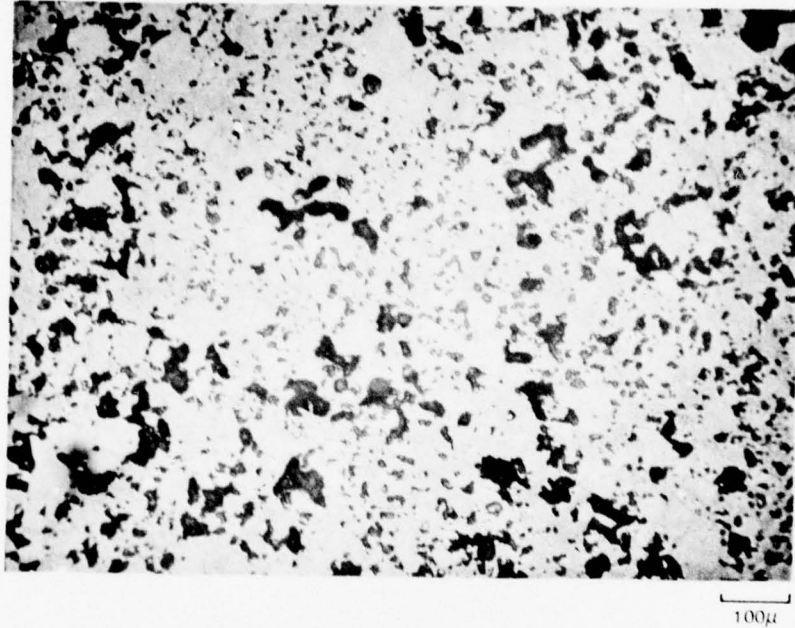


Figure 33 Microstructure of β - O Composition 30.3.1

78-08-138-2

A. SAMPLE 30.4.1



B. SAMPLE 30.5.1

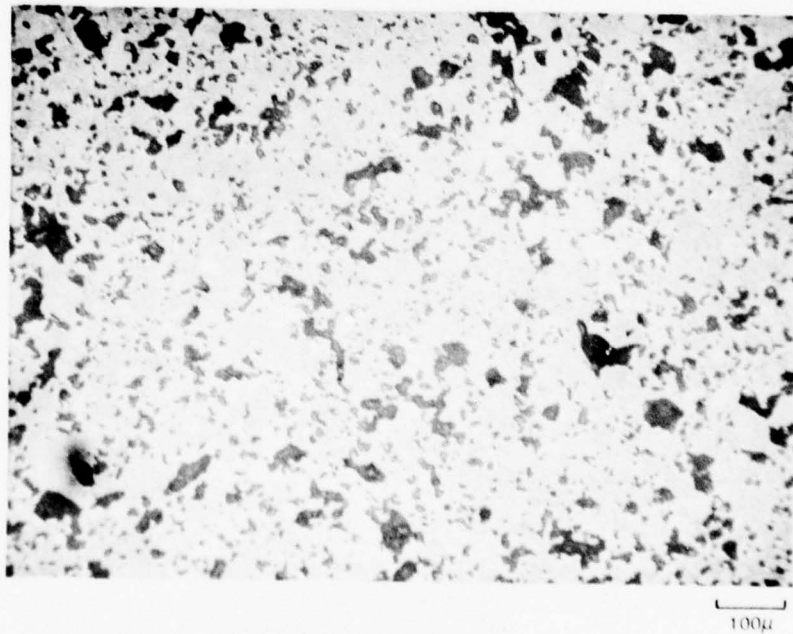


Fig 34. Polished Sections of Process 2 Composition 30 (β' -0) Sampler

1) Preparation and Microstructure of β' -X Phase Samples

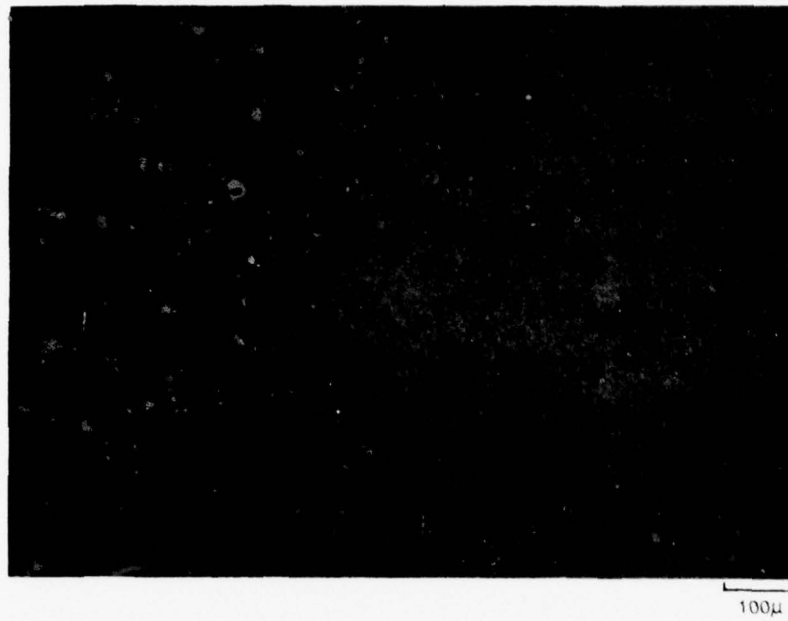
Samples were fabricated from master batches given in Table 12. Fabrication and test data are presented in Table 19. Polished and etched sections of samples 27.3.3 and 31.1.1 are shown in Figs. 35 and 36 respectively. Higher magnification micrographs of the etched samples are shown in Fig. 37. Although the porosity data of Table 19 indicates zero apparent porosity for all the samples, the polished sections disclose some closed porosity. In batch 27.3 samples, only a few closed pores on the order of 10μ in diameter are present. Some regions that could either be rich in second phase, or contain microporosity, are visible in the polished section, but details cannot be clearly resolved. These areas are more prominent in the etched section, suggesting that they could be areas rich in a glassy phase. However, SEM micrographs of fracture surfaces to be shown later disclose that some regions of microporosity do exist in batch 27.3 samples. Also noteworthy in the microstructure of all of the composition 27 samples is their virtual freedom from metallic inclusions that invariably occur when significant sample decomposition has occurred.

In contrast to samples of composition 27, the composition 31 samples show a considerable concentration of closed pores ranging in diameter up to about 30μ . The more complete densification of the composition 27 sample compared with the composition 31 samples under identical firing conditions may be related to the fact that the former composition partitions to a higher volume fraction of liquid phase at the firing temperature than does the latter. This can be seen in a qualitative way by examining Fig. 19. Drawing a line through composition points 27 and X phase and extending this to the β' homogeneity line establishes the β' composition in equilibrium in X phase. Assuming the X phase composition to be that of the liquid and applying the lever rule shows that composition 27 would have almost twice the concentration of liquid as composition 31. (This exercise can be done quantitatively by plotting the composition points on Fig. 2, and drawing tie lines between liquid and β' compositions parallel to those established by Naik.) While examining Fig. 19, it can be noted that the β' constituent of the body having an overall composition 27 has the composition 12 e/o Al, 8 e/o O, or about $\text{Si}_{2.5}\text{Al}_{.5}\text{O}_{.5}\text{N}_{3.5}$. This represents β' composition with the lowest Al concentration that can be expected as the major phase in a sinterable body which does not contain additional components.

2) Powder Pack Studies

Samples 27.3, .6, .7, and .8 were heated to 1600°C for 15 hrs in a powder of composition $\text{SiAl}_4\text{O}_2\text{N}_4$ (15R Phase). XRD patterns were obtained from the reacted surface, and from internal surfaces exposed by grinding away material to different depths below the original surface. A photoreduction of the diffractometer traces obtained from sample 27.3.6 in this fashion are compared to that obtained from the surface of the untreated sample 27.3.2 in Fig. 38.

A. POLISHED



B. ETCHED



Fig 35. Polished and HF Etched Surfaces of (β' -X) Sample 27.3.3

A. POLISHED



B. ETCHED

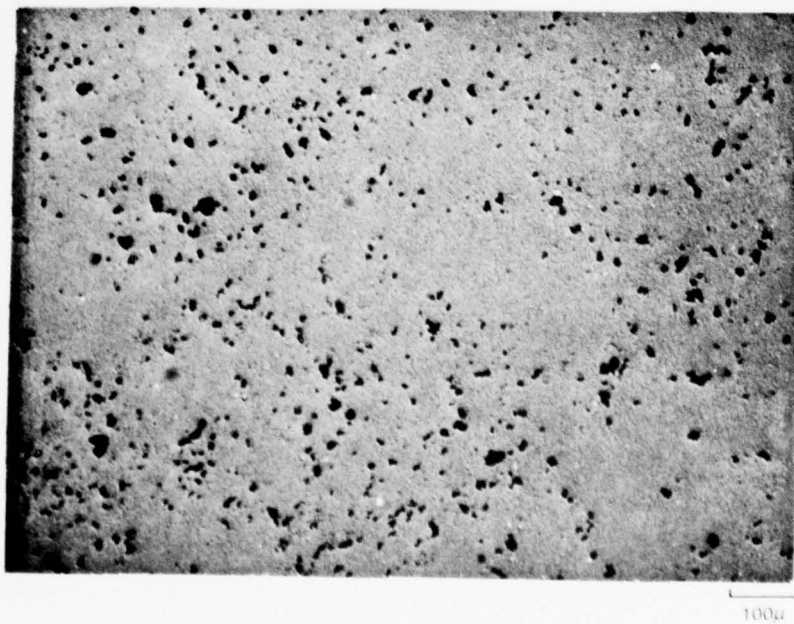
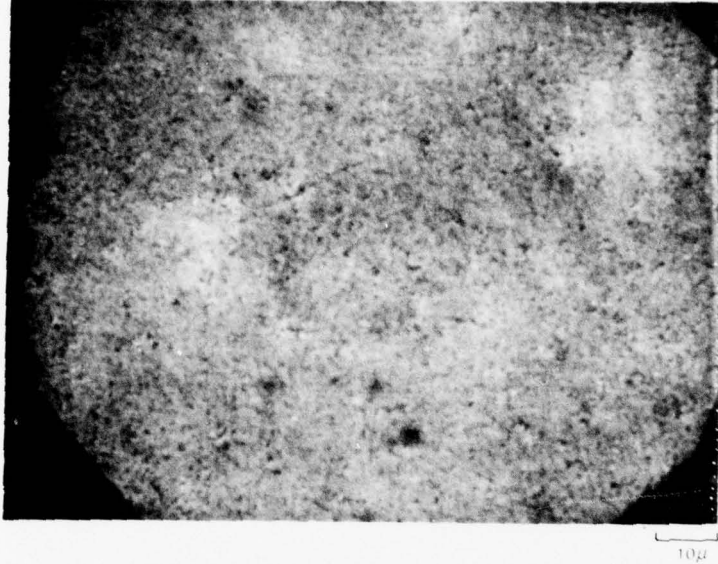


Fig 36. Polished and HF Etched Surfaces of (β' -X) Sample 31.1.1

A. 27.3.3



B. 31.1.1



Fig 37. Comparison of the Microstructure of (β' -X) Samples 27.3.3 and 31.1.1 at High Magnification

Note that the patterns obtained 0.010" and 0.015" below the surface of 27.3.6 are virtually indistinguishable from that of the unreacted sample. The weak crosshatched lines in the patterns are the strongest peaks of X phase. Note that there is little if any diminution in intensity of the X phase peaks in traces B and C relative to trace D. There is a substantial diminution in intensity of the X phase peaks at the surface, to the point where they are of the same order as the background noise. Also note a broadening and shift two higher d spacings of the β' peaks in the surface trace, particularly the (101) peak.

Samples 27.3.9, .10 and .11 were similarly heat treated in 15R powder at 1600°C for 50 hrs. After this heat treatment a marked change had occurred in the sample. A highly stressed surface layer had formed which tended to spall from the sides of the test bars. Photographs of the top and side faces of heat treated bar 27.3.9 are shown in Fig. 39A and B. The shape of the spalled regions suggests that compressional stresses exist in the reaction layer. After being photographed, the bar was mounted in resin and a polished cross section prepared. A micrograph of the cross-section is shown in Fig. 39C. It can be seen that a reaction rim penetrates to a depth of at least 250 μ (0.010"). Below this (and to the center of the cross section) the sample exhibits a grainy microstructure quite different from that of the original sample. (Compare with Fig. 35A).

XRD patterns were taken from the external, and various internal surfaces of sample 27.3.10 and a photoreduction of these as shown in Fig. 40. The diffraction pattern obtained from the surface shows β' peaks that have become broadened, reduced in intensity, and shifted to higher d values. A single strong, broad peak at 2.63 Å is superimposed on the β' pattern. This could be the strongest peak of the 15R phase (or possibly the U Phase) pattern given in Table 7. Below the reaction rim, (i.e., 0.010" below the surface) and to the center of the sample (0.050" below the surface), the β' pattern is broad and reduced in intensity, but the X phase pattern is still present, being broadened and reduced in intensity in roughly the same ratio as the β' phase pattern. From the above experiments it is apparent that it is not possible to convert grain boundary X phase to the β' phase by a pack diffusion process and still maintain a sound specimen.

E. Properties

1) Flexural Strengths

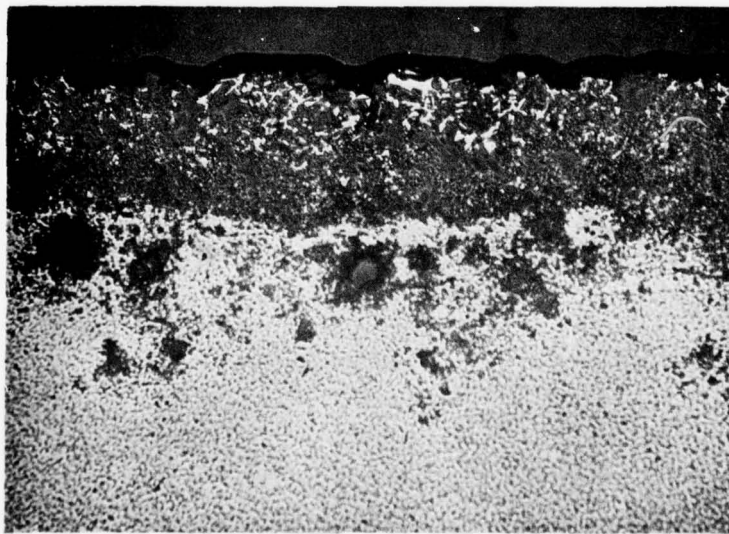
Flexural strength values for selected samples were recorded in Tables 16 and 19. The average room temperature strength of process $2\beta'$ samples (Table 16) was 110 MPa (16 ksi) and that of the process $2\beta'-0'$ samples (Table 18) was 115 (17 ksi). A representative fracture surface of the β' group (sample 33.1.1) is shown in Fig. 41, and from the $\beta'-0$ group (sample 30.4.4) in Fig. 42. In



A. TOP SURFACE (x7)



B. EDGE SURFACE (x14)



C. POLISHED AND ETCHED CROSS SECTION

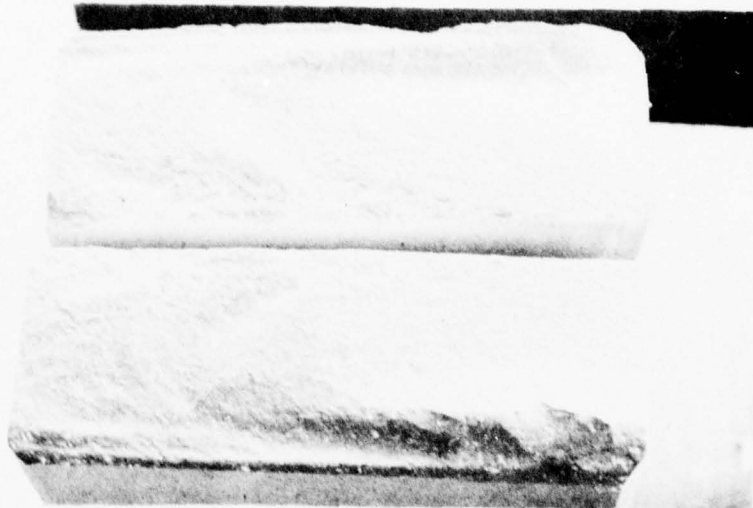
100 μ

Fig 39. Macro and Micrographs of Sample 27.3.9 after Heat Treatment in 4 AINSiO₂ Powder at 1600°C for 50 Hrs.

77-01
 Date: 10/20/77
 Operator: J. H. ...
 Sample: 27.3.10
 Run No: 1
 Run Time: 10:00
 Run Date: 10/20/77
 Run Time: 10:00
 Run Date: 10/20/77

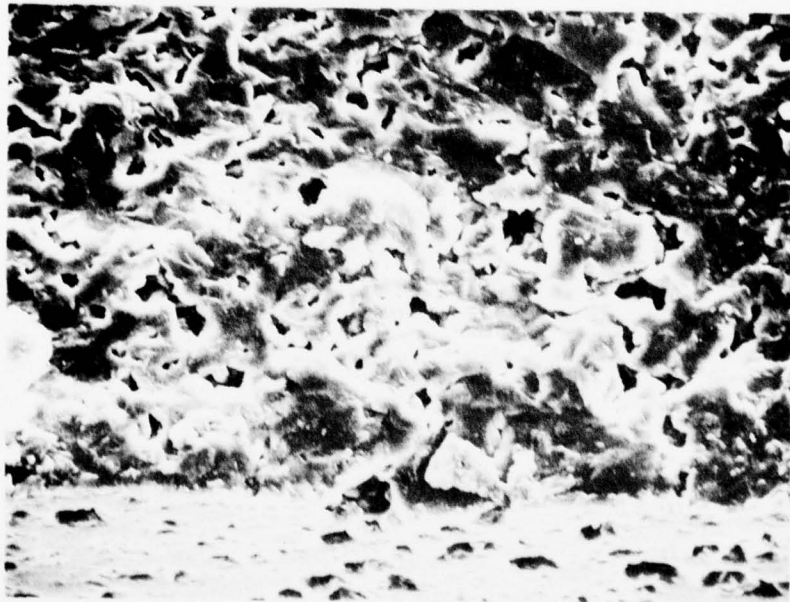


Fig 40. XRD Pattern from Different Areas at Powder Pack Heat Treated Sample 27.3.10



A. OVERALL

1000 μ



B. INITIATION SITE

20 μ

Fig. 41 Fracture Surface of Sample 33.1.1

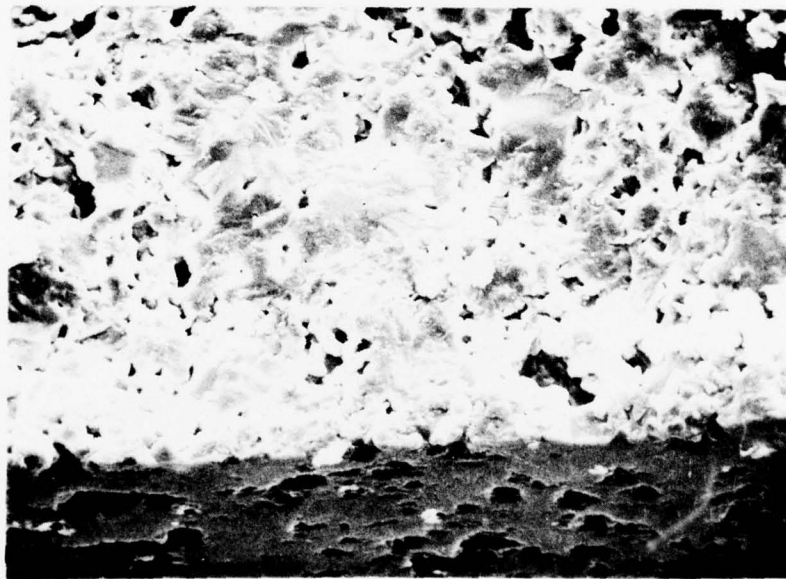
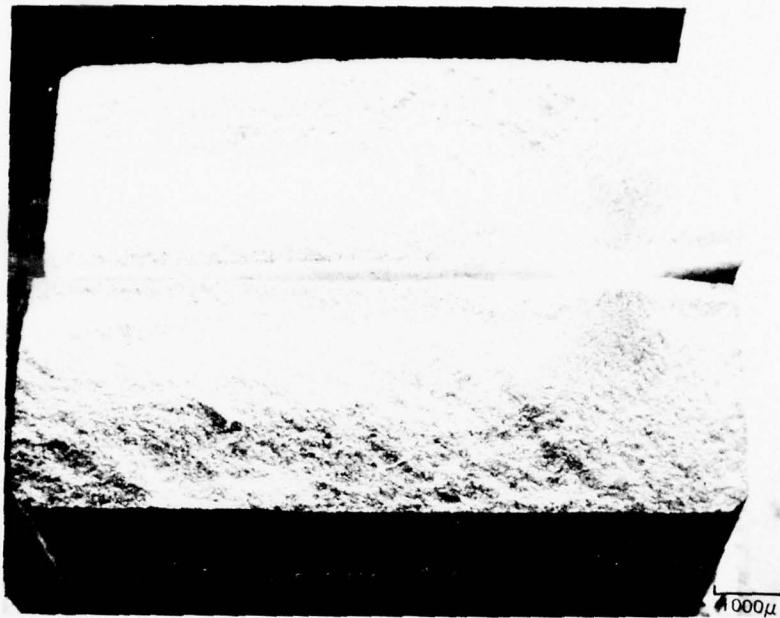


Fig. 42 Fracture Surface of Sample 30.4.4

both instances (as in all cases examined) fracture initiated in the neighborhood of a large pore at or near the tensile surface. The more dense β' -X phase samples (Table 19) had an average room temperature strength of 250 MPa (36 ksi). The samples prepared from batch 27.3 were consistently stronger (average value 310 MPa, 45 ksi) than the samples prepared from batch 27.1 (average value 195 MPa, 28 ksi). In both sets of samples, fractures initiated at isolated voids exemplified in Figs. 43 and 44. The average 1370°C strength for batch 27.3 samples was 267 MPa (39 ksi) and that of 27.4 samples was 290 MPa (42 ksi). Strength at 1370°C was still controlled by large isolated voids as exemplified by in Fig. 45. This contrasts strongly with the fracture behavior of previously fabricated samples (Ref. 5, pp. 63-66) having composition closer to the Al rich end of the β' solid solution limit. In the latter case, strength at 1370°C was limited by the intergranular phase to about 180 MPa (26 ksi).

The average room temperature and 1370°C strength of batch 27.3 samples and the average 1370°C strength of the batch 27.4 samples are plotted on Fig. 46, and the data compared to that for hot pressed Si_3N_4 (NC-132) and two reaction sintered Si_3N_4 bodies (Ref. 8). The strength of the SiAlON bodies is seen to be comparable to that of NC-350; somewhat stronger at room temperature and not as strong at 1370°C.

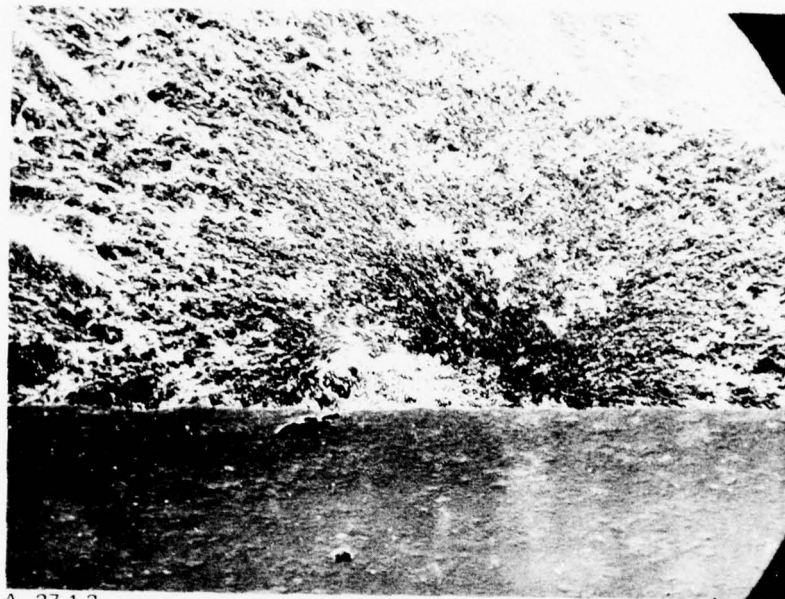
The voids that control the strength of β' -X samples both at room temperature and at 1370°C must be considered as processing flaws, and it is assumed that elimination of these defects through processing refinements could result in substantial improvement in high, as well as low temperature strength of the SiAlON bodies.

2) 1370°C Creep

The 1370°C, 10 ksi, creep curve for β' -X phase sample 27.3.15 is presented in Fig. 47. The secondary creep rate calculated from the curve is 1.5×10^{-4} hr⁻¹. This point is plotted, along with previous data from Ref. 5 and literature data for an MgO doped Sialon (Ref. 6), two hot pressed Si_3N_4 bodies, and two reaction sintered Si_3N_4 bodies (Ref. 7) in Fig. 48. The creep rate is seen to be comparable to that of the 65C Sialon material, less than that of NC-132 but much greater than that of RSSN Materials. It is presumed that batch 27.4 materials should exhibit lower creep than 27.3 because of the higher purity, especially the freedom from low melting constituents introduced by the high alumina grinding media. The effect of these impurities is discussed below.

3) Oxidation Behavior

Weight gain data for several of the SiAlON bodies are summarized in Table 20. All of the β' -X phase samples tested showed no measurable weight gain after 100 hrs exposure to air at 1000°C. Weight gains at 1400°C were small.



A. 27.1.3

100μ



B. 27.1.4

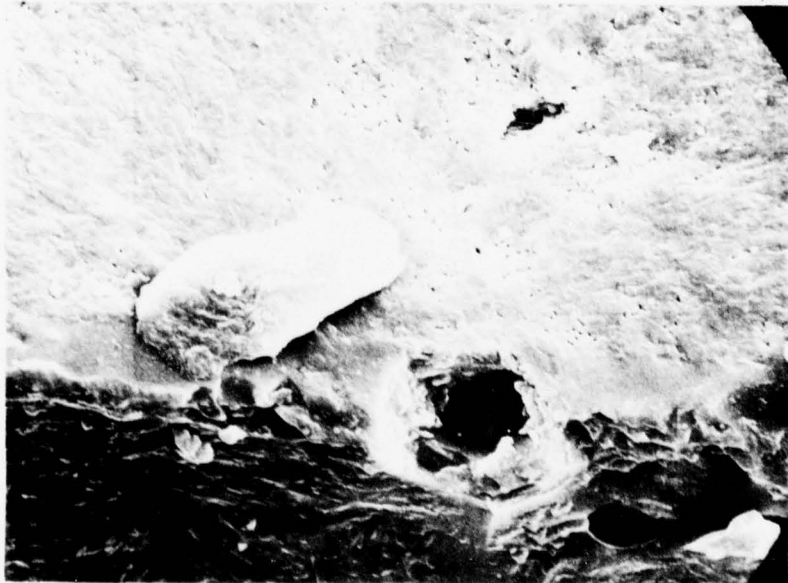
10μ

Fig. 43 Room Temperature Fracture Origins of Sampler 27.1.3 and 27.1.4



A. 27.3.3

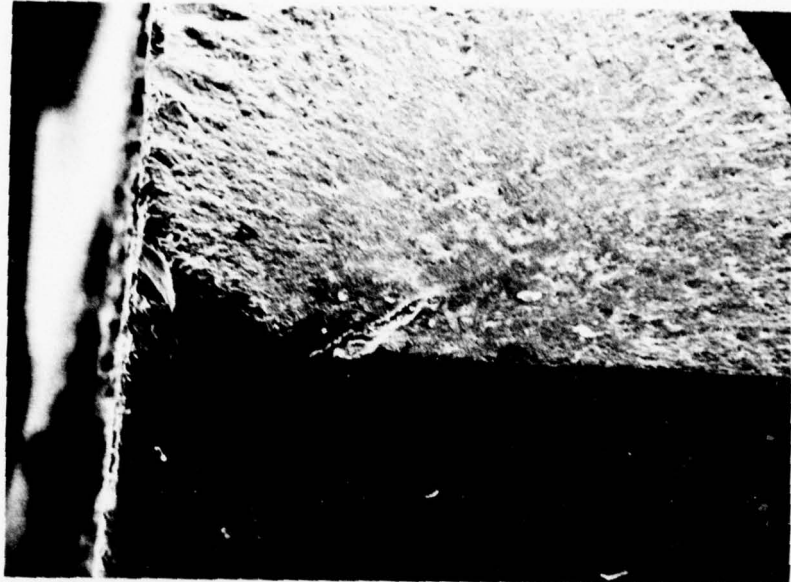
20 μ



B. 27.3.4

10 μ

Fig. 44 Room Temperature Fracture Origins of Sampler 27.3.3 and 27.3.4



A. SAMPLE 27.4.2

$\sigma = 280 \text{ MPa}$

100 μ



B. SAMPLE 27.4.3

$\sigma = 320 \text{ MPa}$

100 μ

Fig. 45 1370°C Fracture Origins of Sampler 27.4.2 and 27.4.3

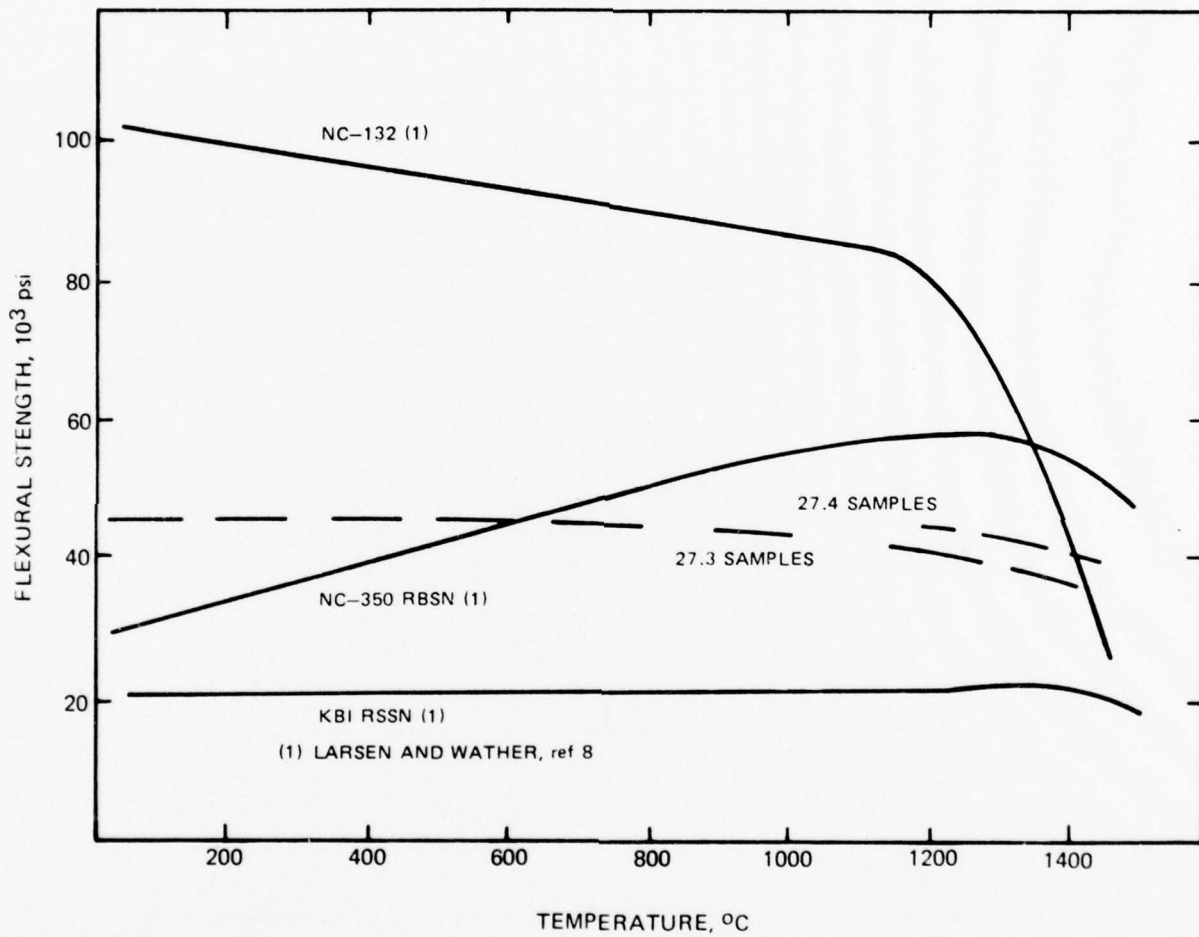


Fig. 46 Flexural Strength of Some Si_3N_4 and Sialon Materials

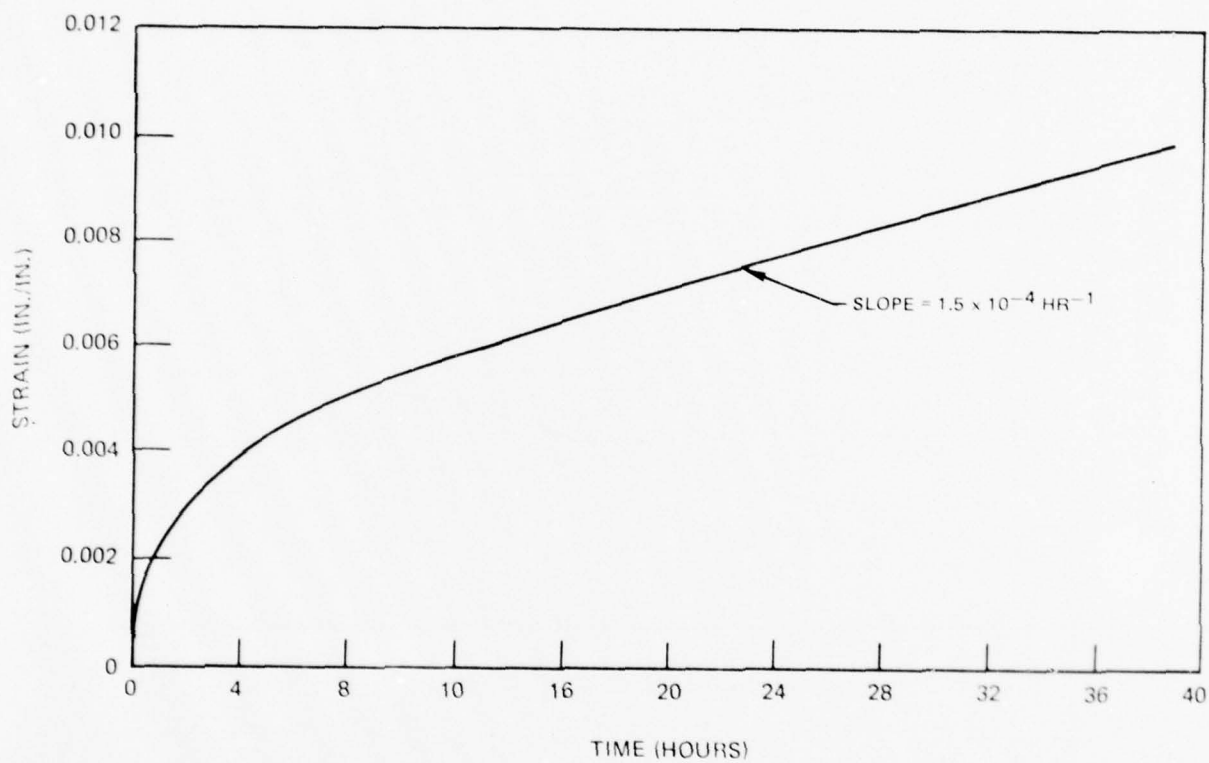


Fig. 47 Strain vs Time at 1370°C and 10,000 psi Stress for Sample 27.3.15

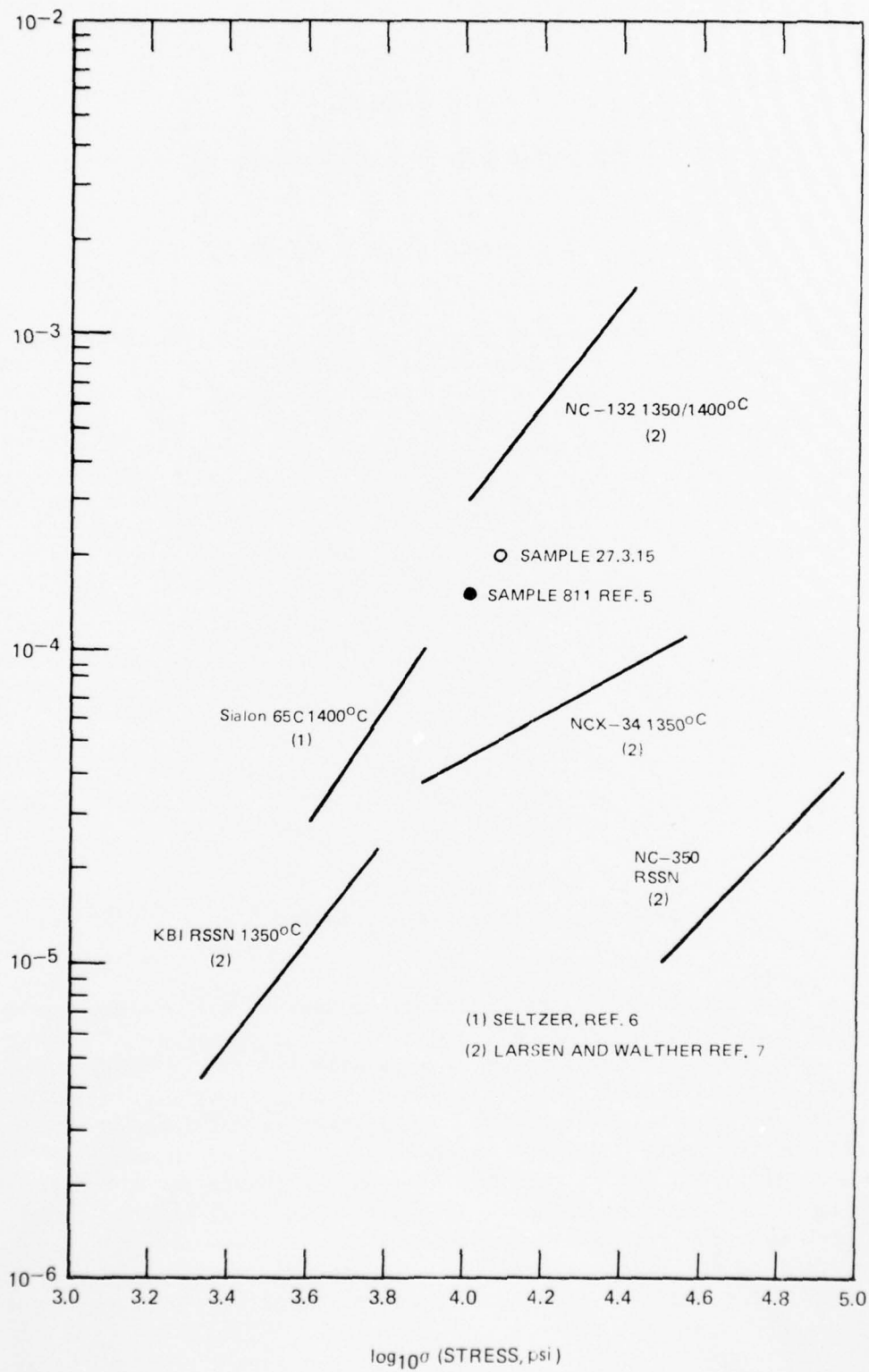


Fig. 48 Creep Rate vs Applied Stress for Some Si_3N_4 and Sialon Materials

TABLE 20

OXIDATION DATA FOR SiAlON SAMPLES

1000°C, 100 hr Data

Samples 27.1.2b, 27.3.13b, 27.4.1b, and 31.1.1b:
No weight gain (± 0.00005 g)

1400°C Data

$$\left(\frac{\Delta W}{A}\right)^2 \quad (\text{g}^2 \text{ cm}^{-4} \times 10^8)$$

Sample Number	(Hrs)				rate constant*
		1	5	72	($\text{g}^2 \text{ cm}^{-4} \text{ t}^{-1} \times 10^{10}$)
27.1.2a		0.04	0.8	2.0	1.7
27.3.13a		1.0	4.0	17.0	18.0
27.4.1a		0.04	0.5	1.5	1.4
31.1.1a		0.00	0.09	0.6	0.8
NC-132					270

*Assuming parabolic kinetics for $5 \text{ hr} < t < 72 \text{ hrs}$

The parabolic oxidation rate constants for the various SiAlONs are compared with that of hot pressed HS-130 (Ref. 9), and are seen to be orders of magnitude less. No such simple comparison can be made with the oxidation behavior of RSSN. These materials tend to exhibit a high initial weight gain followed by a very flat weight gain vs. time curve. The initial weight gain is a function of the density of the RSSN, and tends to be greater at intermediate (1000°C) temperatures (Refs. 10, 11). For both NC-132 and RSSN, strength tends to fall after exposure to air at high temperature. Strength after long term oxidation exposure has not been measured for the Sialon materials. However, micrographs of polished cross sections of oxidized samples, shown in Fig. 49, suggest that, at least for batch 27.4 formulations, strength would be unimpaired, since there is no visible degradation of the surface.

AD-A070 469

UNITED TECHNOLOGIES RESEARCH CENTER EAST HARTFORD CONN F/G 11/2
INVESTIGATION OF SILICON-NITROGEN CERAMICS FOR GAS TURBINES.(U)
JAN 79 G K LAYDEN N62269-77-C-0248

UNCLASSIFIED

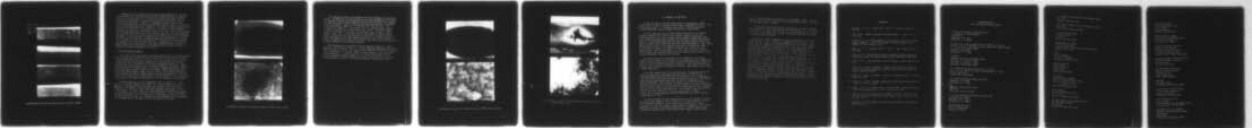
UTRC/R79-914147-4

NADC -77063-30

NL

2 OF 2

AD
A070469



END
DATE
FILMED
7-79
DDC

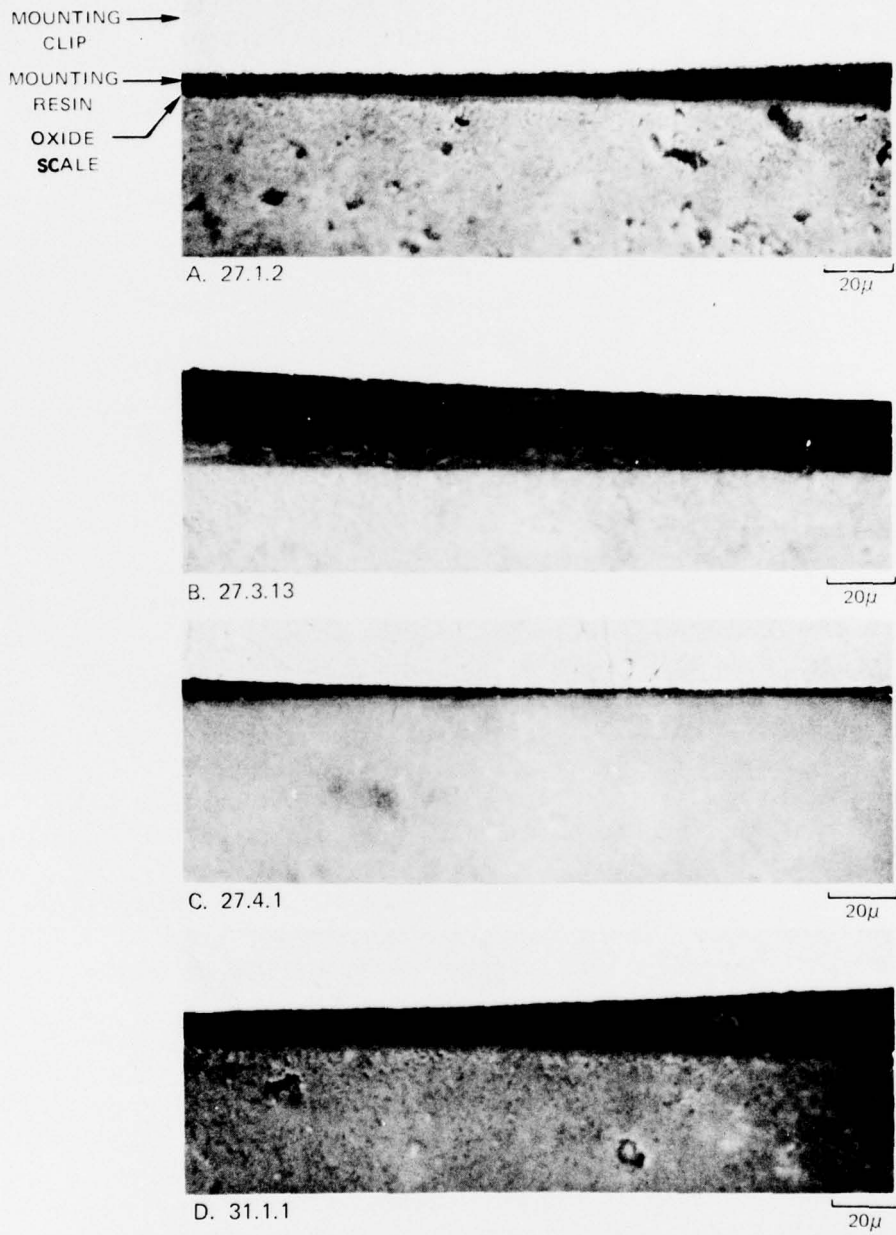


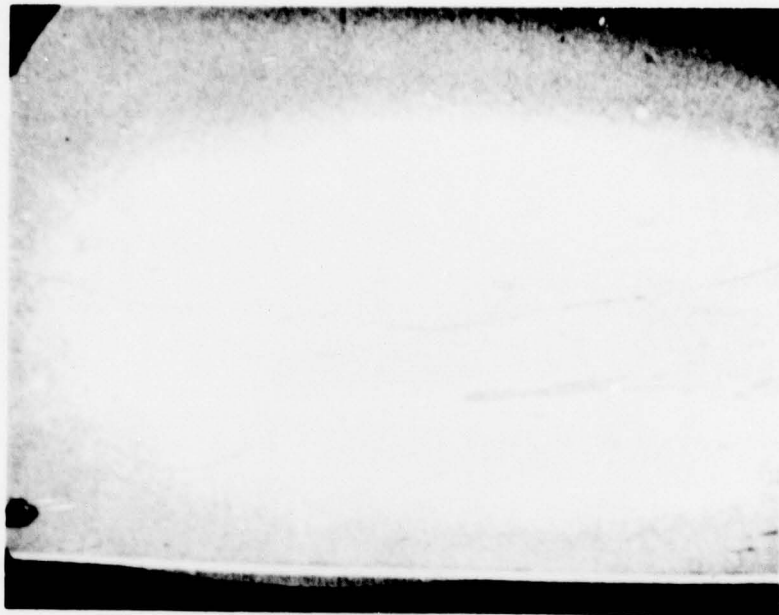
Fig. 49 Polished Cross Sections of Samples Oxidized for 72 HRS. at 1400° C

Examination of the polished cross sections shows differences in the oxide scale thickness that correlate with the relative weight gains of the samples. It can be seen that sample 27.4.1, which was prepared using SN402 Si_3N_4 and milled with Si_3N_4 media, has a grain structure and scale that cannot be resolved in the micrograph. Sample 27.1.2 prepared from KBI Si_3N_4 and also milled with Si_3N_4 media exhibits some significant porosity, and has a relatively thin scale averaging about 4μ in thickness. In contrast to these samples, 27.3.13, which has the same chemical constituents of 27.1.2 but was milled with high alumina media, exhibits a fairly thick scale of 15 or 20μ . From the media weight loss and composition (Table 4) one can calculate that batch 27.3 picked up about 0.04 grams or 0.05 w/o of foreign oxides from the media, all of which are fluxes from SiO_2 . It is reasonable to assume that the more rapid oxidation of sample 27.3.13 compared to the other four samples milled Si_3N_4 media is the result of the fluxing of the scale by these impurities. It may also be postulated that these impurities are concentrated in the grain boundary phase(s) in batch 27.3 samples, where their fluxing action would substantially alter the elevated temperature mechanical properties of the body.

4) Oxidation-Erosion Behavior

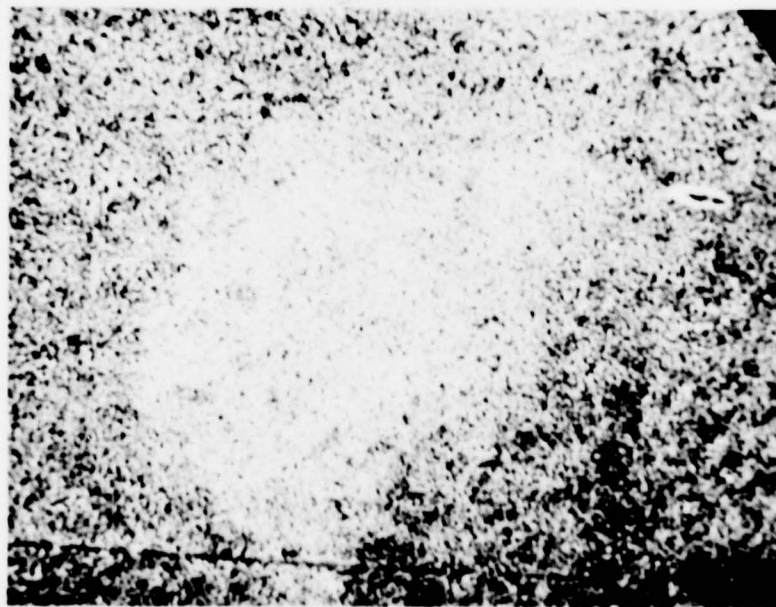
Difficulties were experienced in obtaining reproducible firing conditions and long term temperature stability during erosion tests at Mach 0.8 flame velocity. These problems were aggravated by the fact that heat transferred from the flame to materials tested (β' -X phase composition 27.3 and NC-132) was different, possibly because of differences in emissivity and thermal conductivity. Torch settings that heated sample 27.3.1 to a nominal temperature of 1400°C , heated a NC-132 sample to only around 1270°C . This was the maximum temperature to which the NC-132 samples could be heated with the torch. Different propane:oxygen ratios were then required to heat 27.3.2 to 1270°C as were used for NC-132 and still maintain the correct chamber pressure for Mach 0.8 operation, so that the flame stoichiometry was quite different for the two materials. Thus a quantitative comparison of the erosion characteristics of the two materials was impossible.

SEM photographs of the flame impingement region of Sample 27.3.2 after firing to a nominal temperature of 1270°C for 3 hrs are shown in Fig. 50. Difficulty was experienced in obtaining good resolution in the SEM because of tendency of the sample to become electrically charged, particularly in the eroded region. It can be seen in the high magnification photograph that there was no evidence for flow of material at this temperature. The grainy appearance of the eroded surface is on the same scale as the graininess exhibited by the polished section (see Fig. 49). However the grain boundaries are very prominent on the eroded surface and appear to have been etched by the flame.



A. OVERALL FLAME IMPINGEMENT AREA

1000 μ



B. CENTER OF IMPINGEMENT AREA

40 μ

Fig. 50 Surface of Sample 27.3.2 Subjected to Mach 0.8, 1270°C Flame for 3 HRS.

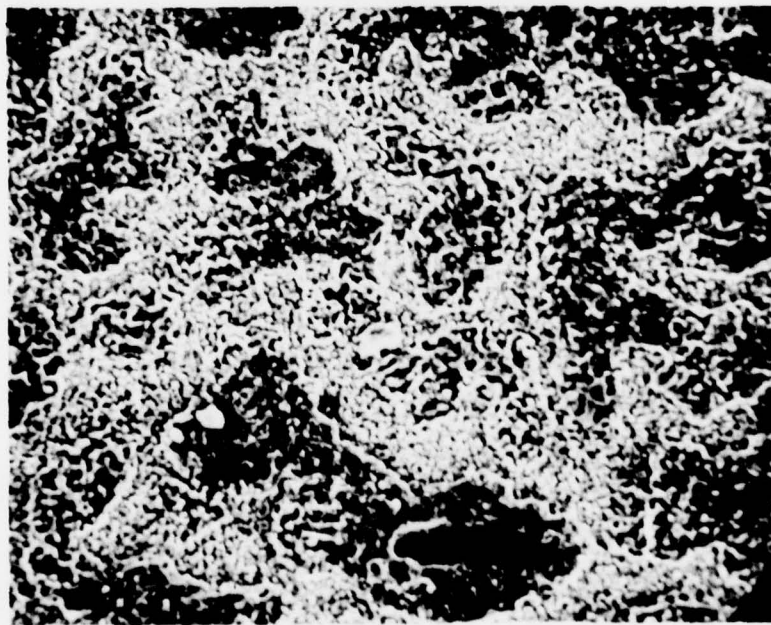
This sample was found to be cracked when it was unclamped from the support blocks. The edges of the cracks as seen in the lower photograph are sharp and not excessively eroded, which suggests that the crack occurred during cooldown. The crack may herald a thermal shock problem with this material; this remains to be investigated. Sample 27.3.1 tested at 1400°C did not crack. SEM photographs of Sample 27.3.1 are shown in Fig. 51. Here the central region is seen to be pitted on a scale of about 100 μ (.004"). The "land" between pits has a graininess on the order of that seen in Figs. 49 and 50. There appears to be a rim of once-molten material (presumably the glass oxidation product) around each pit, but there does not seem to be a general transport of matter down stream as one might imagine would be the case. The mechanism of this pit formation is not clear at the present time, but may involve the fluxing of grain boundaries by the oxidation product.

SEM photographs of the surface of NC-132 subjected to Mach 0.8, 1270°C flame for 2 hrs as shown in Fig. 52. A severe charging problem with this sample made SEM imaging difficult. The grains on the surface of the impinged region are coarse compared to 27.3 samples. Again, material appears to have been etched from between grains, as with Sample 27.3.2. Thus for both materials, the erosion mechanism at 1270°C and Mach 0.8 seems to involve first an etching of grain boundaries followed by its mechanical removal of unsupported grains.



A. OVERALL FLAME IMPINGEMENT AREA

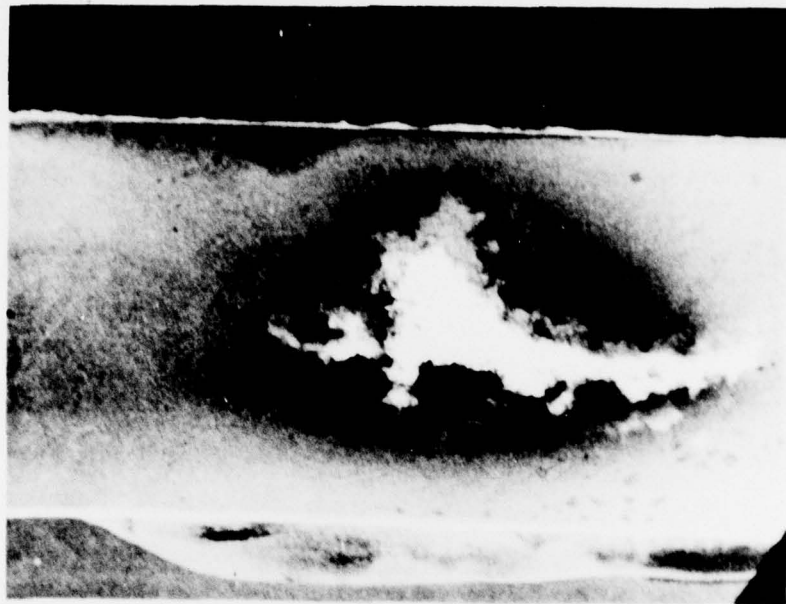
1000 μ



B. CENTER OF IMPINGEMENT AREA

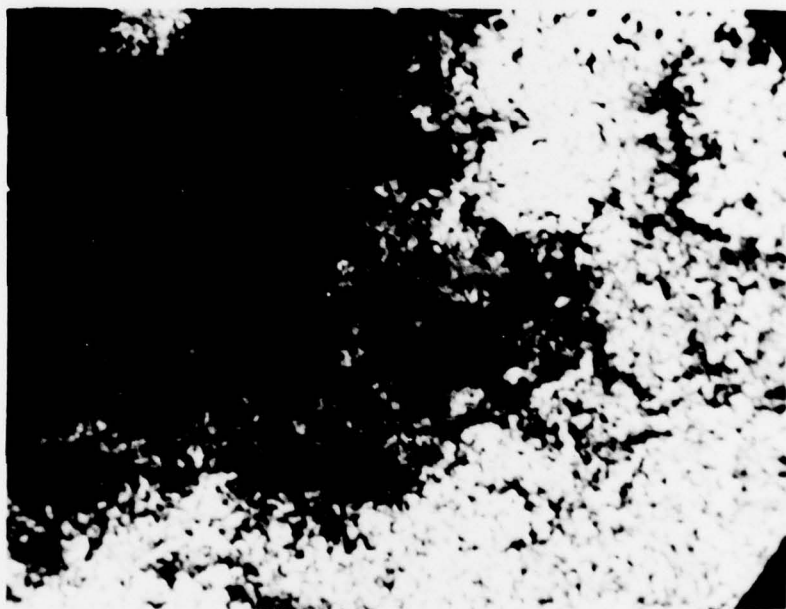
40 μ

Fig. 51 Surface of Samples 27.3.1 Subjected to Mach 0.8, 1400°C Flame for 2 HRS.



A. OVERALL FLAME IMPINGEMENT AREA

1000 μ



B. CENTER OF IMPINGED AREA

40 μ

Fig. 52 Surface of Sample of Hot Pressed Si_3N_4 (NC 132) Subject to Mach 0.8 1270°C Flame for 2 Hours.

IV SUMMARY AND CONCLUSION

Attempts were made to produce single phase β' $\text{Si}_{3-x}\text{Al}_x\text{O}_x\text{N}_{4-x}$ ceramic ceramic bodies, as well as two phase bodies having compositions in the β' - 15R ($\text{Si Al}_4\text{O}_2\text{N}_{4ss}$) and β' - O' ($\text{Si}_2\text{N}_2\text{O}_{ss}$) phase fields. Different approaches to using a transient liquid to promote sintering were investigated.

The first approach that was studied employed mixtures of fine grained compatible phases β' and 15R with coarse grained X phase ($\text{Si}_3\text{Al}_6\text{O}_{12}\text{N}_2$). It was postulated that lack of intimate contact between incompatible phases would hinder solid state reaction that would otherwise consume X-phase during heat up. It was further postulated that when the sample reached the melting point of X phase, liquid would form and wet-out and consolidate the body. These postulates were correct in all respects except that of consolidation. What in fact occurred was that the fine particles bonded into a porous structure during heat up. When liquid formed, it ran into the pores of the structure leaving behind voids that were replicas of the original X-phase particles, and no gross shrinkage or densification occurred.

While this result is discouraging from the standpoint of producing a dense β' body by pressureless sintering, it did demonstrate that segregation of X-phase into large particles will yield liquid at the melting point, where this would not occur in an all-fine-grained formulation. This could therefore be the basis for hot pressing to theoretical density a fine-grained body of single β' phase composition.

The second approach that was studied employed a fine-grained mixture of Si_3N_4 and Al_2O_3 with a coarse grain fraction of AlN. In this system it was postulated that isolation of the AlN constituent of a β' formulation would again hinder solid state reaction during heat up so that the fine-grained Si_3N_4 and Al_2O_3 constituents would react to form a β' composition and liquid above 1750°C . While some net shrinkage occurred with this system, it appeared that bridging of the coarse particles prevented a uniform fine-grained-matrix shrinkage. Large pores associated with bridged particles were generated resulting in a very coarse microstructure. The original large AlN particles none the less were converted to β' $\text{Si}_{3-x}\text{Al}_x\text{O}_x\text{N}_{4-x}$, and the bodies, through coarse grained, appeared chemically homogeneous as judged from EDAX element maps of Si and Al.

The third approach that was investigated was the heat treatment of dense β' -X phase bodies packed in 15R by diffusion via the grain boundary X-phase. Heat treatment at 1600°C for 50 hrs converted the surface for a depth of about .010" (250 μ) to a highly stressed mixture of expanded β' and a second phase that could not be positively identified by the single strong, broad, extraneous diffraction line. This stressed layer tended to spall from the

interior body which remained a mixture of β' and X-phase. Both the β' and X-phases in the interior exhibited diffraction peaks which were greatly broadened and diminished in intensity.

From the above experiments one can conclude that it is highly unlikely that a pressureless sintering technique can be devised that can yield fully dense bodies of β' composition (or β' -X or β' -O) although fully dense bodies of overall β' composition could probably be produced by hot pressing using the isolated X-phase technique.

Bodies of β' -X phase compositions can be easily sintered to near theoretical density. There is evidence to suggest that the preferred β' composition as far as mechanical and thermal properties are concerned would be that with the highest Si_3N_4 content (Refs. 10, 11, 12). The β' composition with the highest Si_3N_4 concentration that can be expected as the major phase in a sinterable body that does not contain extraneous liquid producing components is about $\text{Si}_{2.5}\text{Al}_{0.5}\text{N}_{3.5}$. Samples were fabricated which had a composition 20 ϵ/o Al, 20 ϵ/o O. This composition should partition into very nearly 80 w/o β' $\text{Si}_{2.54}\text{Al}_{0.46}\text{Si}_{0.46}\text{N}_{3.54}$ plus 20 w/o X-phase. These samples were evaluated in terms of room temperature and 1370°C flexural strength, 1370°C flexural creep, 1000 and 1400°C oxidation behavior and Mach 0.8 flame erosion at 1270°C. Mechanical and oxidation test results are compared with literature data for hot pressed Si_3N_4 (NC-132) and reaction sintered Si_3N_4 (NC-350 are KBI RSSN). The strength of SiALON bodies was comparable to that of NC-350 at room temperature and 1370°C. Strength was controlled by processing flaws (voids) at both temperatures, and is therefore subject to improvement with processing refinements. Creep rate at 1370 was less than that of NC-132 but much higher than that of the RSSN materials. Oxidation behavior was superior to either hot pressed or reaction sintered Si_3N_4 .

REFERENCES

1. Gauckler, L. J., H. L. Lukas, and G. Petzow: *J. American Ceram. Soc.*, 58, 346.
2. Jack, K. H.: SiAlONs and Related Nitrogen Ceramics. *J. Mat. Sci.*, 11 1135, 1976.
3. Layden, G. K.: Process Development for Pressureless Sintering of SiAlON Ceramic Components. Final Report, Naval Air System Command Contract N00019-75-C-0232, February 3, 1976.
4. Naik, I. K., L. J. Gauckler, and T. Y. Tien: *J. Amer. Ceram. Soc.*, 61, 332, 1978.
5. Layden, G. K.: Pressureless Sintering of SiAlON Gas Turbine Components, Final Report, Naval Air Systems Command Contract N62269-76-C-108, 1977.
6. Seltzer, M. S.: High Temperature Creep of Ceramics. Report AFML-TR-76-97. 1976.
7. Larsen, D. C. and G. C. Walther: Property Screening and Evaluation of Ceramic Turbine Engine Materials Semiannual Interim Technical Report #6 Contract F33615-75-C-5196.
8. Larsen, D. C. and G. C. Walther: Report No. 11tR1-D6114-1TR-2-4, Contract F33615-75-C-5196.
9. Tripp, W. C. and H. C. Graham: Oxidation of Hot-Pressed Silicon Nitride, *J. Mat. Sc*, 10, 1375 (1975).
10. Lange, F. F., H. J. Siebeneck and D. P. H. Hasselman: Thermal Diffusivity of Four SiAlON Compositions, *J. Amer. Ceram. Soc.* 59 1976.
11. Wills, R. R., R. W. Stewart and J. M. Wimmer: Effect of X-Phase on the Intrinsic Properties of Reaction Sintered Sialon, *Amer. Ceram. Soc. Bull.* 56, 194, 1977.
12. Layden, G. K.: Development of Sialon Materials NASA CR 135290, Contract NAS3-19712, 1977.

DISTRIBUTION LIST
(One copy unless otherwise noted)

(3 copies plus balance after distribution)

U. S. Naval Air Systems Command
(AIR-52031B)
Department of the Navy
Washington, D. C. 20361

(9 copies for internal distribution by AIR-954, as follows:)

AIR-954 (7 copies), AIR-536B1 (1 copy), AIR-330A (1 copy) AIR-330B
U. S. Naval Air Systems Command
Department of the Navy
Washington, D. C. 20361

(2 copies)

Commander, Naval Air Development Center
Code 302A, A. Fletcher (1 copy)
Code 30232, E. Tankins (1 copy)
Warminster, Pennsylvania 18974

U. S. Naval Air Propulsion Test Center (2 copies)
Attn: J. Glatz (PE-43) (1 copy) A. Martino (AT-1) (1 copy)
1440 Parkway Avenue
Trenton, New Jersey 08628

U. S. Naval Sea Systems Command (Code 035)
Department of the Navy
Washington, D. C. 20362

Commander, Naval Weapons Center
Code 5516
China Lake, California 93555

U. S. Naval Ships Engineering Center (Code 6146)
Department of the Navy
National Center, Bldg. 4
Washington, D. C. 20362

Naval Weapons Laboratory
Attn: W. Mannschreck
Dahlgren, VA 22448

U. S. Naval Ships Research and Development Center
Code 2812
Annapolis, Maryland 21402

Naval Surface Weapons Center (Metallurgy Division)
White Oaks
Silver Springs, Maryland 20910

Bell Aerosystems Company
Technical Library
P.O. Box 1
Buffalo, New York 14240

General Electric Company
Aircraft Engine Group
Materials and Processes Technology Laboratories
Evendale, Ohio 45215

Solar
(Dr. A. Metcalfe)
2200 Pacific Highway
San Diego, California 92112

Stellite Division
Cabot Company
Technical Library
P.O. Box 746
Kokomo, Indiana 46901

(2 copies)
General Electric Company
Corporate Research and Development
Attn: W. Hillig (1 copy)
R. Charles (1 copy)
Schenectady, New York 12301

Norton Company
Protective Products Division
(N. J. Ault)
Worcester, Massachusetts 01606

Research Library and Development Division
The Carborundum Company
P.O. Box 337
Niagara Falls, New York 14302

Ford Motor Company
Product Development Group
(E. A. Fisher)
2000 Rotunda Drive
Dearborn, Michigan 48121

General Electric Company
AEG Technical Information Center
Mail Drop N-32, Bldg. 700
Cincinnati, Ohio 45215

Professor Richard E. Tressler
Ceramic Science Section
Pennsylvania State University
201 Mineral Industries Bldg.
University Park, Pennsylvania 16802

Metals and Ceramics Information Center
Battelle Columbus Laboratories
505 King Avenue
Columbus, Ohio 43201

The Johns Hopkins University
Applied Physics Laboratory
(Maynard L. Hill)
Johns Hopkins Road
Laurel, Maryland 20810

AVCO RAD
201 Lowell Street
Wilmington, Massachusetts 01887

Detroit Diesel Allison Division
General Motors Corporation
Materials Laboratories
Indianapolis, Indiana 46202

Pratt & Whitney Aircraft
(Mr. A. Magid)
Florida Research and Development Center
West Palm Beach, Florida 33402

Westinghouse Electric Company
Materials and Processing Laboratory
(Ray Bratton)
Beulah Road
Pittsburgh, Pennsylvania 15235

Westinghouse Electric Company
Lester Branch 9175
(A. N. Holden)
Philadelphia, Pennsylvania 19113

Chief, Materials Engineering Dept.
Dept. 93-39M
AiResearch Manufacturing Co. of Arizona
402 South 36th Street
Phoenix, Arizona 85034

Lycoming Division
AVCO Corporation
Stratford, Connecticut 06497

Curtis Wright Company
Wright Aeronautical Division
Woodridge, New Jersey 07075

(2 copies)
Director
Naval Research Laboratory
Code 6360 (1 copy)
Code 6400 (1 copy)
Washington, D. C. 20375

Office of Naval Research
The Metallurgy Program, Code 471
Arlington, Virginia 22217

Director
Army Materials and Mechanics Research Center
(A. Gorum)
Watertown, Massachusetts 92172

Commanding Officer
Army Research Office (Durham)
Box CM, Duke Station
Durham, North Carolina 27706

U. S. Army Aviation Material Laboratories
Fort Eustis, Virginia 23604

Air Force Materials Laboratory
Code LLM
Wright-Patterson Air Force Base
Dayton, Ohio 45433

Air Force Propulsion Laboratory
Code TBP
Wright-Patterson Air Force Base
Ohio 45433

National Aeronautics and Space Administration
Code RWM
Washington, D. C. 20546

(3 copies)
National Aeronautics and Space Administration
Lewis Research Center
C. M. Ault (1 copy)
H. P. Probst (1 copy)
W. A. Sanders, MS 49-1 (1 copy)
21000 Brookpark Road
Cleveland, Ohio 44135

U. S. Energy Research and Development Administration
Division of Reactor Development
Mail Station F-309 (A. Van Echo)
Washington, D. C. 20545